LIETUVOS SVEIKATOS MOKSLŲ UNIVERSITETAS

Ieva Ceslevičienė

FLIUKSOMINIŲ METODŲ TAIKYMAS NAVIKO LĄSTELIŲ METABOLIZMUI TIRTI

Daktaro disertacija
Gamtos mokslai,
biologija (N 010)

Kaunas, 2020

Disertacija rengta 2014–2020 metais Lietuvos sveikatos mokslų universiteto Medicinos akademijos Kardiologijos instituto Vaistinių medžiagų ikiklinikinių tyrimų laboratorijoje.

Mokslinis vadovas

dr. Sergio Bordel Velasco (Lietuvos sveikatos mokslų universitetas, gamtos mokslai, biologija – N 010).

Konsultantai

prof. dr. Vytenis Arvydas Skeberdis (Lietuvos sveikatos mokslų universitetas, gamtos mokslai, biofizika – N 011);
prof. habil. dr. Algirdas Boguševičius (Lietuvos sveikatos mokslų universitetas, medicinos ir sveikatos mokslai, medicina – M 001).

Disertacija ginama Lietuvos sveikatos mokslų universiteto biologijos mokslo krypties taryboje:

Pirmininkė

prof. dr. Rasa Ugenskienė (Lietuvos sveikatos mokslų universitetas, gamtos mokslai, biologija – N 010).

Nariai:

prof. dr. Ilona Sadauskienė (Lietuvos sveikatos mokslų universitetas, gamtos mokslai, biologija – N 010);
prof. dr. Artūras Kašauskas (Lietuvos sveikatos mokslų universitetas, gamtos mokslai, biologija – N 010);
prof. dr. Rimantas Daugelavičius (Vytauto Didžiojo universitetas, gamtos mokslai, biologija – N 010);
prof. dr. Mindaugas Andrulis (Ulmo universitetas, medicinos ir sveikatos mokslai, medicina – M 001).

Disertacija ginama viešame biologijos mokslo krypties tarybos posėdyje 2020 m. rugpjūčio 27 d. 14 val. Lietuvos sveikatos mokslų universiteto Kardiologijos instituto Posėdžių salėje.

Adresas: Sukilėlių pr. 15, LT-50162 Kaunas, Lietuva.

LITHUANIAN UNIVERSITY OF HEALTH SCIENCES

Ieva Ceslevičienė

APPLICATION OF FLUXOMIC METHODS TO STUDY TUMOR CELL METABOLISM

Doctoral Dissertation
Natural Sciences,
Biology (N 010)

Kaunas, 2020

Dissertation has been prepared at the Institute of Cardiology of Medical Academy of Lithuanian University oh Health Sciences during the period of 2014–2020.

Scientific Supervisor

Dr. Sergio Bordel Velasco (Lithuanian University of Health Sciences, Natural Sciences, Biology – N 010).

Consultant

Prof. Dr. Vytenis Arvydas Skeberdis (Lithuanian University of Health Sciences, Natural Sciences, Biophysics – N 011);
Prof. Habil. Dr. Algirdas Boguševičius (Lithuanian University of Health Sciences, Medical and Health Sciences, Medicine – M 001).

Dissertation is defended at the Biology Research Council of the Lithuanian University of Health Sciences:

Chairperson

Prof. Dr. Rasa Ugenskienė (Lithuanian University of Health Sciences, Natural Sciences, Biology – N 010).

Members:

Prof. Dr. Ilona Sadauskienė (Lithuanian University of Health Sciences, Natural Sciences, Biology – N 010);
Prof. Dr. Artūras Kašauskas (Lithuanian University of Health Sciences, Natural Sciences, Biology – N 010);
Prof. Dr. Rimantas Daugelavičius (Vytautas Magnus University, Natural Sciences, Biology – N 010);
Prof. Dr. Mindaugas Andrulis (Ulmo University, Medical and Health Sciences, Medicine – M 001).

Dissertation will be defended at the open session of the Biology Research Council of the Lithuanian University of Health Sciences on 27th of August 2020 at 2 p.m. in Conference Hall of Institute of Cardiology of Lithuanian University of Health Sciences.

Address: Sukilėlių 15, LT-50162 Kaunas, Lithuania.

TURINYS

SANTRUMPOS

7-AAD	–	7-aminoaktinomicinas D
ACC	–	acetilo kofermento A karboksilazė
Acetil-KoA	–	acetilo kofermentas A
ADP	–	adenozin-5'-difosfatas
AKT	–	baltymo kinazė B (angl. *protein kinase B*)
ALDH	–	aldehido dehidrogenazė
ALT	–	alanino transaminazė
AMPK	–	AMP aktyvuoto baltymo kinazė (angl. *5' AMP-activated protein kinase*)
AP-1	–	aktyvatoriaus baltymas 1 (angl. *activator protein 1*)
ASMC	–	žmogaus kvėpavimo takų lygiųjų raumenų ląstelės (angl. *airway smooth muscle cells*)
AST		aspartato transaminazė
ATP		adenozin-5'-trifosfatas
BCAT	–	šakotosios grandinės aminorūgščių transferazė (angl. *branched-chain amino acid transferase*)
BCAT2	–	mitochondrinė šakotos grandinės aminorūgščių transferazė 2 (angl. *mitochondrial branched-chain amino acid transferase 2*)
BCC	–	krūties vėžio pirminių ląstelių kultūra (angl. *breast cancer cells*)
BCAA	–	šakotosios grandinės aminorūgštis (angl. *branched-chain amino acid*)
BCKA	–	šakotosios grandinės keto rūgštis (angl. *branched-chain keto acid*)
BCSC	–	krūties vėžio kamieninės ląstelės (angl. *breast cancer stem cells*)
BT-474	–	krūties naviko ląstelių linija
CAF	–	su naviku susiję fibroblastai (angl. *cancer-associated fibroblasts*)
CCCP	–	karbonilo cianido m-chlorfenilo hidrazonas (angl. *carbonyl cyanide m-chlorophenyl hydrazone*)
CCL2	–	monocitų chemotaktinis baltymas – 1 (angl. *monocyte chemoattractant protein-1*)
CD	–	diferenciacijos antigenai (angl. *cluster of differentiation*)
CPT1C	–	karnitino palmitoiltransferazė 1C (angl. *carnitine palmitoyltransferase 1C*)
CSC		vėžio kamieninės ląstelės (angl. *cancer stem cells*)
CXCL7	–	pagrindinis trombocitų bazinis baltymas (angl. *chemokine (C-X-C motif) ligand 7*)
DBT	–	dihidrolipoamido šakotos grandinės transacilazė (angl. *dihydrolipoamide branched chain transacylase*)
DLT	–	dihidrolipoilo transacetilazė
DMEM	–	dulbeko modifikuota Eagle terpė (angl. *Dulbecco's Modified Eagle Medium*)
DNR	–	deoksiribonukleorūgštis
ECHS1	–	trumposios grandinės enoil-KoA hidratazė 1 (angl. *enoyl-CoA hydratase, short chain 1*)
ECM	–	tarpląstelinis užpildas (angl. *extracellular matrix*)
EGF	–	epiderminis augimo veiksnys (angl. *epidermal growth factor*)

EMT	–	epitelinis–mezenchiminis virsmas (angl. *epithelial–mesenchymal transition*)
EM	–	elementarus metabolinis vienetas (angl. *elementary metabolite unit*)
ER	–	estrogenų receptoriai
F12	–	Ham's F-12 maistinių medžiagų mišinys (angl. *Ham's Nutrient Mixture F-12*)
FADH	–	redukuotas flavino adenino dinukleotidas (angl. *reduced form of flavin adenine dinucleotide*)
FAO	–	riebalų rūgščių oksidacija (angl. *fatty acid oxidation*)
FAS	–	riebalų rūgščių sintezė (angl. *fatty acid synthesis*)
FASN	–	riebalų rūgščių sintazė (angl. *fatty acid synthase*)
FGF	–	fibroblastų augimo veiksnys (angl. *fibroblast growth factor*)
FJS	–	fetalinis jaučio serumas (angl. *fetal bovine serum*)
FOXC2	–	šakės galvutės dėžutės baltymas C2 (angl. *forkhead box protein C2*)
FOXO	–	šakės galvutės dėžutės baltymas O (angl. *forkhead box protein O*)
FOXP3	–	šakės galvutės dėžutės baltymas P3 (angl. *forkhead box protein P3*)
GSMM	–	Genomo apimties metabolinis modelis (angl. *Genome Scale Metabolic Model*)
GAPDH	–	gliceraldehido-3-fosfato dehidrogenazė
HADHA	–	Hidroksiacil-KoA dehidrogenazės trifunkcinis daugiafermentinis komplekso alfa subvienetas (angl. *hydroxyacyl-CoA dehydrogenase trifunctional multienzyme complex subunit alpha*)
HER2	–	epidermio augimo veiksnio receptorius 2 (angl. *human epidermal growth factor receptor 2*)
HIBADH	–	3-hidroksiizobutirato dehidrogenazė
HIF1A	–	hipoksijos sukeliamas 1-alfa veiksnys (angl. *hypoxia-inducible factor 1-alpha*)
IFN	–	Interferonas
IL	–	Interleukinas
JC1	–	5,5',6,6'-tetrachloro-1,1',3,3'-tetraetilbenzimidazolilkarbocianino jodidas
Ki67	–	ląstelių proliferacijos žymuo
KoA	–	kofermentas A
LEF1	–	limfoidą stiprinantis veiksnys-1 (angl. *lymphoid enhancer-binding factor 1*)
Malonil-KoA	–	malonilo kofermentas A
MAPK	–	mitogenų aktyvinama baltymų kinazė (angl. *mitogen-activated protein kinase*)
MCF-10A	–	Ląstelių linija išskirta iš normalaus krūties audinio (angl. *Michigan Cancer Foundation-10A*)
MCF-7	–	Krūties naviko ląstelių linija (angl. *Michigan Cancer Foundation-7*)
MCT	–	monokarboksilato transporteris (angl. *monocarboxylate transporter*)
ME	–	malato dehidrogenazė (angl. *malic enzyme*)
MET	–	mezenchiminis-epitelinis virsmas;
MMP	–	tarpląstelinio užpildo metalo proteinazė (angl. *matrix metalloproteinase)*
MSC	–	mezenchiminės kamieninės ląstelės (angl. *mesenchymal stem cells*)
NAD	–	nikotinamido adenino dinukleotidas
NADH	–	redukuotas nikotinamido adenino dinukleotidas

NADPH	–	redukuotas nikotinamido adenino dinukleotido fosfatas
NK	–	natūralus žudikas (angl. *natural killer*)
NKT	–	T ląstelės žudikės (angl. *natural killer T*)
OXPHOS	–	mitochondrijų oksidacinis fosforilinimas (angl. *mitochondrial oxidative phosphorylation*)
PBS	–	fosfatinis buferis (angl. *phosphate-buffered saline*)
PDH	–	piruvato dehidrogenazė
PI3K	–	fosfoinozidido 3-kinazė (angl. *phosphoinositide 3-kinase*)
PPAR-δ	–	reroksisomos proliferatoriaus aktyvinti δ izoformos receptoriai
PER	–	progesteronų receptoriai
R/G	–	raudonos ir žalios fluorescencijos santykis (angl. *red/green*)
RNR	–	ribonukleino rūgštis
ROS	–	aktyviosios deguonies formos (angl. *reactive oxygen species*)
siRNR	–	trumpos grandinės nekoduojanti ribonukleino rūgštis (angl. *small interfering RNA*)
SP1	–	transkripcijos veiksnys (angl. *specificity protein 1*)
Sukcinil-KoA	–	sukcinilo kofermentas A
TAM	–	su naviku susiję makrofagai (angl. *tumor-associated macrophages*)
TCA	–	trikarboksirūgštis (angl. *tricarboxylic acid*)
TGFβ	–	transformuojantis augimo veiksnys beta (angl. *transforming growth factor beta*)
TNF-α	–	navikų nekrozės veiksnys alfa (angl. *tumor necrosis factor α*)
TNF-β	–	navikų nekrozės veiksnys beta (angl. *tumor necrosis factor β*)
TP53	–	naviko baltymas p53 (angl. *tumor protein p53*)
VEGF	–	kraujagyslių endotelio augimo veiksnys (angl. *vascular endothelial growth factor*)
WB	–	baltymų imunoblotingas (angl. *Western blot*)

ĮVADAS

Viena didžiausių chemoterapijos problemų yra jos šalutinis poveikis. Dauguma chemoterapijoje naudojamų vaistų yra nukreipti į DNR replikaciją arba pagrindinius ląstelių ciklo reguliatorius. Tai neigiamai veikia ne tik piktybines ląsteles, bet ir sveikas besidauginančias ląstelės (tame tarpe ir kamienines ląsteles), todėl sutrinka jų atsinaujinimas ir sveikų audinių funkcija [1]. Siekiant išvengti ar bent sumažinti šalutinį poveikį, būtina nustatyti sisteminius navikinių ir sveikų ląstelių skirtumus bei apskaičiuoti potencialių vaistinių medžiagų terapinius langus. Naujos našios genomikos, transkriptikos, proteomikos ir metabolomikos tyrimų technologijos, tokios kaip cDNR mikrogardelės ir RNR sekoskaita, leido sukaupti duomenų bazėse informaciją, kurią galima panaudoti sisteminių skirtumų tarp sveikų ir navikinių ląstelių nustatymui. Tikimasi, kad šie transkripciniai skirtumai suteiks pagrindą terapijai, nukreiptai į navikines ląsteles, nepažeidžiant sveikų ląstelių.

Navikinės ląstelės yra kilusios iš sveikų kamieninių ląstelių [2, 3], kuriose įvyksta mutacijos, sukeliančios tumorogeninį fenotipą. Atlikti žmogaus navikų RNR sekos tyrimai atskleidė šimtus mutacijų, susijusių su naviku atsiradimu [4], tačiau labai mažai mutavusių genų pasikartojo didelėse tiriamų mėginių frakcijose. Kiekvieno naviko tipo atveju tik maždaug keturi mutavę genai kartojasi daugiau negu 20 proc. tirtų mėginių [5]. Nustatyta, kad dažniausiai mutavęs būna navikų supresoriaus TP53 genas [6]. Nežiūrint į didelį piktybines transformacijas sukeliančių genų heterogeniškumą, vėžį galima charakterizuoti pagal kelis pagrindinius bruožus: stabilios proliferacijos išlaikymą; augimo supresorių išvengimą; invazijos ir metastazavimo aktyvinimą; replikacijos imortalizavimą; angiogenezės indukciją; apoptozės išvengimą [7]. Šie bruožai siejasi su transkripciniais pokyčiais, kurie neegzistuoja sveikose ląstelėse. Siekdami įvertinti šiuos skirtumus, išanalizavome didelį kiekį sveikų ir navikinių ląstelių genų raiškos duomenų ir eksperimentiškai parodėme, kad šakotosios grandinės aminorūgščių transaminazės 2 (BCAT2, angl. *branched-chain amino acid transaminase 2*) slopinimas gali pasitarnauti, kaip terapinis langas, selektyviai veikiantis navikines ląsteles, nesant poveikio sveikoms ląstelėms.

Kadangi navikinių ląstelių gyvybingumas ir proliferacija priklauso nuo riebalų rūgščių sintezės ir oksidacijos, tolimesniais tyrimais, panaudodami ^{13}C žymėtą glutaminą, siekėme nustatyti, ar šie abu procesai koegzistuoja krūties navikų ląstelėse.

DARBO TIKSLAS IR MOKSLINIS NAUJUMAS

Darbo tikslas

Fliuksominių metodų taikymas sveikų ir navikinių ląstelių metabolizmo ir transkripcinių skirtumų analizei ir priešnavikinių taikinių paieškai.

Uždaviniai

1. Krūties naviko ląstelių pirminės kultūros sukūrimas.
2. Terapinio lango paieška, atliekant sveikų ir navikinių ląstelių transkripcinių skirtumų analizę.
3. Eksperimentinis terapinio lango įvertinimas, slopinant sveikų ir navikinių ląstelių šakotosios grandinės aminorūgščių transaminazę 2.
4. Ištirti riebalų rūgščių sintezės ir oksidacijos sąveikos įtaką navikinių ląstelių gyvybingumui, panaudojant ^{13}C žymėtą glutaminą.

Mokslinio darbo naujumas

Daugumai navikinių ląstelių būdinga sustiprėjusi aerobinė glikolizė – Varburgo efektas. Vėžinės ląstelės pasižymi dideliu gliukozės sunaudojimo greičiu ir pieno rūgšties gamybą, net ir esant didelei deguonies koncentracijai. Anksčiau manyta, kad vėžinės ląstelės pasižymi sutrikusiu kvėpavimu dėl funkcinių mitochondrijų trūkumų, ir joms labiau būdinga aerobinė glikolizė, nei oksidacinis fosforilinimas. Tačiau naujausi tyrimai parodė, kad vėžinių ląstelių mitochondrijos funkcionuoja gerai, o energijos gamybai svarbus tiek oksidacinis fosforilinimas, tiek laktinė fermentacija [8].

Mes iškėlėme hipotezę, kad navikinėse ląstelėse didžioji adenozintrifosfato (ATP) dalis gaunama naudojant alternatyvius substratus, t. y. aminorūgštis. Siekiant kiekybiškai įvertinti alternatyvių energijos šaltinių įtaką, panaudojome genomo apimties metabolinius modelius (GSMM, angl. *Genome Scale Metabolic Model*). Remiantis šios analizės duomenimis, nustatėme, kad MCF-7 ląstelių linijoje ~50 proc. ATP yra gaunama iš šakotosios grandinės aminorūgščių (BCAA, angl. *branched chain amino acids*) valino, leucino ir izoleucino.

Tyrime naudojame siRNR, slopinančią fermento BCAT2 raišką, kuris katalizuoja BCAA, t. y. valino, leucino ir izoleucino, pirmąjį degradacijos etapą. Nustatėme, kad šio geno nutildymas sumažino navikinių ląstelių proliferaciją.

Galimos dvi pagrindinės interpretacijos apie riebalų rūgščių oksidacijos (FAO, angl. *fatty acid oxidation*) funkcijas vėžinėse ląstelėse. Manoma, kad FAO apsauginę funkciją gali turėti tik esant metaboliniam stresui, kai prara-

dus sukibimą su tarpląsteliniu užpildu, susilpnėja gliukozės įsisavinimas ir katabolizmas [9]. Tokiomis sąlygomis FAO veiktų kaip alternatyvus ATP [10] arba NADPH [11] šaltinis, o riebalų rūgščių sintezė (FAS, angl. *fatty acid synthesis*) darytų neigiamą poveikį ląstelių išgyvenimui, nes padidėtų ATP ir NADPH suvartojimas [11]. Kaip alternatyva buvo pasiūlyta, kad FAO ir FAS gali vykti vienu metu ir palaikytų viena kitą [12]. Šią hipotezę įrodo tai, kuomet paveikus ląsteles orlistatu (lipidų sintezės inhibitoriumi) sumažėjo deguonies suvartojimo greitis [13], kas buvo paaiškinta tuo pačiu metu ląstelėse vykstančia lipidų sinteze ir oksidacija. FAO ir FAS koegzistavimą įrodo tai, kad tuo pat metu nukreipus FAS ir FAO, sustiprėja terapinis poveikis prostatos vėžiui [14] ir mielomai [15]. Tačiau turimi įrodymai nėra tiesioginiai. Šiame darbe siekėme tiesiogiai patikrinti, ar egzistuoja FAS ir FAO, atlikdami metabolinių srautų analizę, panaudojant ^{13}C pažymėtą glutaminą bei genų nutildymą, panaudojant trumpą nekoduojančią RNR (siRNA). Taip pat parodėme, kad ląstelės, kuriose vienu metu vyksta FAO ir FAS yra mažiau jautrios oksidaciniam stresui.

1. LITERATŪROS APŽVALGA

1.1. Navikas ir jo aplinka

Navikas – tai pakitusių, neribotai besidauginančių organizmo ląstelių darinys. Daugėja įrodymų, kad pasikeitęs metabolizmas yra vienas iš skiriamųjų navikinių ląstelių požymių. Naviko mikroaplinka – tai sudėtingas tinklas, kurį sudaro stromos ląstelės (mezenchiminės kamieninės ląstelės (MSC, angl. *mesenchymal stem cells*)), su vėžiu susiję fibroblastai (CAF, angl. *cancer-associated fibroblasts*), adipocitai, endotelio, imuninės ląstelės ir kitos ląstelės (1.1.1 pav.), ir tarpląstelinio užpildo (ECM, angl. *extracellular matrix*) komponentai, citokinai, augimo veiksniai. Taip pat, naviko mikroaplinkai būdinga hipoksija [16]. CAF ypač gausu daugelio navikų, įskaitant krūties, prostatos ir kasos karcinomas, stromoje [17]. CAF yra nevienalytės populiacijos ir jų santykinė sudėtis labai skiriasi tarp skirtingų navikų. Pagrindiniai aktyvatoriai yra α-lygiųjų raumenų aktinas ir specifinis fibroblastų baltymas. Per didelė trombocitų sukeliamo augimo veiksnio receptorių β ir fibroblastų aktyvinimo baltymo raiška dažnai buvo stebimas solidinių navikų stromos fibroblastuose [18, 19]. Stromos fibroblastų ekspresuojami baltymai turi įtakos navikų formavimuisi. Bloga prognozė yra susijusi su padidėjusia p53 baltymo raiška CAF duktalinės krūties karcinomos atveju [20], padidėjusia karboanhidrazės IX raiška žmogaus plaučių adenokarcinomos atveju [21] ar padidėjusia periostino raiška cholangiokarcinomos atveju [22]. ECM yra audinių ir organų karkasas, susidarantis iš skirtingų ląstelių komponentų. Transformuojantis augimo veiksnys beta (TGFβ, angl. *transforming growth factor beta*), kurį išskiria navikinės ląstelės, fibroblastai ar imuninės ląstelės, gali skatinti tarpląstelinio užpildo metalo proteinazių (MMP, *angl. matrix metalloproteinases*) aktyvaciją, ląstelių migraciją ir navikinių ląstelių invaziją [23]. TGFβ gali paveikti ECM komponentų raišką. TGF-β reguliuoja įvairius ECM genus per SMAD ir MAP-kinazės signalinius kelius.

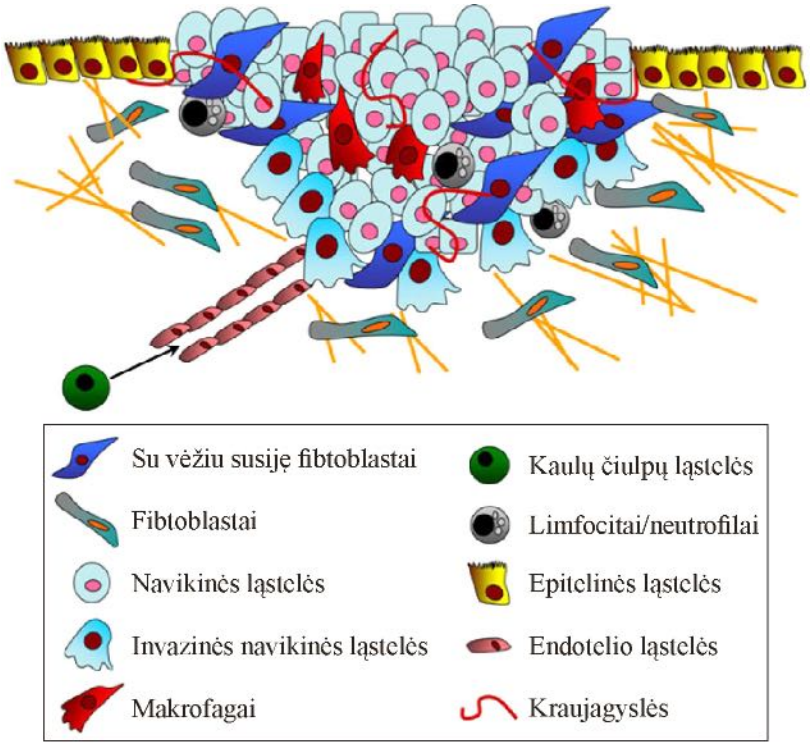

1.1.1 pav. *Stromos sandara, iš kurios išsivysto su vėžiu susiję fibroblastai*

Adaptuota iš Paolo Cirri ir kt. [16]

Bazinės membranos degradacija leidžia navikinėms ląstelėms sąveikauti su stromos fibroblastais, taip padarydama jų fenotipą panašų į CAF. Taip pat CAF gali susidaryti ir iš kaulų čiulpų MSC, kurių diferenciaciją skatina naviko kilmės dirgikliai. Navikinės ląstelės išskiria augimo veiksnius, kurie stimuliuoja angiogenezę ir uždegimą, bei suaktyvina endotelio ląsteles, makrofagus ir neutrofilus. Taigi, šios aktyvuotos stromos ląstelės kartu su navikinėmis ląstelėmis išskiria keletą EMC degradacijos fermentų (MMP, urokinazės tipo plazminogeno aktyvatorius ir katepsinai), kurių bendras aktyvumas tik dar labiau skatina stromos CAF bei vėžinių ląstelių invazyvumą [16] (1.1.1 pav.).

Makrofagai yra pagrindiniai naviko angiogenezės veiksniai. Stromoje esantys makrofagai gali išskirti įvairius citokinus. Svarbiausia makrofagų funkcija yra dalyvavimas imuninėje sistemoje, tačiau patekę į naviko aplinką tampa su naviku susijusiais makrofagais (TAM, angl. *tumor-associated macrophages*), kurie neatlieka savo imuninės funkcijos, o palaiko naviko augimą ir angiogenezę. Klinikiniai tyrimai parodė koreliaciją tarp padidėjusio TAM kiekio ir blogos krūties, prostatos, kiaušidžių, gimdos kaklelio, endo-

metriumo, stemplės ir šlapimo pūslės vėžio prognozės [24]. T, B limfocitai, natūralios žudikės (NK, angl. *natural killer*) ir T ląstelės žudikės (NKT, angl. *natural killer T*) aptinkami naviko stromoje ir apie naviką esančiuose audiniuose. Augant navikui, pažeidžiami T ir B limfocitai, kurie turėtų būti atsakingi už organizmo imuninę apsaugą, todėl atsiranda imunosupresija, kuri yra naviko progresavimo sudedamoji dalis. T reguliacinės ląstelės yra svarbi imuninės sistemos dalis naviko atžvilgiu, kadangi jos sekretuoja du pagrindinius imunosupresinius citokinus IL-10 ir TGF-β, kurie slopina specifinių efektorinių T limfocitų ir įgimto imuniteto NK ląstelių aktyvumą. Nors NK ląstelių yra naviko mikroaplinkoje, jos nesugebės atlikti savo naikinimo funkcijos. Navikinės stromos NK ląstelės turi anerginį fenotipą, kurį sukelia piktybinis ląstelių gautas TGF-β [25]. Angiogeniniai veiksniai, tokie kaip kraujagyslių endotelio augimo veiksnys (VEGF, angl. *vascular endothelial growth factor*) ir fibroblastų augimo veiksnys, kuriuos gamina piktybinės ląstelės, stimuliuoja endotelio ląsteles ir naujų kraujagyslių formavimą. Taip pat jie atsakingi ir už limfangiogenezę, kuri svarbi naviko metastazavime ir imuniniame atsake.

1.2. Epitelinis–mezenchiminis virsmas ir navikų metastazavimas

Kancerogenezė yra sudėtingas, kelių pakopų procesas, apimantis keletą mechanizmų, tokių kaip ląstelių proliferacija, diferenciacija, apoptozė, epitelinis-mezenchiminis virsmas (EMT, angl. *epithelial-mesenchymal transition*) ir angiogenezė [26, 27]. EMT yra suskirstyta į tris tipus: embriogenezė, fibrozė ir navikogenezė. 1-o ir 2-o tipo EMT prisideda prie organų vystymosi ir audinių regeneracijos. 3 tipo EMT dalyvauja kancerogenezėje ir yra reikšmingai susijęs su invaziškumu, tolimosiomis metastazėmis ir bloga klinikine baigtimi [28–34]. EMT dalyvauja reguliuojant keletą ląstelių funkcijų, įskaitant ląstelių adheziją, migraciją, proliferaciją, diferenciaciją, signalo perdavimą, išgyvenamumą ir metastazavimą [31, 35]. Tai apima hormonų receptorių ir ląstelių tarpusavio sąveikos baltymų praradimą. *In vitro* krūties naviko MCF-7 ląstelėse estrogeno nutildymo modelis parodė, kad estrogenų receptorių (ER) raiškos praradimas buvo reikšmingai susijęs su EMT procesu, buvo skatinamas ląstelių dauginimasis ir migracija, ECM ir MMP pokyčiai [36]. Pirminio naviko stromos fibroblastai arba kaulų čiulpų ląstelės diferencijuojasi į CAF ir padidina navikinių ląstelių agresyvumą ir invaziją dėl EMT. Atsiranda atsparumas hipoksijai, rūgštinei terpei ar chemoterapiniams vaistams, taip pat jų metabolizmas palaiko naviko masės augimą, net ribojant naviko maistines medžiagas. Ląstelės, kurios metastazuoja, iš pirminio židinio keliauja kartu su CAF, kurie apsaugo nuo apoptozės ir palengvina ekstra-

vazaciją. CAF išskiria citokinus/chemokinus, kurie reguliuoja galutinį metastazavusio naviko įsitvirtinimą, reguliuoja mezenchiminį-epitelinį virsmą (MET) ir leidžia vėliau augti kolonijoms [16] (1.2.1 pav.).

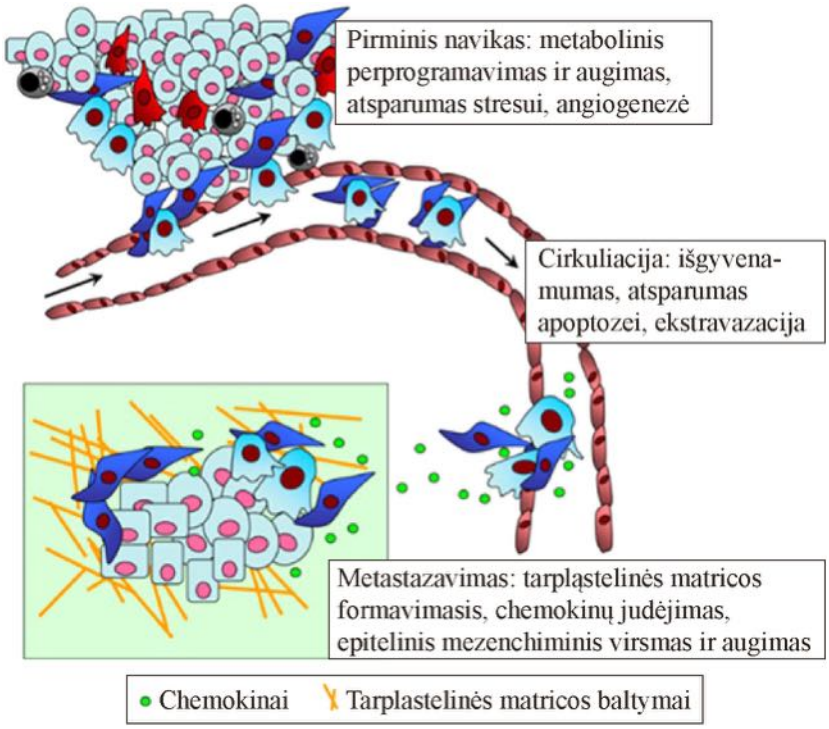

1.2.1 pav. *Su vėžiu susijusių fibroblastų vaidmuo naviko metastazavime*

Adaptuota iš Paolo Cirri ir kt. [16]

EMT aktyvacijai būdingas epitelinių ląstelių žymenų, tokių kaip E-kadherino, okliudino, sandarių jungčių baltymų ir desmogleino, raiškos sumažėjimas, dėl ko prarandama adhezija tarp ląstelių. Be to, tuo pat metu padidėja mezenchiminių ląstelių žymenų, įskaitant N-kadheriną, citokeratiną, aktiną ir fibronektiną, kiekis [37]. E-kadherino raiškos sutrikimas tarpląstelinėje adhezijoje sukelia naviko ląstelių metastazes. EMT pasireiškia keliais signalo perdavimo keliais, įskaitant TGF-β, PI3K / AKT, Ras / MAPK, Wnt kelius. Šie signalo perdavimo keliai funkcionuoja aktyvuodami susijusius transkripcijos veiksnius. Pavyzdžiui, TGF-β aktyvina SNAIL2, „Twist1“ ir ZEB1 / 2 ir iš naujo reguliuoja FOXC2, taip sukeldamas EMT aktyvaciją. TGF-β kanoninis ir nekanoninis Wnt signalo perdavimo kelias sinergetiškai indukuoja EMT ląstelėse, po to automatiškai palaikant intersticinių ląstelių būklę [38]. VEGF yra stipriausias šiuo metu aptiktas angiogeninis veiksnys, stimuliuojantis

endotelio ląstelių dauginimąsi, skatinantis kraujagyslių pralaidumą, ląstelių migraciją ir naviko ląstelių metastazavimą. TGF-β1 yra stiprus VEGF induktorius navikinėse ląstelėse. Jis taip pat dalyvauja naviko mikroaplinkoje, reguliuodamas naviko ląstelių invaziją ir angiogenezę [39]. Navikinių ląstelių EMT turi įtakos transkripcijos veiksnio (SP1, angl. *specificity protein 1*) ir Wnt signalinio kelio sąveika. EMT taip pat yra susijęs su fermentų, dalyvaujančių BCAA (valino, leucino ir izoleucino) degradacijoje, raiškos padidėjimu.

1.3. Krūties navikai

Krūties navikas yra dažniausia moterų onkologinė liga, paplitusi tiek išsivysčiusiuose, tiek besivystančiuose regionuose, ir užimanti antrą vietą tarp visų navikų atvejų (10,9 proc.). 2018 m. diagnozuota 2 mln. naujų krūties naviko atvejų [40]. Krūties navikas yra kliniškai ir biologiškai heterogeninė liga, pasireiškianti specifiniais morfologiniais ir imunohistocheminiais radiniais bei įvairia klinikine eiga [41]. Individualizuotos medicinos epochoje padaryta reikšminga pažanga, atliekant krūtų vėžio potipių molekulinę analizę. Krūties navikai skirstomi į 5 tipus [42] (1.3.1 lentelė). Kiekvienas tipas turi skirtingas biologines savybes, klinikines išeitis, atsaką į chemoterapiją ir padeda pasiūlyti pacientėms tikėtinai efektyviausią gydymo metodą [43]. Biologiniai naviko tipai (subtipai) apibrėžiami imunohistocheminiu tyrimu nustačius ER, progesteronų receptorių (PR), epidermio augimo veiksnio receptorių 2 (HER2) ir ląstelių proliferacijos žymens Ki-67 raišką [44] (1.3.1 lentelė). Biologiniai žymenys, susieti su klinikiniais-patologiniais prognoziniais veiksniais, tokiais kaip naviko dydis, diferenciacijos laipsnis, piktybinio proceso invazija į limfagysles bei limfmazgių būklė, svarbūs ir skirstant ligonius į prognozines grupes. Iki šiol pripažinti ir kasdieninėje praktikoje rekomenduojami tik keli ankstyvajam krūties navikui gydyti svarbūs biologiniai žymenys, turintys patikimą prognozinę vertę. Vienas svarbiausių predikcinių krūties naviko žymenų yra ER, leidžiantis nustatyti ligos eigą ir numatyti atsaką į hormonų terapiją. PR yra taip pat plačiai praktikoje naudojamas žymuo, nors duomenų apie jo vertę sukaupta mažiau. Šias gretas papildė HER2 biožymuo, leidžiantis patikimai prognozuoti ligos eigą, bei svarbus skiriant terapiją trastuzumabu [45]. Siekiant pacientams parinkti tinkamiausią gydymą, farmacinių kompanijų kuriami antikūnai prieš naviką gydymui aprobuojami tik kartu naudojant klinikinį testą, skirtą nustatyti konkretaus biologinio žymens raišką [46]. Žinoma, kad Vakarų pasaulyje taikomas sisteminis pooperacinis gydymas leido sumažinti mirtingumą nuo krūties naviko [47]. Tačiau taip pat žinoma, kad nemažai daliai pacientų taikomas gydymas sutei-

kia labiau toksinį nei gydomąjį poveikį [48]. Nors epidemiologinių tyrimų rezultatai rodo, kad mirtingumas nuo krūties naviko mažėja, ši liga vis dar išlieka dažniausia mirties priežastimi tarp moterų, sergančių piktybiniais navikais [49]. Tai skatina ieškoti naujų diagnostikos ir gydymo galimybių bei naujų prognozinių veiksnių.

1.3.1 lentelė. *Krūties navikų tipai*

Krūties naviko tipas	Biologinių žymenų raiška
Luminalinis A	ER(+) ir/arba PR(+); HER2(–); Ki67 (<14 proc.)
Luminalinis B	ER(+) ir/arba PR(+); HER2(–); Ki67 (>14 proc.)
Luminalinis B HER2+	ER(+) ir/arba PR(+); HER2(+); Ki67 (bet koks)
HER2+	HER2(+); ER(–); PR(–)
Trejopai neigiamas	ER(–); PR(–); HER2(–)

MSC yra daugiaplanės mezenchiminės stromos ląstelės, kurios gali kilti iš kaulų čiulpų ar normalios krūties stromos. Įrodyta, kad iš kaulų čiulpų gauti MSC gali padidinti krūties vėžio kamieninių ląstelių (BCSC, angl. *breast cancer stem cells*) populiaciją, ekspresuojant IL-6 ir CXCL7 (pagrindinis trombocitų bazinis baltymas) [50]. CAF skatina vėžio, ypač krūties vėžio, progresavimą. CAF gali reguliuoti BCSC dėl tokių veiksnių kaip CCL2 (monocitų chemotaktinis baltymas-1), IL-6 ir IL-8 [51]. BCSC gali reguliuoti CAF per įvairius signalo perdavimo kelius. Wnt signalinis kelias susijęs su navikinių ląstelių metabolizmo pokyčiais. Transkripciniai pokyčiai, kuriuos sukelia Wnt, sukelia β-katenino stabilizavimą, kuris gali perprogramuoti navikinių ląstelių metabolizmą, pvz., padidindamas aerobinę glikolizę. ROS gamyba iš mitochondrijų kvėpavimo grandinės gali β-kateniną skatinti prisijungimą prie FOXO transkripcijos veiksnių. FOXO geno transkripcija suaktyvina genus, kurie kovoja su oksidaciniu stresu, todėl skatina ląstelių išgyvenimą [52]. Imuninės ląstelės, ypač TAM, yra glaudžiai susijusios su naviko dauginimusi. Naviko ląstelės gamina makrofagų kolonijas stimuliuojantį veiksnį, kad išplistų TAM, tuo tarpu TAM gamina TNFα ir TGFβ [53]. Sergant krūties vėžiu, TAM gali skatinti BCSC per parakrino EGFR / Stat3 / Sox-2 signalo perdavimo kelią [54]. Tuo tarpu hialurono rūgšties sintazės 2 reguliavimas CD44+/ CD24–/ESA+ BCSC gali sustiprinti sąveiką tarp BCSC ir TAM, todėl BCSC auga [55]. Kitos imuninės ląstelės, tokios kaip naviką infiltruojantys limfocitai (TIL, įskaitant CD4+, CD8+ ir FOXP3+ TILs), taip pat yra glaudžiai susijusios su BCSC fenotipais, terapiniu atsaku ir krūties vėžio prognoze [56]. Adipocitai yra pagrindinė krūties stromos sudedamoji dalis, teikianti protumorogeninius signalus, sergant krūties vėžiu [57]. Riebalinis audinys išskiria adipsiną, kad sustiprintų BCSC savybes [58]. Endotelio ląstelės yra būtinos

naviko angiogenezei, kuri svarbi maistinių medžiagų ir deguonies tiekimui naviko mikroaplinkoje. Taip pat endotelio ląstelės gali praturtinti CD44+/CD24 žymenimis krūties navikines ląsteles [59].

1.4. Varburgo efektas ir atvirkštinis Varburgo efektas

Oto Varburgas (Otto Warburg) 1924 m. nustatė pasikeitusį vėžinių ląstelių metabolizmą. Jis aprašė savo stebėjimus, kad vėžinės ląstelės pasižymi dideliu gliukozės sunaudojimo greičiu ir pieno rūgšties gamyba. Panaudodamas savo sukurtą manometrą, Varburgas su kolegomis atrado, kad vėžinės ląstelės nesunaudoja daugiau deguonies nei normalios ląstelės, net ir normoksijos sąlygomis, todėl atrodė, kad vėžinės ląstelės mieliau renkasi aerobinę glikolizę nei oksidacinį fosforilinimą. Varburgas iš pradžių teigė, kad vėžinės ląstelės pasižymi sutrikusiu kvėpavimu dėl mitochondrijų funkcijos sutrikimų. Vėliau buvo nustatyta, kad vėžinės ląstelės neatsisako ir oksidacinio fosforilinimo [60, 61]. Po daugiau nei pusės šimtmečio tyrinėjimų, Varburgo efektas patvirtintas daugumoje vėžinių ląstelių tipų, bet tikrosios priežastys, kodėl ląstelės pereina į anaerobinį gliukozės skaidymo kelią ir jo fiziologinė prasmė nėra pilnai suprantami. Manoma, kad Varburgo efektas gali suteikti vėžinėms ląstelėms privalumų dauginantis. Dėl nekontroliuojamo augimo vėžinių ląstelių metabolizmas, kaip ir visų besidauginančių ląstelių, turi būti pritaikytas tam, kad būtų palengvintas maistinių medžiagų įsisavinimas ir prijungimas į biomasę naujų ląstelių gaminimui (tai apima aminorūgščių bei baltymų sintezę, DNR dublikaciją ir biomembranų lipidų sintezę) [62]. Naujausi tyrimai parodė, kad vėžinių ląstelių mitochondrijos funkcionuoja gerai, o energijos gamybai svarbus tiek oksidacinis fosforilinimas, tiek anaerobinis kvėpavimas [63, 64]. Mikroaplinkos hipoksija ir tarpląsteliniai keliai, suaktyvinantys su hipoksija susijusį genų atsaką, vėžinių ląstelių metabolizmą perkelia į anaerobinius kelius [65, 66]. Daugeliu vėžio atvejų nustatytos metabolinių fermentų anomalijos ir mutacijos. Normaliuose audiniuose gliukozė virsta piruvatu ir pernešama į mitochondrijas oksidaciniam fosforilinimui (OXPHOS) Krebso cikle, arba OXPHOS yra reikalingi kvėpavimo substratai, kuriais gali būti piruvatas, malatas, glutamatas, sukcinatas ar kitas Krebso ciklo tarpinis metabolitas, kurio oksidacijos metu susidaro redukuoti kofermentai (NADH ir $FADH_2$) ir ADP.

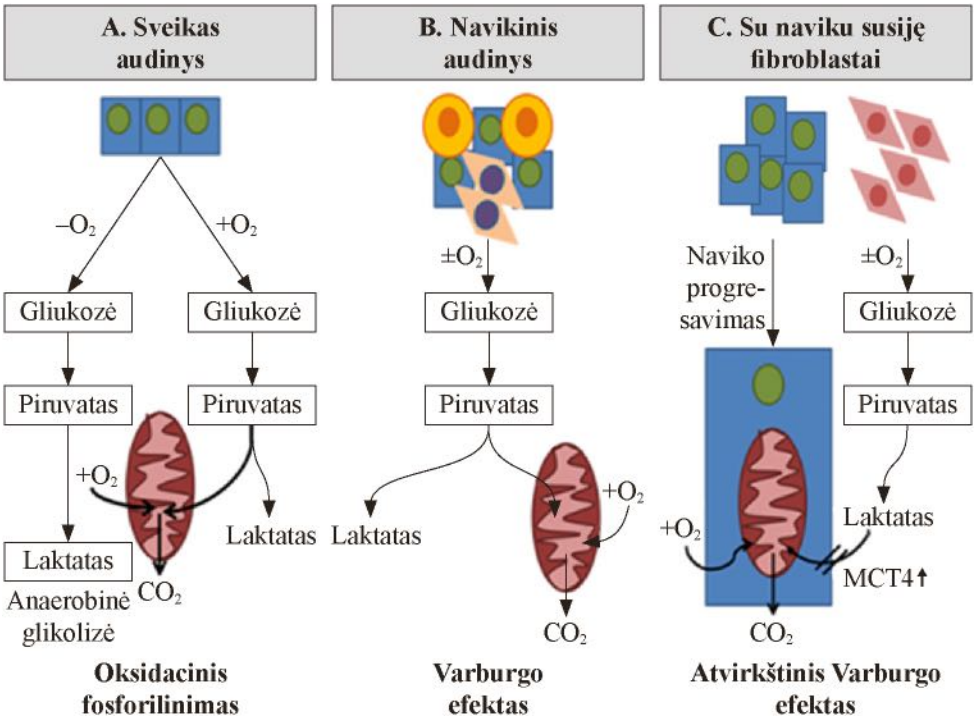

1.4.1 pav. *Varburgo efektas ir atvirkštinis Varburgo efektas*

(A) Sveikuose audiniuose gliukozė virsta piruvatu, kuris pernešamas į mitochondrijas oksidaciniam fosforilinimui. **(B)** Daugelis naviko rūšių dalyvauja glikolizėje, nepriklausomai nuo deguonies (aerobinė glikolizė arba Varburgo efektas). **(C)** Kai kurios vėžio ląstelės perprogramuoja su vėžiu susijusius fibroblastus, kad jie atliktų aerobinę glikolizę ir išskirtų daug energijos turinčias maistines medžiagas, kurios, patekusios į vėžio ląstelių mitochondrijas, dalyvautų oksidaciniame metabolizme. Adaptuota iš Paolicchi Elisa ir kt. [67]

Navikinėse ląstelėse glikolizė yra aktyvesnė nei sveikose, dėl ko susidaro didelis laktato kiekis. Aerobinės glikolizės reguliavimas susijęs su onkogeno aktyvacija. Manoma, kad beveik kiekvienas pagrindinis onkogenezę skatinantis onkogenas taip pat skatina padidėjusį gliukozės metabolizmą. Nustatyta, kad aktyvinančios BRAF, PTEN ir KRAS mutacijos aktyvina svarbiausių metabolinių fermentų transkripciją ir slopina bei perprogramuoja glutamino metabolizmą [68–70]. Stabilizavus hipoksijos sukeliama 1-alfa veiksnį (HIF1A), pastebima, kad vėžio ląstelės padidina glikolizę, kai nemaža dalis gliukozės virsta laktatu, o ne patenka į oksidacinį fosforilinimą, todėl susidaro rūgštinė mikroaplinka ir neefektyviai gaminamas ATP [71]. Gerai žinoma, kad šis pokytis yra svarbus išgyvenimui hipoksijos sąlygomis ir koreliuoja su vėžio kamieninių ląstelių (CSC, angl. *cancer stem cells*) susidarymu. Pavyzdžiui, plaučių vėžio ir leukemijos CSC turi mažą mitochondrijų DNR kiekį, oksidacinį fosforilinimą, deguonies sunaudojimo greitį, tarpląstelinį ATP ir

specifinius biožymenis (ALDH, CD24, CD44, CD133), atsakingus už jų susidarymą ir išgyvenimą [72]. Tačiau šie įrodymai neturėtų klaidinti dėl mitochondrijų vaidmens CSC. Buvo pastebėta, kad CSC dauginimasis ir išgyvenamumas priklauso nuo mitochondrijų biogenezės, o tai rodo, kad mitochondrijų metabolizmas, nors ir sumažėjęs, yra labai svarbus CSC išgyvenimui. Visų pirma, įrodyta, kad CSC yra priklausomi nuo oksidacinio fosforilinimo. Panaudojus ATP-sintazės inhibitorius, CSC paprastai žūva [72]. Reiškia mitochondrijų aktyvumo pokyčiai gali būti silpnoji vieta CSC [73]. Panaudojus labiau specifinius mitochondrijų inhibitorius, nustatyta, kad specifinis monokarboksilato transporterio (MCT) inhibitorius AR-C155858, kuris blokuoja mitochondrijų degalų, tokių kaip laktatas, įsisavinimą ląstelėse, galėtų veiksmingai sumažinti CSC susidarymą [74]. Tūkstančiai genų reguliuojamų laktatu, kartu gali sudaryti transkripcijos tinklą, susijusį su ląstelių perprogramavimu, įgalinant laktogenezę ir kancerogenezę [74–76]. Kai kurių navikų ląstelės nėra visiškai priklausomos nuo pagreitėjusios glikolizės. Įdomu tai, kad jie „maitinami“ aktyvinant normalias stromos ląsteles, supančias vėžio ląsteles [77]. HIF1A aktyvacija vyksta CAF, ir tai pagerina aerobinę glikolizę ir laktato gamybą, kuri paverčiama piruvatu ir naudojama mitochondrijų oksidacinį fosforilinimą navikinėse ląstelėse [78, 79]. Šis reiškinys buvo vadinamas „atvirkštiniu Varburgo efektu“, kuris rodo padidėjusią šalia vėžinių ląstelių esančių stromos CAF aerobinę glikolizę, išskiriančią daug energijos turinčias maistines medžiagas, kurios maitina navikinės ląsteles, sukeliančias naviko augimą ir piktybiškumą [80]. Šiam procesui taip pat būdingas kaveolino-1 molekulės, kuri atsakinga už HIF1A aktyvavimą stromos ląstelėse, praradimas ir padidėjęs MCT aktyvumas, ypač MCT4, kuris atsakingas už tiek energijos tiekimą, tiek viduląstelinį pH reguliavimą [81].

1.5. Krebso ciklas

Trikarboksirūgščių (TCA) arba citrinos rūgšties ciklas dar vadinamas Krebso ciklu. Hansas Krebsas pirmasis aprašė šį ciklą ir už tai 1953 m. buvo apdovanotas Nobelio medicinos premija. Krebso ciklas – tai pagrindinis metabolizmo kelias, vykstantis mitochondrijose, kur randami ir visi Krebso ciklo fermentai (1.5.1 pav.). Šio ciklo metu, oksidacijos ir redukcijos reakcijų metu potencinė energija elektronų forma perduodama elektronų nešikliams (kofermentams). Pagrindinis toks kofermentas yra nikotinamido adenino dinukleotidas (NAD^+). Piruvo rūgšties junginys ar riebalų rūgštys yra oksiduojamos, o kofermentai – redukuojami. Piruvo rūgštis, glikolizės produktas, negali tiesiogiai patekti į Krebso ciklą. Pereinamojoje reakcijoje iš piruvo rūgšties pašalinama viena CO_2 molekulė. Šis procesas vadinamas dekarboksilinimu.

Tada piruvo rūgšties molekulė tampa du anglies atomus turinčiu junginiu, vadinamu acetilo grupe. Ši grupė per aukštos energijos ryšį prisijungia prie kofermento A. Susidaręs junginys vadinamas acetil-KoA. Šios reakcijos metu piruvo rūgštis yra oksiduojama, o NAD^+ yra redukuojamas į NADH. Acetil-KoA reaguoja per pirmąją aštuonių reakcijų seką, apimančią Krebso ciklą. Jį sudaro NADH ir $FADH_2$ generuojančių reakcijų skaičius, kurias paeiliui galima panaudoti oksidacinio fosforilinimo keliu ATP susidarymui [82]. Riebalų rūgštys sintetinamos iš citozolio acetil-KoA, kuris pats iš dalies gaunamas iš citrinos rūgšties. Citrinos rūgštis yra kilusi iš TCA ciklo ir gabenama į citozolį. Riebalų rūgščių oksidacija vyksta mitochondrijose, gaunamas mitochondrijų acetil-KoA, kuris maitina TCA ciklą. Riebalų rūgštis iš citozolio į mitochondrijas perneša karnitino šaudyklė, ir jų atomai patenka į TCA ciklą.

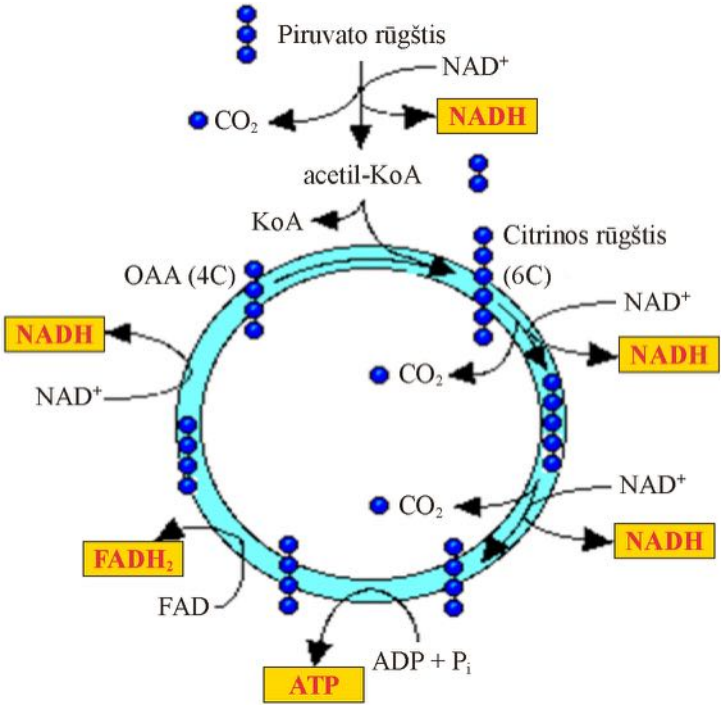

1.5.1 pav. *Krebso ciklas*

Adaptuota iš *http://americanboard.org/Subjects/general-science/cellular-energetics/*

1.6. Riebalų rūgščių sintezė ir oksidacija bei jų reguliavimo ypatumai

Riebalų rūgščių biosintezė yra svarbi ląstelių augimui, diferenciacijai ir homeostazei. Naviko ląstelių gyvybingumą ir proliferaciją veikia citozolinė FAS ir mitochondrinė FAO. FAS ir mitochondrinė FAO [83]. Neoplastinių audinių proliferacija, remiasi *de novo* FAS [84]. Nustatyta, kad riebalų rūgščių sintazės (FASN) genas yra prognozinis žymuo, sergant krūties [83], prostatos [85], kepenų [86] ir kitais epitelio navikais. ATP citrato liazė, kuri yra atsakinga už žinduolių ląstelių citozolinio acetil-KoA ir riebalų rūgščių sintezę, taip pat turi įtakos ląstelių transformacijai ir navikų formavimui. Slopinant acetil-KoA karboksilazę (ACC), kuri katalizuoja acetil-KoA virsmą į malonil-KoA ir yra reikalinga riebalų rūgščių biosintezei, galima sulėtinti naviko ląstelių dauginimąsi [87]. Padidėjusi onkogeninio Ras raiška yra susijusi su ilgesne riebalų rūgščių grandine [88]. Nesmulkialąsteliniuose plaučių vėžio audiniuose taip pat pastebėta ilgesnė riebalų rūgščių grandinė [89]. Genų raiškos metaanalizė, kurios metu genai buvo suskirstyti į grupes ir sudarė metabolinius tinklus [90], parodė, kad metabolinių tinklų, susijusių su riebalų rūgščių sinteze ir pailgėjimu, raiška teigiamai koreliuoja su ląstelių proliferacijos greičiu (naudojant NCI-60 duomenų kolekciją) ir neigiamai koreliavo su storosios žarnos vėžiu sergančių pacientų išgyvenimo prognozėmis. Įdomu tai, kad tas pats buvo pastebėtas metabolinių potinklių, susijusių su riebalų rūgščių skilimu ir β-oksidacija, metu. Šie stebėjimai lėmė hipotezę, kad abu reiškiniai egzistuoja tose pačiose ląstelėse.

FAO įtaka vėžio ląstelių gyvybingumui ir dauginimuisi pritraukia vis didesnį dėmesį [91]. Nustatyta, kad FAO slopina leukemijos ląstelių apoptozę [13]. Įrodyta, kad peroksisomos proliferatoriaus aktyvinti receptoriai (PPAR) skatina FAO, o tai savo ruožtu skatina ATP gamybą ir apsaugo vėžio ląsteles nuo apoptozės, kurią sukelia sukibimo su tarpląsteliniu užpildu praradimas [92].

Karnitino palmitoiltransferazė 1C (CPT1C) dalyvauja citozolinių riebalų rūgščių pernešime iš citozolio į mitochondrijas, kur vyksta riebalų rūgščių oksidacija [93]. CPT1C yra nustatytas kaip onkogenas [94, 95]. Manoma, kad dėl malonil-KoA, kuris yra FAS tarpinis produktas, slopinamų CPT1 baltymų vienu metu negali vykti FAS ir FAO. Malonil-KoA gali gaminti du fermentai – ACC1 ir ACC2 [96]. ACC2 gaminamas malonil-KoA slopina CPT1 baltymus ir todėl blokuoja riebalų rūgščių pernešimą į mitochondrijas ir jo vėlesnę β oksidaciją. Tuo tarpu ACC1 gaminamas malonil-KoA neslopina CPT1 baltymų [97]. Tikriausiai taip yra todėl, kad malonil-KoA tiesiogiai iš ACC1 nukreipiamas į FASN, neišlaisvinant citozolyje.

FASN – riebalų rūgščių sintazė yra daugelio fermentų baltymas, katalizuojantis FAS. Pagrindinė jo funkcija yra katalizuoti palmitato sintezę iš acetil-KoA ir malonil-KoA, panaudojant NADPH. Bendras skirtingų navikų, tokių kaip kolorektalinis [98], kiaušidžių [99], krūties [100], prostatos [101], minkštųjų audinių sarkomos [102], gliomų [103] ir melanomos [104] bruožas yra per didelė FASN raiška. FASN geno slopinimas turi įtakos NADPH kaupimuisi. Aktyvuojama NADPH oksidazė slopina AMP-aktyvuoto baltymo kinazę, kuri atlieka svarbų vaidmenį, koordinuojant įvairius metabolizmo kelius. Perteklinis NADPH substrato kiekis dėl FASN slopinimo skatina NADPH oksidazę generuoti aktyvią deguonies formą (ROS, angl. *reactive oxygen species*) ir yra susijęs su apoptozės indukcija [105-107].

Trumposios grandinės enoil-KoA hidratazė 1 (ECHS1, angl. *enoyl-CoA hydratase, short chain 1*) mitochondrijose katalizuoja antrąjį FAS etapą ir dalyvauja valino, leucino ir izoleucino metabolizme [108, 109].

ME dalyvauja piruvato metabolizme ir anglies atomų fiksavime. Jis katalizuoja reakciją, kurios metu gaminamas NADPH, kuris yra būtinas vėžio ląstelių augimui, palaikant redokso pusiausvyrą ir biosintezės procesus citoplazmoje [110]. ME1 aktyvumas priklauso nuo NADP, ir jis atlieka svarbų vaidmenį lipidų sintezėje ir riebalų rūgščių desaturacijoje [111]. Sergant kepenų ląstelių karcinoma, padidėja ME1 raiška ir sumažėja bendras išgyvenamumas, lyginant su normaliu ME1 lygiu [110]. ME1 raiška koreliuoja su ligos progresavimu, diferenciacija ir trumpesniu išgyvenimo laiku.

1.7. Oksidacinis stresas, aktyviosios deguonies formos

Oksidacinis stresas – tai organizmo būsena, kai sutrinka biocheminė pusiausvyra, padidėja laisvųjų radikalų gamyba arba sutrinka jų neutralizacija ir dėl to vyksta ląstelių bei audinių pažeidimas. Laisvieji radikalai – tai molekulės, turinčios neporinį elektroną, todėl tai nestabilios molekulės, atakuojančios kitas molekules ir prisijungiančios elektroną. Molekulė yra stabili tik tuomet, jeigu turi porinį elektronų skaičių. Laisvieji radikalai pažeidžia ląstelės membranos lipidus ir fermentus, baltymus, ląstelės branduolio membraną, DNR. Nors fiziologinės koncentracijos yra nepaprastai svarbios užtikrinant ląstelių išgyvenimą, ROS perteklius daro žalą ląstelėms ir yra laikomas pagrindiniu vystymosi veiksniu tokių ligų, kaip navikai [112], neurodegeneracinės ligos bei širdies ir kraujagyslių sistemos sutrikimai [113]. ROS yra normalios ląstelių apykaitos produktai ir vaidina gyvybiškai svarbų vaidmenį stimuliuojant signalinius kelius ląstelėse, reaguojant tarpląstelinės aplinkos sąlygų pokyčius. Daugiausia ROS ląstelėse sukuria mitochondrijų kvėpavimo grandinė. Endogeninių metabolinių reakcijų metu aerobinėmis sąlygomis

ląstelės gamina ROS, tokias kaip superoksido anijonas (O_2^-), vandenilio peroksidas (H_2O_2), hidroksilo radikalas (OH•) ir organiniai peroksidai, kaip normalūs biologinio molekulinio deguonies redukcijos produktai. Elektronų perkėlimas į molekulinį deguonį vyksta kvėpavimo grandinės lygyje, o elektronų pernešimo grandinės yra mitochondrijų membranose. Hipoksijos sąlygomis mitochondrijų kvėpavimo grandinė taip pat gamina azoto oksidą (NO), kuris gali suaktyvinti malondialdehido raišką sukeldamas per didelę lipidų peroksidaciją.

1.8. Mitochondrijų membranos potencialas

Eukariotiniuose organizmuose pagrindinė naudojamos energijos forma yra ATP ryšyje sukaupta energija. Pagrindinė dalis viso ląstelėse gaminamo ATP susidaro oksidacinio fosforilinimo būdu, kuris vyksta mitochondrijose. ATP ląstelėse yra ne tik pagrindinė energijos forma, tačiau jis reikalingas ir baltymų fosforilinimo reakcijoms, kurių pagalba yra keičiamas daugybės biologinių sistemų aktyvumas. Be to gali tiesiogiai dalyvauti signalo perdavime keisdamas keleto tipų jonų kanalų aktyvumą. Krebso ciklo metu susidarę redukuoti NADH ir $FADH_2$ perduoda elektronus galutiniam akceptoriui O_2 per elektronų transporto grandinę – vyksta oksidacija. Elektronų transporto grandinė sudaryta iš keturių baltymų kompleksų, kurie yra įsitvirtinę vidinėje mitochondrijų membranoje (1.8.1 pav.). Tai vadinamieji kvėpavimo grandinės kompleksai: NADH dehidrogenazė; sukcinato dehidrogenazė, citochromo C oksido reduktazė ir citochromo oksidazė. NADH ir $FADH_2$ yra oksiduojama, kadangi atiduoda savo elektronus, o tuo pačiu iš mitochondrijų užpildo į tarpmembraninę erdvę yra išstumiami H^+. Protonų išmetimą vykdo trys grandinės kompleksai. Išstumtų į tarpmembraninę erdvę protonų koncentracija čia yra žymiai didesnė nei užpilde. Labai svarbų vaidmenį vaidina vidinė mitochondrijų membrana – dėl mažo jos laidumo susiformuoja elektrocheminis H^+ gradientas skirtingose membranos pusėse. Protonai į užpildą sugrįžta tik per ATP sintazę, kuri panaudoja protonų gradiento energiją ADP fosforilinimui iki ATP. Protonų gradientas tarnauja kaip kuras ATP sintazei. Tuo būdu redukuotų kofermentų NADH ir $FADH_2$ oksidacija yra glaudžiai susijusi su ADP fosforilinimu, todėl šis kompleksinis procesas vadinamas oksidaciniu fosforilinimu. Mitochondrijų membranos potencialo ir ATP lygiai ląstelėje palaikomi gana stabilūs, nors abiejų šių veiksnių svyravimai gali būti riboti, atsižvelgiant į normalų fiziologinį aktyvumą. Ilgalaikis mitochondrijų membranos potencialo normalaus lygio sumažėjimas ar padidėjimas gali sukelti nepageidaujamą ląstelių gyvybingumo praradimą ir būti įvairių patologijų priežastimi. Be kitų veiksnių, mitochondrijų membranos

potencialas vaidina pagrindinį vaidmenį mitochondrijų homeostazėje selektyviai pašalinant disfunkcines mitochondrijas. Tai taip pat yra jonų (išskyrus H^+) ir baltymų, reikalingų sveikam mitochondrijų funkcionavimui, pernešimo jėga [114, 115].

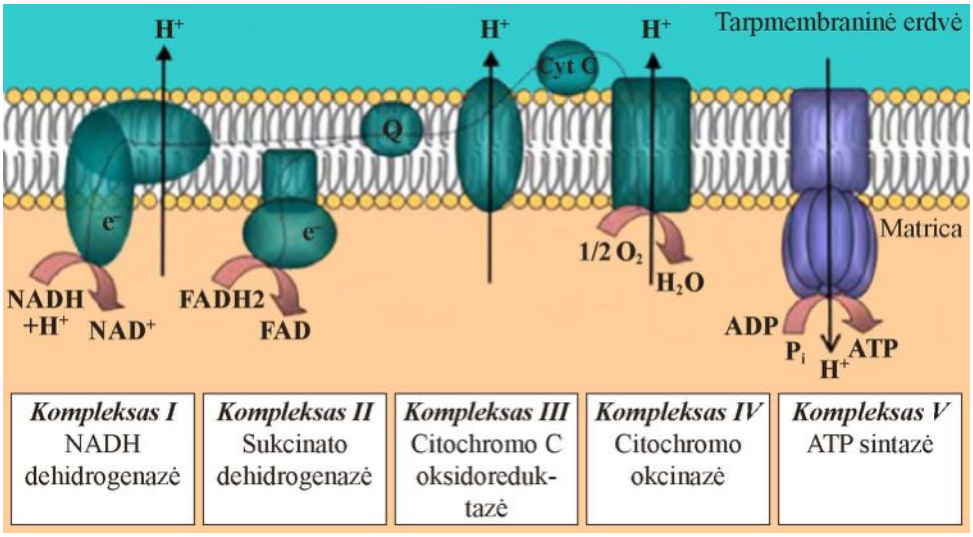

1.8.1 pav. *Mitochondrijų kvėpavimo grandinė*

Oksidacinio fosforilinimo sistemą sudaro keturi kvėpavimo grandinės kompleksai (I–IV kompleksai) ir du tarpiniai substratai (kofermentas Q ir citochromas c). Tarpinio metabolizmo metu gaminami $NADH^+$, H^+ ir $FADH_2$ toliau oksiduojami mitochondrijų kvėpavimo grandinėje, kad būtų sukurtas elektrocheminis protonų gradientas, kurį ATP sintazė (V kompleksas) galiausiai panaudoja ATP sintezei. Paveikslėlis adaptuotas pagal Bellance Nadege ir kt. [116].

1.9. Šakotosios grandinės aminorūgštys

Šakotosios grandinės aminorūgštys (BCAA) – leucinas, izoleucinas ir valinas – yra nepakeičiamos aminorūgštys. Ląstelėse BCAA yra tiesiogiai inkorporuojamos į baltymus arba metabolizuojamos. BCAT katalizuojant, BCAA amino grupė virsta į α-ketogrupę, gauname glutamatą ir šakotosios grandinės α-ketorūgštį (BCKA). BCKA oksiduojama ir paverčiama į galutinius produktus (acetil-KoA ir sukcinil-KoA), dalyvaujančius TCA cikle (1.9.1 pav.) [117].

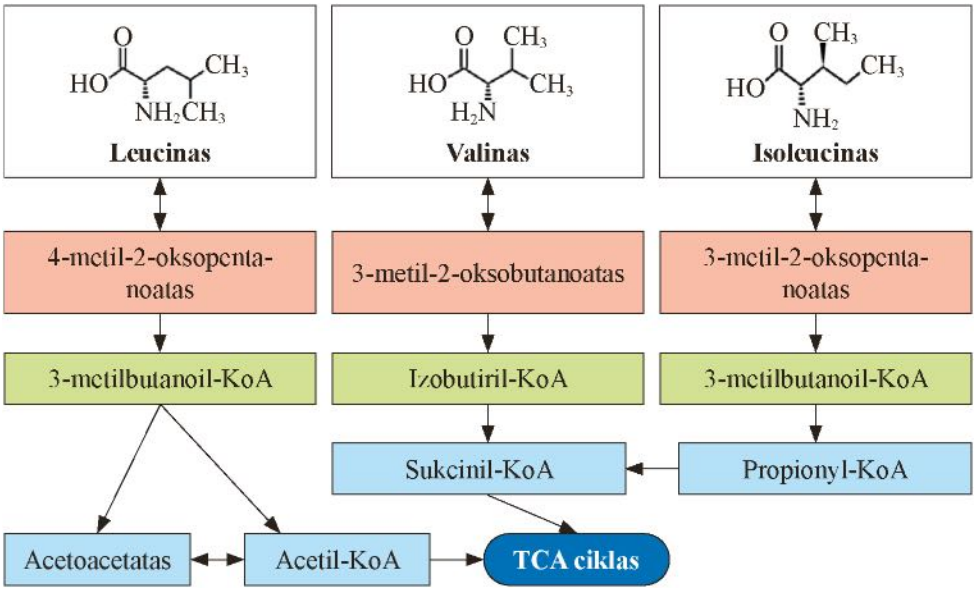

1.9.1 pav. *Pagrindiniai BCAA katabolizmo žingsniai*

BCAA katabolinės reakcijos katalizuojamos fermentų, o galutiniai produktai patenka į TCA ciklą. Adaptuota pagal Nie ir kt. [118].

Aminotransferazės katalizuoja α-amino grupės pernešimą iš aminorūgšties į 2-ketoglutaratą, kad susidarytų glutamatas. Šie fermentai reguliuoja glutamato susidarymą iš daugelio aminorūgščių. Alanino aminotransferazė (ALT) alanino amino grupę paverčia į 2-ketoglutaratą, o aspartato aminotransferazė (AST) – aspartato amino grupę į 2-ketoglutaratą, abiem atvejais pagaminamas glutamatas. Tuo pačiu metu alanino aminotransferazė formuoja piruvatą, o aspartato aminotransferazė – oksaloacetatą:

L-aspartatas + α-ketoglutaratas ⇌ oksaloacetatas + L-glutamatas
L-alaninas + α-ketoglutaratas ⇌ piruvatas + glutamatas

BCAT katalizuoja BCAA ir α-ketoglutarato konversiją į BCKA ir glutamatą. Tokiu būdu dauguma aminorūgščių gali virsti BCAA per transaminimo reakcijas [117].

α-ketorūgštis + glutamatas ⇌ α-ketoglutaratas + BCAA

BCAA yra būtinas naviko augimui ir gali veikti kaip mTORC1 agonistas blokuodamas baltymų sintezę ir tapdamas azoto (neesminėms aminorūgštims ir nukleotidų biosintezei) ir anglies (TCA ciklui ir energijos gamybai) šaltiniu [119].

1.10. Bioinformacinių metodų taikymas onkologijoje

Bioinformatika naudoja pažangius kompiuterinius metodus ir technologines platformas duomenų saugojimui, valdymui, analizavimui ir interpretavimui. Biomedicininių tyrimų metu surinktų biologinių duomenų kiekis iš esmės išaugo dėl galingų naujų tyrimų technologijų. Šių duomenų prieinamumas ir jų įžvalgos apie ligos biologiją veda prie tiksliosios medicinos: prevencijos, diagnozavimo ir gydymo, atsižvelgiant į paciento ligos molekulines savybės. Niekur šis iššūkis nėra akivaizdesnis nei onkologijoje, nes didžioji dalis visų duomenų yra gaunama iš navikais sergančių pacientų. Norint paspartinti pažangą, vėžio tyrėjams reikia prieigos prie daugelio skirtingų institucijų kuruojamų duomenų bazių. Bioinformatikos tikslas yra sukurti infrastruktūrą, kuri padėtų tyrėjams saugoti, analizuoti, integruoti, pasiekti ir vizualizuoti didelius biologinių duomenų ir susijusios informacijos kiekius. Šiuo metu tyrėjai naudoja daugybę skirtingų įrankių ir platformų biologiniams duomenims saugoti ir analizuoti, įskaitant viso genomo sekoskaitą, pažangiąją vaizdų analizę, išsamią biologinių mėginių baltymų analizę ir klinikinius duomenis. Dažnai sunku integruoti ir analizuoti šių įvairių platformų duomenis. Be to, tyrėjai dažnai neturi prieigos prie kitų studijų pirminių duomenų arba jiems trūksta kompiuterinių pajėgumų. Pastaraisiais metais virtualios saugyklos pagerino prieigą prie tyrimų duomenų, tačiau daugelis šių pastangų vis dar yra pradiniame etape (*https://www.cancer.gov/research/ncirole/bioinformatics*).

1.11. Genomo apimties metaboliniai modeliai (GSMM)

Gerai žinoma, kad navikinių ląstelių metabolizmas skiriasi nuo normalių ląstelių metabolizmo. Vanderio Heideno apžvalgoje [120] pabrėžiama, kad šiuo metu yra apie 30 metabolinių fermentų, kurie gali būti tinkamais priešvėžinių vaistų taikiniais skirtinguose vėžio vystymosi etapuose. Tai susiję su medžiagų apykaitos procesais, tokiais kaip nukleorūgščių sintezė, aminorūgščių metabolizmas, lipidų sintezė, glikolizė, TCA ciklas ir kt. Naudojant priešvėžinius vaistus, didelė žala padaroma sveikoms ląstelėms, atsakingoms už normalų atsinaujinimo procesą, todėl svarbu kurti medžiagas, selektyviai veikiančias navikines ląsteles. Skirtingų pacientų atsakas į tuos pačius vaistus gali būti labai skirtingas, todėl individualizuota medicina tampa nauju tikslu. Dažnai skirtingais medžiagų apykaitos keliais galima gauti tą patį galutinį metabolinį produktą. Tačiau nepageidaujamų šalutinių poveikių sveikoms ląstelėms būtų galima išvengti, nustačius, kurie metaboliniai apykaitos keliai tam tikram galutiniam produktui pasiekti sveikose ląstelėse yra dubliuojami, o navikinėse nedubliuojami. Norimo efekto galima nepasiekti, jeigu yra keli

metaboliniai keliai, o blokuojamas tik vienas. Metabolizmas yra labiausiai žinomas biologinis tinklas, o metabolinių terapinių langų radimo problemą galima išspręsti naudojant GSMM. GSMM [121, 122] yra pilnas metabolinių reakcijų, vykstančių tam tikrame organizme, rinkinys. Kiekvieną reakciją katalizuoja vienas ar keli fermentai, kiekvienas iš jų koduojamas genu. Taigi egzistuoja tiesioginis ryšys genas-baltymas-reakcija. Metabolinio tinklo struktūrą gali atspindėti jo stechiometrinė matrica su kiekvienos reakcijos metabolitų stechiometriniais koeficientais. Darant prielaidą, kad kiekvieno metabolito koncentracija yra nusistovėjusi, galima apibūdinti tikėtinus srautų pasiskirstymus ir įvertinti ląstelės metabolinius pajėgumus. GSMM gali būti naudojami metabolinių srautų pasiskirstymams apskaičiuoti, naudojant linijinį programavimą. Šiam skaičiavimui reikia nustatyti viršutinę ir apatinę kiekvieno metabolinio srauto ribą, taip pat pasirinkti objektyvią maksimizuojamą funkciją. Ši funkcija paprastai pasirenkama, kaip biomasės gamyba, kuri modeliuose vaizduojama kaip biomasės stechiometrinė lygtis, apimanti biomasės vienetą sudarančių makromolekulių proporcijas. Vanderis Heidenas savo apžvalgoje teigia, kad vėžio ląstelių metabolinio tinklo srautų nustatymas gali padėti surasti sėkmingus fermentinius taikinius. Dabartinius metabolinių srautų pasiskirstymo matavimo metodus, tokius, kaip ^{13}C pažymėtų substratų panaudojimas, apriboja santykinai nedidelis centrinio anglies metabolizmo srautų skaičius. Eksperimentiškai išmatuoti srautai gali būti naudojami nustatant GSMM parametrus, kad būtų galima gauti ir srautų, kurie tiesiogiai neišmatuoti, apskaičiavimus (vidurkius ir standartinius nuokrypius) [123]. Tačiau tiesioginiai ar netiesioginiai metabolinių srautų matavimai yra brangesni, ilgiau trunka ir yra mažiau išsamūs, negu kai kurie kiti didelio našumo eksperimentiniai metodai, tokie kaip RNR sekvenavimas – RNA-seq. Neseniai sukurtas didelio našumo vienos ląstelės RNR-seq metodas [124] leidžia greitai nustatyti skirtingų navikų ląstelių populiacijų genų raiškos profilius. Dėl šių priežasčių mes siekėme sukurti kompiuterinį metodą, kuris leistų rasti personalizuotus terapinius langus naudojant GSMM ir RNR-seq duomenis.

2. TYRIMŲ METODIKA

2.1. Ląstelių išskyrimas

Tirtos išskirtos iš operacinės medžiagos krūties vėžio ląstelės. Aprašyti krūties navikų histologiniai tipai bei ER, PR, HER2 ir Ki-67 raiška. Duomenys gauti iš pacientų medicinos dokumentų išrašų.

Leidimą atlikti tyrimą išdavė Kauno regioninis biomedicininių tyrimų etikos komitetas (leidimo Nr. P2-137/2006; išdavimo data: 2017 m. gruodžio 8 d.).

2.1.1 lentelė. *Navikų histopatologiniai tipai ir žymenų raiška*

Išskirta ląstelių kultūra	Histopatologinis naviko tipas	ER raiška	PR raiška	HER2 raiška
BC1	Infiltracinė lobulinė karcinoma	+	+	–
BC2	Infiltracinė duktalinė karcinoma	+	+	–
BC4	Infiltracinė duktalinė karcinoma	+	+	+
BC5	Infiltracinė duktalinė karcinoma	–	–	+
BC6	Infiltracinė duktalinė karcinoma	+	+	–

Operacijos metu gauti audiniai sudėti į lėkštutę, užpilti 2 ml fosfatinio buferio druskos tirpalo (PBS) ir susmulkinti žirklutėmis. BC4 ir BC5 mėginiai tuomet užpilti 1 ml 0,025 proc. tripsino tirpalo ir perkelti į 15 ml mėgintuvėlį. Mėginiai 60 min. laikyti kratytuve (37 °C, 350 rpm), po to 5 min. centrifuguoti (420 × g). Supernatantas nupilamas, o likusi medžiaga perkeliama į flakonėlį ir užpilama 4 ml auginimo terpės, paruoštos iš DMEM (Dulbeko modifikuota Eaglo terpė, Sigma) ir 10 proc. FJS (fetalinio jaučio serumo, Sigma).

BC2 ir BC6 mėginiai apdoroti tripsinu (0,025 proc.) ir III tipo kolagenaze (150 U/ml). Abu mėginiai, juos susmulkinus, padalinti į du mėgintuvėlius ir centrifuguoti 5 min. (420 × g). Supernatantas nupiltas, o ant likusios medžiagos užpilta 1 ml tripsino arba III tipo kolagenazės tirpalo. Mėginiai tuomet 60-čiai min. perkelti į kratytuvą (37 °C, 350 rpm), tada 5 min. centrifuguoti (420 × g). Supernatantas nupilamas, o likusi medžiaga perkeliama į lėkštutę ir užpilama 4 ml DMEM/Ham's F12 terpės, papildytos 10 proc. FJS. Ląsteles pavyko išskirti iš mėginių, apdorotų abiejų fermentų tirpalais.

BC1 mėginys apdorotas šiais fermentais: tripsino (0,05 proc.) tirpalu (1 atvejis), III tipo kolagenazės (125 U/ml) ir proteinazės K (8 U/ml) tirpalu (2 atvejis) arba III tipo kolagenazės (125 U/ml) ir hialuronidazės IV-S (408U/ml) tirpalu (3 atvejis). Susmulkintas mėginys iš pradžių padalintas į

tris mėgintuvėlius ir 5 min. centrifuguotas (420 × g). Supernatantas nupilamas, o ant likusios medžiagos užpilama skirtingi fermentų tirpalai (po 1 ml). Mėgintuvėliai tada perkeliami į kratytuvą (60 min., 37 °C, 350 rpm). Fermentų tirpalai nupilami, o ant likusios medžiagos užpilama po 1 ml PBS (pirmu ir trečiu atveju) arba, antru atveju, 1 ml III tipo kolagenazės tirpalo (125 U/ml). Mėgintuvėliai vėl 60-čiai min. perkelti į kratytuvą (37 °C, 350 rpm). Mėginiai 10 min. centrifuguoti (420 × g), supernatantas nupilamas, o mėgintuvėlyje likusi medžiaga perkeliama į lėkštelę ir užpilama 4 ml DMEM/Ham's F12 terpės, papildytos 10 proc. FJS. Ląsteles pavyko išskirti iš audinio, apdoroto 0,05 proc. tripsino tirpalu (1 atvejis).

Pirmines ląstelių kultūros išskirtos iš mėginių, apdorotų 0,025 proc. tripsino tirpalu, 0,05 proc. tripsino tirpalu arba III tipo kolagenazės tirpalu (150 U/ml).

Tolimesniems eksperimentams buvo naudojamos BC4 ląstelės (infiltracinė duktalinė karcinoma ER(+) PER(+) HER2(+)), kuri toliau vadinama, kaip BCC ląstelių linija.

2.2. Ląstelių saugojimas užšaldant

Nuo ląstelių nupilama terpė, jos du kartus nuplaunamos PBS ir atlipinamos 0,05 proc. tripsino tirpalu. Tuomet ląstelės perkeliamos į mėgintuvėlį ir centrifuguojamos 5 min. 420 × g. Supernatantas nupilamas ir ląstelės užpilamos 1 ml šaldymo terpės, kurią sudaro DMEM/Ham's F12, 15 proc. FJS ir 10 proc. dimetilsulfoksido. Ląstelės suspenduojamos šaldymo terpėje ir suspensija perkeliama į kriomėgintuvėlį, kuris laikomas –20 °C ir, susidarius ledo kristalams, perkeliamas į –80 °C.

2.3. Ląstelių kultivavimas

Krūties vėžinės ląstelės BCC ir MCF-7 (žmogaus krūties adenokarcinomos ląstelių linija; CLS-Cell Lines Service, Eppelheim, Vokietija) auginamos DMEM/Ham's F12 terpėje, papildytoje 10 proc. FJS ir 1 proc. penicilino / streptomicino (100 U/ml). Žmogaus kvėpavimo takų lygiųjų raumenų ląstelės (ASMC) maloniai dovanotos prof. R. Gosens, Groningeno universitetas, Nyderlandai [125]. ASMC buvo auginamos DMEM terpėje, kurioje yra 10 proc. FJS ir penicilino/streptomicino mišinio (100 U/ml). MCF-10A ląstelės (ATCC, Wesel, Vokietija) buvo auginamos DMEM / F-12 terpėje, papildytoje 5 proc. arklio serumu (GE Healthcare Life Sciences, Logan, JAV), 20 ng/ml EGF (Life Technologies, Carlsbad, CA). JAV), 10 μg/ml insulino („Life Technologies", Carlsbad, CA, JAV), 0,5 μg/ml hidrokortizono ir

100 ng/ml choleros toksino bei penicilino/streptomicino mišinio. Ląstelės laikomos inkubatoriuje („Binder“), drėgnoje aplinkoje, palaikant 37 °C temperatūrą ir 5 proc. CO_2 dujų koncentraciją. Ląstelių monosluoksniui padengus apie 70 proc. indo dugno ploto, jos persėjamos. Nuo ląstelių nupilama ląstelių kultūrų auginimo terpė. Ląstelės du kartus nuplaunamos naudojant PBS ir atlipinamos 0,05 proc. tripsino tirpalu 5 min. inkubuojant 37 °C temperatūroje. Atlipusios ląstelės užpilamos šviežia auginimo terpe ir 1/5 ląstelių suspensijos perkeliama į naujus auginimo indelius.

2.4. Ląstelių proliferacijos tyrimas tripano mėlio testu

Ląstelės $1{,}5 \times 10^4$ buvo sėjamos į 6 šulinėlių plokšteles. Ląstelės papildytos skirtingos koncentracijos (20, 50, 100 μM) Amb19149142 junginiu (GreenPharma, Prancūzija), kuris buvo ištirpintas 0,1 proc. etanolyje. Į mėgintuvėlį su 50 μl ląstelių suspensijos pridedama 50 μl 0,4 proc. tripano mėlio dažų, ištirpintų fiziologiniame tirpale (Life Technologies, Carlsbad, CA, JAV). 10 μl ląstelių suspensijos su dažais pernešama su pipete į hemocitometro kamerą (Neubauer), (Sigma-Aldrich, Steinheim, Vokietija). Matavimai atlikti po 120 val.

2.5. siRNR transfekcija

Genų slopinimas su siRNR buvo atliekamas pagal standartinę gamintojo nustatytą procedūrą, naudojant Jet Prime reagentą („Polyplus-transfection® SA“, Prancūzija). Buvo naudojamos galutinės 10 nM ECHS1 siRNR (ATGATGTGTGATATCATCTAT; Qiagen, Germantown, MD, JAV), FASN siRNR (CAGGCTTCAGCTCAACGGGAA; Qiagen) arba 5 nM BCAT2 siRNR (5′-CCAUGAACAUCUUUGUCU; Invitrogen, USA) koncentracijos. Ląstelės tuo pačiu metu buvo transfekuotos trimis skirtingais siRNR prieš skirtingus malato dehidrogenazės (ME1, ME2 ir ME3) genus: 4 nM ME1 (UGCCAUGACUCAGCGUUCtt; Ambion, Waltham, MA, JAV), 4 nM ME2 (GGGUGUCUAUGGAAUGGGAtt; Ambion) ir 4 nM (GCCUUUACCCUUGAAGAAAtt; Ambion). Visos šios procedūros buvo atliktos 24 val. po siRNR transfekcijos. Kaip kontrolė buvo naudojama mėginio transfekcija.

2.6. Metabolitų žymėjimas izotopine anglimi

Ląstelės buvo inkubuotos DMEM be gliukozės, L-glutamino ir piruvatų (Sigma, Schnelldorf, Vokietija), papildytos 10 proc. FJS ir antibiotikais. Į galutinę 4 mM koncentraciją buvo pridėta L-glutamino-$^{13}C_5$ (Aldrich, Hamburgas, Vokietija). Ląstelės buvo inkubuojamos 24 val.

MS metabolitų, žymėtų su L-glutamino-$^{13}C_5$ (Aldrich, cat# 605166), analizė buvo atliekama tandeminiu masės spektrometru Waters Acquity, ląstelių mėginiai buvo ruošiami pagal protokolą [126]. Gauti masės spektrai buvo naudojami metabolinių srautų pasiskirstymo nustatymui naudojantis elementarių metabolinių vienetų (EMU) metodu [127]. Tai buvo atlikta pasitelkiant programavimą Python kalba [128].

2.7. Metabolinio srauto pasiskirstymas

Metabolinio srauto pasiskirstymui naudojome EMU sistemą [127]. Modelyje buvo nurodyti septyni nepriklausomų reakcijų greičiai. Viena iš jų – piruvato dehidrogenazė (PDH) – buvo nustatyta ties 1, o visos kitos reakcijos buvo palygintos su PDH kiekiu. Likusios nepriklausomos reakcijos buvo riebalų rūgščių oksidacijos greitis, malato dehidrogenazė, α-ketoglutarato susidarymas gautas iš glutaminolizės, α-ketoglutarato karboksilinimo, piruvato karboksilazės ir piruvato importo į mitochondrijas. Visas žymėto malato ir citrato masės dalis išmatavome nuo M0 iki M6 ir sumažinome santykinių skirtumų kvadratinę sumą tarp modelio ir eksperimentinių rezultatų. Mažiausia pavienė reikšmė, lygi nuliui, reikštų, kad yra daug skirtingų metabolinio srauto paskirstymų, kurie lemia tuos pačius ženklinimo modelius, todėl sistemos negalima nustatyti. Siekiant įvertinti kiekvieno metabolinio srauto indėlį į sistemos identifikuojamumą, buvo apskaičiuotos naujos Jacobo matricos, atimant stulpelį, atitinkantį patikrintą metabolinio srauto kitimą, ir atliekant naujos matricos pavienių reikšmių skilimą. Kuo didesnė buvo nauja mažiausia išimtinė reikšmė, tuo sunkiau buvo nustatyti atimtą reikšmę. FAO (pats įdomiausias šiame darbe) buvo sunkiausiai nustatomas. Norėdami išvengti šios problemos, mes atlikome visuotinį eksperimentų, atitinkančių maketų transfekciją ir FASN bei ECHS1 nutildymą, optimizavimą. Šis požiūris grindžiamas prielaida, kad siRNA neturi įtakos visiems nepriklausomiems efektams, išskyrus FAO. α-ketoglutarato karboksilinimo greitis taip pat leido pakeisti mūsų sąlygas, nes šis metabolinio srauto kitimas yra labai jautrus mažiems α-ketoglutarato ir citrinos rūgšties koncentracijų pokyčiams. Reikšmių, atitinkančių ME nutildymą, nustatymas buvo atliekamas, fiksuojant FAO rodiklį ir leidžiant pakeisti visus kitus priedus. Po gydymo staurosporinu buvo paskirstymas, leidžiantis pasikeisti visoms nepriklausomoms

reakcijoms. Kiekvienam apipavidalinimui visų metabolinio srauto reikšmių vertės buvo paeiliui padidintos arba sumažintos 0,001 (neleidžiant joms imti neigiamų verčių). Jei šis padidėjimas lėmė tikslumo funkcijos sumažėjimą, naujos vertės buvo laikomos ir procesas kartojamas. Buvo naudojami skirtingi pradiniai dydžių pasiskirstymo rinkiniai ir išlaikymas, nustatantis mažiausią santykinę paklaidą.

2.8. Skysčių chromatografija - masių spektrometrija (UPLC-ESI-MS)

Masių spektometrinė (MS) metabolitų, izotopiškai žymėtų naudojant L-glutaminą-$^{13}C_5$, analizė buvo atliekama tandeminiu masių spektrometru. Organinių rūgščių atskyrimas mėginiuose buvo atliktas naudojant Acquity H klasės UPLC sistemą (Waters, Milford, MA, JAV) su YMC-Triart C18 (100 × 2,0 mm, 1,9 μm) kolonėle (YMC, Kiotas, Japonija). MS duomenims gauti buvo naudojamas trigubo kvadrupolio tandemo masės spektrometras Xevo TQD (Waters, Milford, MA, JAV) su elektropurškimo jonizacijos (ESI) šaltiniu. Kolonėlės temperatūra buvo palaikoma 40 °C. Gradiento eliuavimas buvo atliekamas su judančiąja faze, susidedančia iš 0,1 proc. skruzdžių rūgšties vandens tirpalo (tirpiklio A) ir acetonitrilo (tirpiklio B), kai oro srauto greitis buvo nustatytas 0,4 ml/min. Pradinės sąlygos buvo nustatytos 95 proc. tirpiklio A. Linijinis gradiento profilis buvo pritaikytas tokiomis tirpiklio A proporcijomis: 0–0,2 min. buvo nustatytas 95 proc., 0,2–1,5 min. – 10 proc. ir 1,5–1,8 min. – 90 proc., bei grįžo į pradines sąlygas. Bendras pusiausvyros analizės laikas buvo 3 min. Analizei atlikta neigiama elektros purškimo jonizacija esant tokiems parametrams: kapiliarų įtampa buvo nustatyta į neigiamą 2 kV, šaltinio temperatūra buvo naudojama 150 °C, tiekiamų azoto dujų desulfuravimo temperatūra buvo nustatyta 400 °C, dujų tėkmės desolvacija – 700 l/val., dujų apyvarta – 20 l/val. Kūgio įtampa buvo 25 V. MS duomenys buvo renkami viso nuskaitymo režimu diapazone nuo 50 m/z iki 250 m/z. Gauti masės spektrai buvo naudojami metabolinių srautų pasiskirstymo nustatymui, naudojantis EMU metodu [127]. Tai buvo atlikta pasitelkiant programavimą Python kalba.

2.9. Tėkmės citometrija

Ląstelės 5×10^4 buvo sėjamos į 35 mm lėkšteles ir užpilamos 2 ml DMEM terpės. Mock ir siRNR transfekuotos ląstelės 20 min. kambario temperatūroje buvo inkubuojamos su terpe, kurioje yra 1 mg/l JC-1 dažų (Biotium, Fremont, CA USA). Po to ląstelės buvo plaunamos PBS, paveiktos tripsinu ir surenkamos centrifuguojant. Tada ląstelės buvo resuspenduotos PBS su 5 mg/l 7-AAD dažais (Millipore, Burlington, MA, JAV) ir inkubuojamos 10 min. Teigiamai kontrolei buvo naudojamas 10 μM karbonilo cianido m-chlorfenilhidrazonas (CCCP). Mėginiai buvo kiekybiškai įvertinti naudojant Guava PCA tėkmės citometrą (Millipore). Duomenys buvo analizuojami naudojant „GuavaSoft 2.7 InCyte“ programinę įrangą. Mitochondrijų membranos potencialas buvo parodytas kaip JC-1 agregatų (raudonos fluorescencijos) ir monomerų (žalios fluorescencijos) santykis (R/G).

2.10. Baltymų imunodetekcija

Imunocitochemijos ir imunoblotingo (WB, angl. *Western blot*) analizei naudoti šie pirminiai antikūnai: triušio prieš PPAR delta (ThermoFisher Scientific, cat# PA1-823A), triušio prieš histoną H3 (ThermoFisher Scientific, cat# 702023), pelės prieš beta-kateniną (ThermoFisher Scientific, cat# CAT-5H10), pelės prieš GAPDH (Ambion, cat# AM4300), triušio prieš BCAT2 (Abcam, cat# ab95976). Naudotas antrinis asilo prieš triušį IgG H&L antikūnas sujungtas su Alexa Fluor 488 (Life technologies, cat# A21206).

Baltymų imunoblotingui BCC ląstelės (3×10^6) buvo lizuotos ant ledo šaltų ląstelių ekstrahavimo buferyje (Invitrogen, Carlsbad, CA, JAV), papildytame 20 μl/ml proteazių slopiklių kokteiliu (Sigma-Aldrich, Vokietija) ir 1 mM PMSF (Abcam, Cambridge, JK) 30 min. Lizatai buvo centrifuguoti 13 000 aps./min. 10 min. 4 °C temperatūroje. Qubit® baltymų analizės rinkinys (Invitrogen) buvo naudojamas, norint nustatyti bendrą baltymų koncentraciją Qubit 3.0 fluorometru (Invitrogen). Ląstelių lizatai (30 μg) buvo atskirti Bolt™ 4–12 proc. Bis-Tris ir geliais (Invitrogen) MES SDS tekančiame buferyje ir pernešti į 0,45 μm PVDF membranas (GEHealthcare, JK). Baltymai buvo nustatyti naudojant pirminius antikūnus, esančius ECHS1 (ab174312), FASN (ab99359) ir BCAT2 (ab95976) (Abcam), PPAR-δ (PA1-823A), ME1 (MA5-23524), ME2 (PA5-38007), ME3 (PA5-36494) ir GAPDH (AM43) („Fisher Science”, JAV) ir „WesternBreeze®“ chemiliuminescencinį rinkinį („Invitrogen“) pagal gamintojo instrukcijas. Juostos buvo vizualizuotos „G:Box Chemi Gel“ dokumentacijos sistema (Syngene, Frederick, MD, JAV).

2.11. Statistinė analizė

Visi eksperimentai su ląstelėmis buvo atliekami mažiausiai 3 pakartojimus (n = 3). Modeliavimo eksperimentuose, duomenų išsibarstymas pateiktas standartine paklaida, kai du eksperimentai buvo lyginami vienas su kitu. Kai prognozuojami izotopomerų pasiskirstymai buvo palyginti su apskaičiuotais, eksperimentinių verčių paklaidų juostos atitinka 95 proc. pasikliautinuosius intervalus. Dviejų verčių palyginimas buvo atliktas naudojant Stjudento t testą. Patikimumo lygmuo buvo $p<0,05$. Statistinė analizė buvo atlikta naudojant „Excel“ ir „scipy.stats“ biblioteką.

3. REZULTATAI

3.1. Krūties naviko ląstelių pirminės kultūros sukūrimas ir charakterizavimas

Ląstelės buvo išskirtos kaip aprašyta Metodų skyriuje, naudojantis įprastiniais protokolais [129]. CD44 ir CD24 yra transmembraniniai glikoproteinai. CD24 raiška stebima navikinėse ląstelėse ir šis žymuo veikia kaip specifinis hialurono rūgšties receptorius, skatinantis piktybinių ląstelių judėjimą. CD44 žymuo navikinėse krūties ląstelėse yra aktyvios formos ir dalyvauja daugelyje viduląstelinių signalų perdavimo kaskadų, taip pat yra susijęs su ląstelių proliferacija, diferenciacija ir judėjimu. Ki-67 yra nehistoninis branduolio baltymas, naudojamas kaip ląstelių proliferacijos žymuo. Padidėjusi Ki-67 raiška būdinga navikinėms ląstelėms ir siejama su bloga ligos prognoze bei geru atsaku į chemoterapiją. Atliktos išskirtos ląstelių linijos linijinės šviesinės mikroskopijos nuotraukos (3.1.1 pav.).

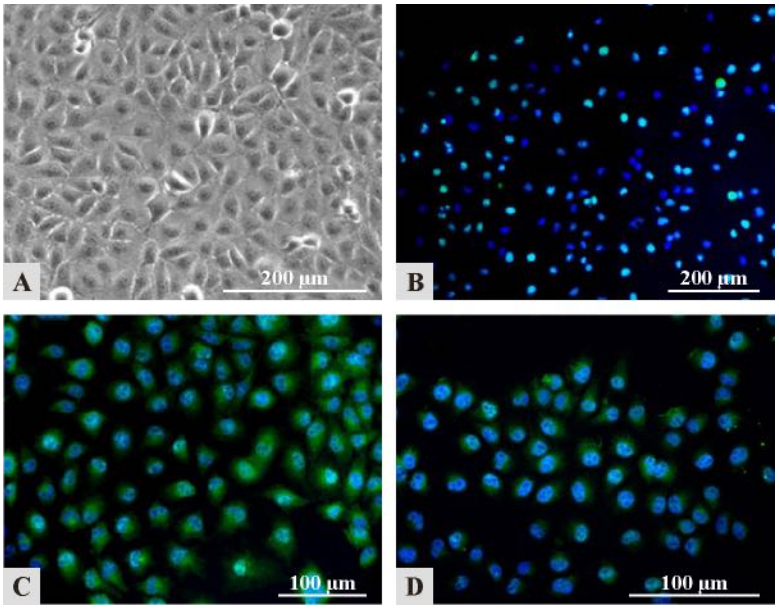

3.1.1 pav. *BCC ląstelių linijos šviesinės mikroskopijos nuotrauka*

(A) BC4 ląstelės; **(B)** Ki-67 imunofluorescencija BCC ląstelėse; **(C)** CD24 imunofluorescencija BCC ląstelėse; **(D)** CD44 imunofluorescencija BCC ląstelėse.

3.2. Lipoamido struktūrinis analogas

Šiame skyriuje eksperimentiškai parodome, kaip GSMM gali būti panaudotas vaistų kūrimui. Prieinamosiose metabolitų duomenų bazėse galima atlikti naujų slopiklių, panašių į metabolitus, paiešką. Nauji slopikliai tai molekulės, kurios jungiasi prie biologinio taikinio ir slopina jo biologinę funkciją. Tanimoto balas – tai skaičiumi išreikštas panašumas tarp vadinamųjų molekulių pirštų antspaudų. Tanimoto balas yra išreikštas nuo nulio (nėra panašumo) iki vieneto (aukštas panašumas). Apskaičiavus ir įvertinus Tanimoto balą, buvo surastas naujas slopiklis, panašus į vieną iš metabolitų, besijungiantis į tą taikinį, kurio substratas yra minėtasis metabolitas. Palyginome žmogaus metabolitų (gautų pagal jų KEGG indeksus) chemines struktūras ir junginius, esančius „DrugBank“ duomenų bazėje. Junginiai, kurių Tanimoto balas yra didesnis nei 0,9, padidina 29,5 karto tikimybę, kad analizuojamoji molekulė jungsis prie to paties taikinio, kaip ir panašus metabolitas, nei atsitiktinai parinkta molekulė. Naudojant RNR-seq duomenis ir žmogaus GSMM, įmanoma įvertinti metabolinių srautų pasiskirstymą ir išmatuoti metabolinių srautų kitimą (pavyzdžiui, naudojant vaistą, kuris slopina katalizuojančius fermentus). Šis metodas leido numatyti skirtingą lipoamidų analogų poveikį MCF-7 (krūties vėžio ląstelių linija) ir ASMC (kvėpavimo takų lygiųjų raumenų ląstelės) dauginimuisi [130]. Norint atlikti eksperimentus, buvo reikalingas susintetintas junginys, kurį būtų galima įsigyti. Lipoamidas yra tarpinis produktas, susidarantis valino, leucino ir izoleucino skilimo metu, kuomet pagaminama didelė ATP dalis, reikalinga navikinėms ląstelėms, kaip energijos šaltinis.

Santykinio augimo greitis priklausė nuo reakcijų, kurių fermentai sąveikauja su lipoamidu, slopinimo. Jokio skirtumo tarp MCF-7 ir ASMC nestebėta esant mažesniam nei 0,8 slopinimui, tačiau esant didesniems slopinimams egzistuoja potencialus terapinis langas (3.2.1 pav.). Tai rodo, kad tinkamos dozės lipoamido analogai gali smarkiai sumažinti MCF-7 ląstelių proliferacijos greitį ir švelniau paveikti ASMC.

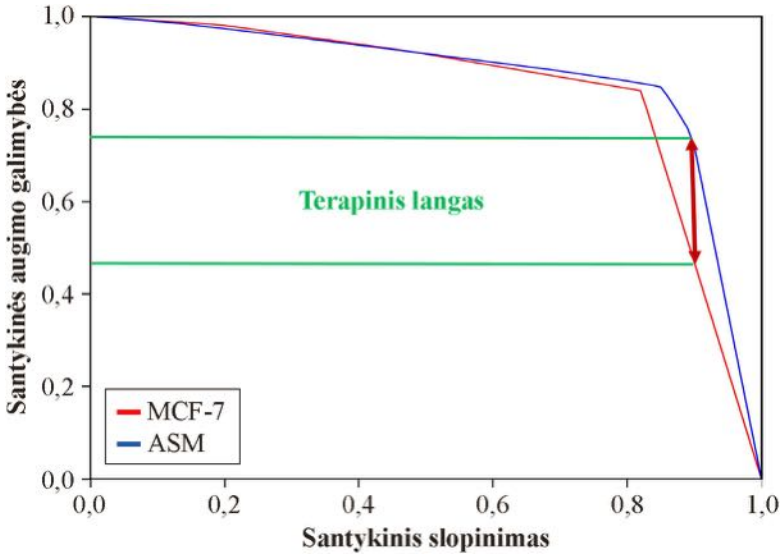

3.2.1 pav. *Terapinio lango nustatymas*

Mes ieškojome junginių, turinčių struktūrinį panašumą į lipoamidą. Buvo patikrintas junginys su penkiakampiu žiedu ir alifatine grandine, užbaigiančia polinę grupę (*http://www.ambinter.com/reference/19149142*), remiantis jo panašumu į lipoamidą. Išbandytas junginys Amb19149142 reikšmingai sumažino MCF-7 ląstelių augimą, tačiau neturėjo statistiškai reikšmingo poveikio ASMC (3.2.2 pav.). Rezultatai rodo, kad srauto balanso analizė, naudojant GSMM, apdorotus pagal RNR-seq duomenis, galėtų būti naudojama numatant terapinius langus ir padedant kurti naujus vaistus.

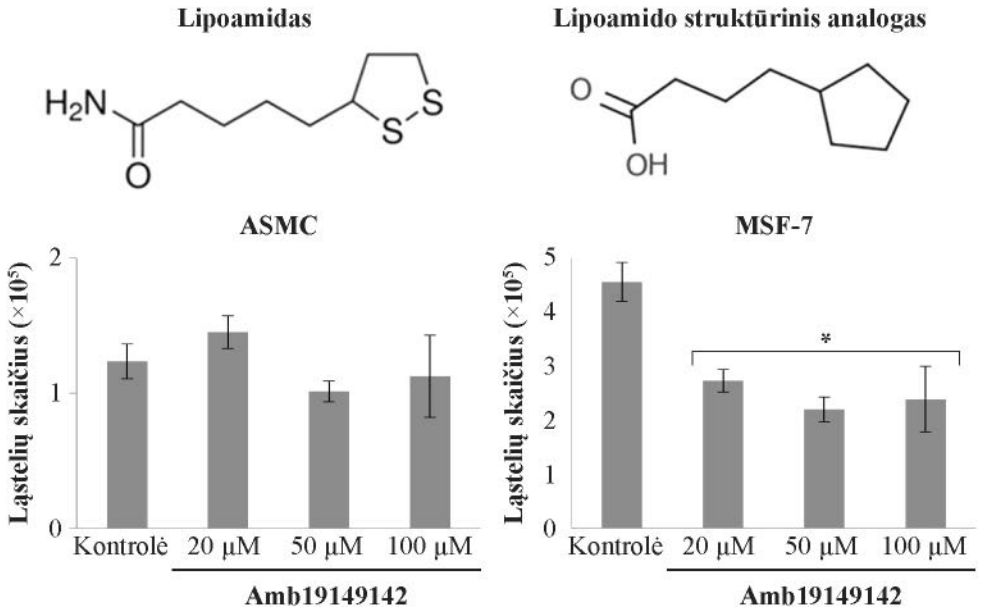

3.2.2 pav. *Lipoamido struktūrinio analogo Amb19149142 poveikis MCF-7 ir ASMC proliferacijai (n = 3). * p<0,05.*

Lipoamido struktūrinio analogo Amb19149142 poveikis tirtas panaudojus tris skirtingas koncentracijas (20, 50 ir 100 μM) ir vertinant po 120 val. Visos trys tirtos koncentracijos mažino MCF-7 ląstelių proliferaciją, tačiau reikšmingo poveikio ASMC neturėjo.

3.3. Šakotosios grandinės aminorūgščių degradacija

Navikų ląstelės didelę dalį ATP pagamina BCAA degradacijos metu. Norėdami kiekybiškai įvertinti šį procesą, mes panaudojome GSMM ir eksperimentinius NCI–60 bibliotekos ląstelių metabolitų įsisavinimo duomenis [131, 132]. Kiekvienai ląstelių linijai apskaičiavome srautų pasiskirstymą, tenkinantį stebimą įsisavinimo ir sekrecijos greitį, minimizuojant visų metabolinių srautų sumą. Iš gauto srautų pasiskirstymo įvertinome bendrą ATP produkciją. Eksperimentiniai pieno rūgšties pagaminimo greičiai ir kiekvienos BCAA suvartojimo tempai buvo panaudoti palyginti ATP gamybą šių procesų metu (3.3.1 pav.). Buvo nustatyta, kad nuo 12 proc. iki 55 proc. viso ATP susidaro, degraduojant BCAA.

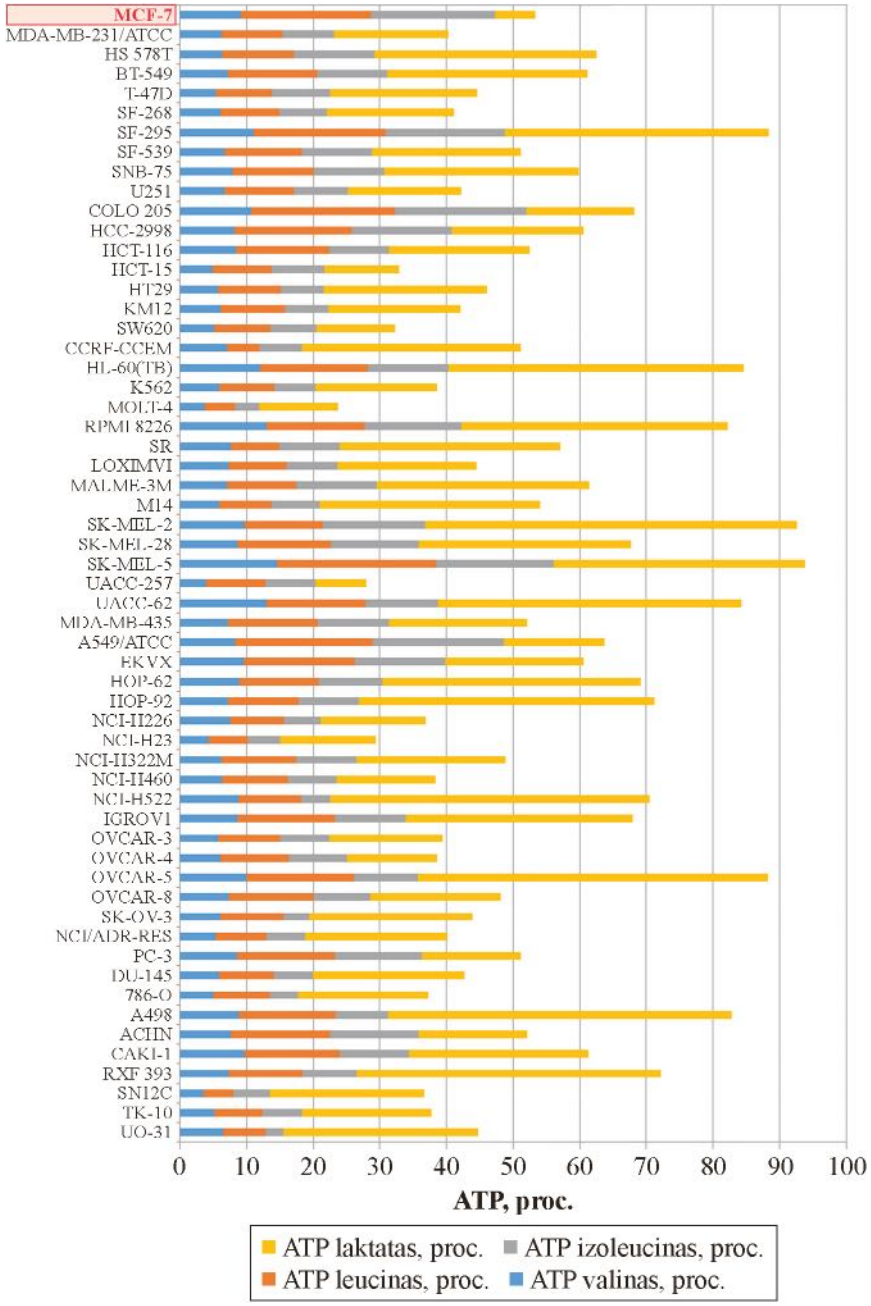

3.3.1 pav. *NCI-60 bibliotekoje esančiose ląstelių linijose apskaičiuotas ATP kiekis, gaunamas iš pieno rūgšties fermentacijos, bei valino, leucino ir izoleucino degradacijos. Raudonai apibrėžta – MCF-7 ląstelėse ~50 proc. ATP gaunama iš valino, leucino ir izoleucino*

Navikinės ląstelės nuo sveikų skiriasi padidėjusia penkių fermentų, dalyvaujančių valino degradacijoje, raiška (BCAT2, DBT, dihidrolipoilo transacetilazės (DLT), HADHA ir HIBADH), keturių iš jų izoleucino degradacijoje (BCAT2, DBT, DLT ir HADHA) ir trijų – leucino degradacijoje (BCAT2, DBT ir DLT). Paminėti penki fermentai nėra tiesiogiai reguliuojami SP1, tačiau jų reguliavimo būdas yra identiškas genų, susijusių su EMT, kuris rodo, kad BCAA skilimą skatina reguliavimo kaskados, susijusios su EMT.

Atliktos 289 mikrogardelių analizės rezultatai parodė, kad navikinės ląstelės, lyginant su sveikomis ląstelėmis, pasižymi dviem reikšmingais transkripcijos pokyčiais: Wnt reguliuojamų genų raiškos padidėjimu ir aktyvatoriaus baltymu 1 (AP-1) reguliuojamų genų raiškos sumažėjimu. SP1 ir Wnt signalinio kelio sąveika turi įtakos navikinių ląstelių EMT. SP1 dalyvauja EMT, kuris Wnt signalo perdavimo kelyje aktyvuoja β-katenino fosforilinimą, apjungiantį LEF1 ir FOXO4 koduojamus transkripcijos veiksmus, lemiančius tikslinių genų raiškos padidėjimą bei navikogenezę (3.3.2 pav.).

EMT taip pat yra susijęs su fermentų, dalyvaujančių BCAA (valino, leucino ir izoleucino) skilime, raiškos padidėjimu. Tyrėme vieno iš šių fermentų (BCAT2) nutildymo poveikį.

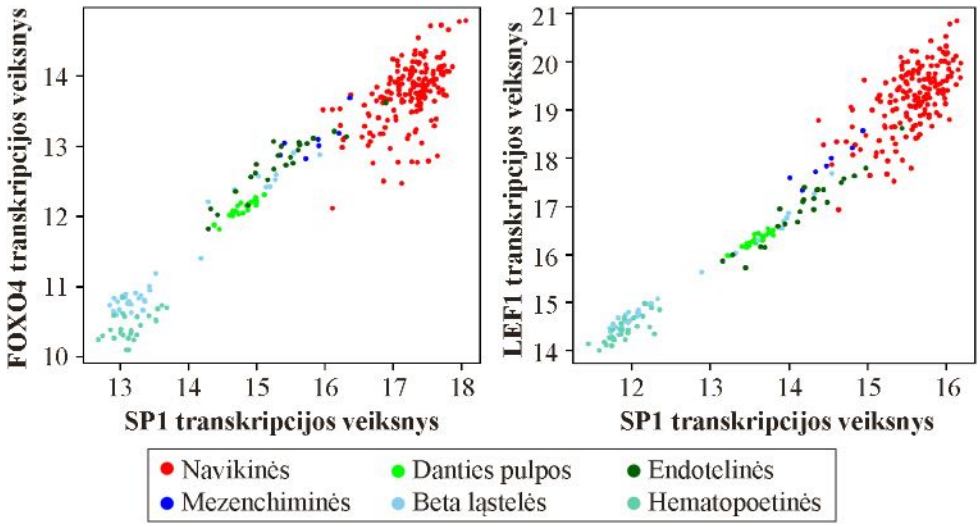

3.3.2 pav. *Koreliacija tarp SP1 ir FOXO4 bei tarp SP1 ir LEF1 transkripcijos veiksnių*

BCAT2 katalizuoja pirmąjį valino, leucino ir izoleucino degradacijos žingsnį. BCAT1 ir BCAT2 raiškos padidėjimas randamas įvairiose navikinėse ląstelėse, tačiau BCAT2 raiškos padidėjimas ir poveikis krūties navikinėse ląstelėse išlieka neaiškus. Į savo eksperimentinius tyrimus įtraukėme BCC, kad nustatytume, ar plačiai naudojamų navikinių ląstelių linijose gautas išvadas galima pritaikyti realių navikų ląstelėms. Kaip sveikas ląsteles pasirinkome kvėpavimo takų lygiųjų raumenų ląstelių liniją (ASMC) ir krūties epitelio ląstelių liniją (MCF-10A). Atliktas imunofluorescencinis tyrimas parodė, kad BCAT2 kiekis navikinėse ląstelėse yra ženkliai didesnis, nei sveikose ląstelėse (3.3.3 pav.).

Norint įvertinti ląstelėse BCAT2 baltymo raišką ir siRNR prieš BCAT2 poveikį, atliktas WB tyrimas. Kontrolėje BCAT2 raiška navikinėse ląstelėse buvo žymiai didesnė, negu sveikose. Paveikus siRNR prieš BCAT2, šio baltymo raiška visose ląstelėse sumažėjo (3.3.4 pav.).

SiRNR prieš BCAT2 sumažino navikinių ląstelių proliferaciją, tačiau sveikų ląstelių proliferacijai įtakos neturėjo. MCF-7 ir BCC skaičius sumažėjo atitinkamai $16{,}6 \pm 2{,}1$ proc. ir $11{,}3 \pm 1{,}5$ proc. ASMC ir MCF-10A ląstelių skaičius nepakito (atitinkamai, $99 \pm 0{,}8$ proc. ir $106 \pm 3{,}4$ proc.) (3.3.5 pav.). Reikia turėti omenyje, kad santykinai nedidelis citotoksinis poveikis gali būti susijęs su tuo, kad siRNR geba išveiklinti tik apie pusę taikinio.

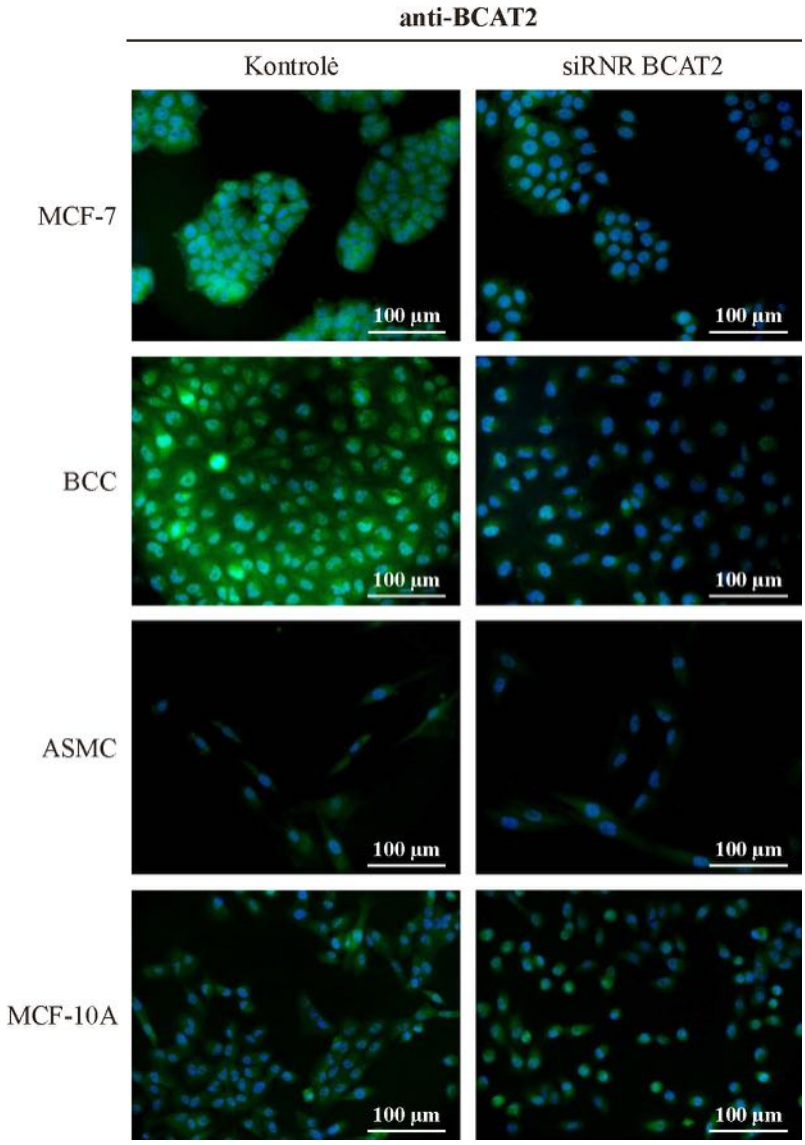

3.3.3 pav. *BCAT2 imunofluorescencija navikinėse (MCF-7 ir BCC) ir sveikose (ASMC ir MCF-10A) ląstelėse kontrolėje ir po siRNR prieš BCAT2 transfekcijos*

Žalia – antriniai triušio IgG-H & L antikūnai, konjuguoti su Alexa Fluor 488; mėlyna – DAPI dažyti branduoliai. Eksperimentai buvo atlikti 24 val. po transfekcijos.

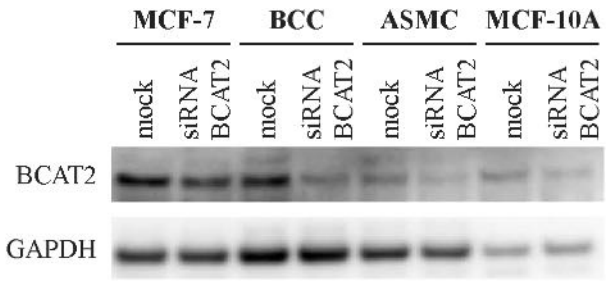

3.3.4 pav. *Baltymo raiška paveikus navikines ir sveikas ląsteles siRNR prieš BCAT2*

Gliceraldehido-3-fosfato dehidrogenazė (GAPDH) – kontrolinis baltymas. Eksperimentai atlikti 24 val. po transfekcijos.

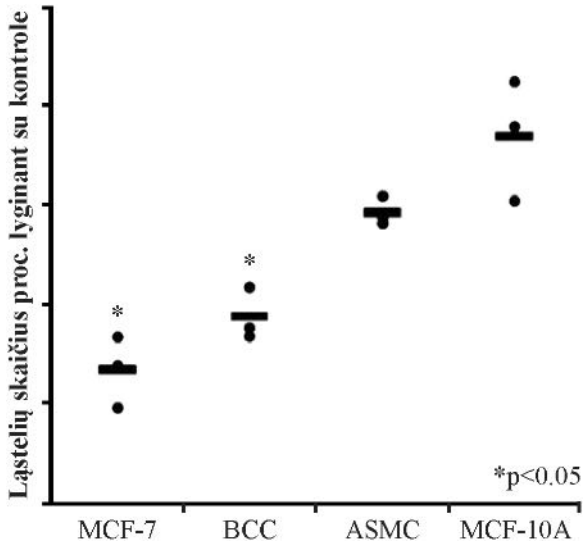

3.3.5 pav. *SiRNR prieš BCAT2 poveikis navikinių (MCF-7 ir BCC) ir sveikų (ASMC ir MCF-10A) ląstelių proliferacijai.*

Tėkmės citometrijos tyrimas, naudojant aneksiną V-PE/7-AAD, parodė, kad siRNR prieš BCAT2 neturėjo poveikio nei navikinių, nei sveikų ląstelių gyvybingumui (3.3.6 pav.).

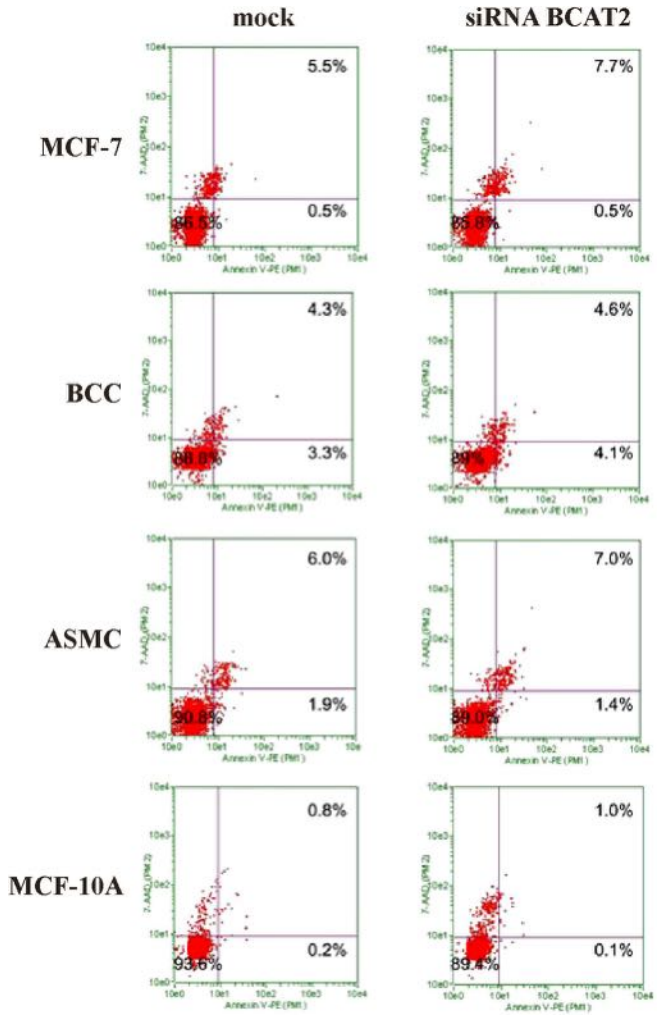

3.3.6 pav. *BCAT2 baltymo nutildymo įtaka ląstelių gyvybingumui*

Kiekvieno grafiko apatiniame kairiajame kvadrante pateikti skaičiai rodo nepakitusių ląstelių kiekį, apatiniame dešiniajame kvadrante – ankstyvoji apoptozė, viršutiniame dešiniajame kvadrante – vėlyvoji apoptozė. Ląstelių gyvybingumas nesiskyrė kontrolėje ir siRNR prieš BCAT2 paveiktose ląstelėse.

Šie rezultatai rodo, kad BCAT2 gali būti tinkamas taikinys naujiems vaistams, siekiant citostatinio poveikio vėžio ląstelėms.

3.4. Vienalaikio FAS ir FAO įvertinimas, panaudojant ^{13}C žymėjimą

Naviko ląstelių gyvybingumą ir proliferaciją veikia FAS citozolyje ir FAO mitochondrijose. Siekiant patikrinti hipotezę, ar naviko ląstelėse vienu metu vyksta FAS ir FAO, naudojome ^{13}C žymėtą glutaminą FAO lygiui įvertinti. Riebalų rūgštys sintetinamos iš citozolio acetil-KoA, kuris pats daugiausiai gaunamas iš citrinos rūgšties. Citrinos rūgštis yra kilusi iš TCA ciklo ir gabenama į citozolį, tačiau gali būti gaunama ir iš glutamino redukuojant α-ketoglutaratą karboksilinimo metu. FAO vyksta mitochondrijose (riebalų rūgštys iš citozolio pernešamos per transporterį), gaunamas mitochondrijų acetil-KoA, kuris maitina TCA ciklą. Vykstant šiems procesams kartu, dalis acetil-KoA, maitinančio TCA ciklą, yra gaunama iš citrato. Žymėtas ^{13}C glutaminas per redukuojantį karboksilinimą pažymi penkis anglies atomus citrate ir paženklina citozolinį acetil-KoA tolimesnėje lipidų sintezėje. Jei šie lipidai tuo pačiu metu skaidomi, paženklintas acetil-KoA pateks į TCA ciklą ir susidarys visiškai paženklintos citrinos rūgšties molekulės (M6 izotopomeras) (3.4.1 pav.).

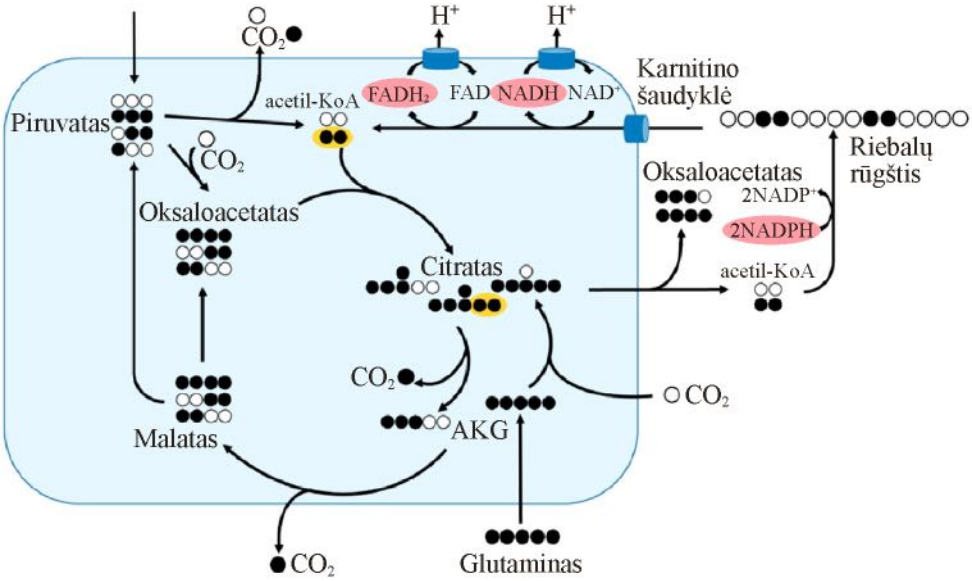

3.4.1 pav. *Metabolizmo modelis su atomų perėjimais*

Metabolinis modelis su atomų perėjimais parodo, kaip riebalų rūgštys, skaidomos dėl glutamato ar ME aktyvumo, gali sukurti M6 citrato izotopomerą. Schema vaizduoja redokso potencialo peršokimą iš citozolinio NADPH į mitochondrijas, susidarančią tuo pat metu vykstant FAS ir FAO. Ženklinti anglies atomai, įeinantys į TCA ciklą iš FAO, pažymėti geltonai. Stipresnė FAO turėtų atitikti didesnę citrato frakciją su 6 žymėtais anglies atomais. Norėdami patikrinti, ar beta oksidacijos greitis gali būti įvertintas pagal citrato žymėjimą, panaudodami siRNR nutildėme FASN, ECHS1, kurios dalyvauja beta oksidacijoje, ir malato dehidrogenazę (ME), kurios dėka visi šeši citrato anglies atomai pažymimi nepriklausomai nuo lipidų metabolizmo. Tyrimams naudojome MCF-7, BT-474 ir BCC ląsteles (3.4.2 pav.). Paženklintas piruvatas, gautas iš malato, veikiant ME, sudaro visiškai paženklintą citratą. Todėl, norėdami įvertinti, ar lipidų metabolizmas iš tikrųjų vaidina svarbų vaidmenį formuojant visiškai pažymėtą citratą, papildomai atlikome genų nutildymą, naudodami siRNR. Norint patikrinti FAS ir FAO egzistavimą tuo pačiu metu buvo pasirinkta BCC linija, nes kitos dvi ląstelių linijos – MCF-7 ir BT-474 – turėjo žymiai mažesnį visiškai pažymėto citrato kiekį. M6 citrato procentinė dalis MCF-7 ląstelėse buvo 1,15 proc., o BT-474 – 0,5 proc.

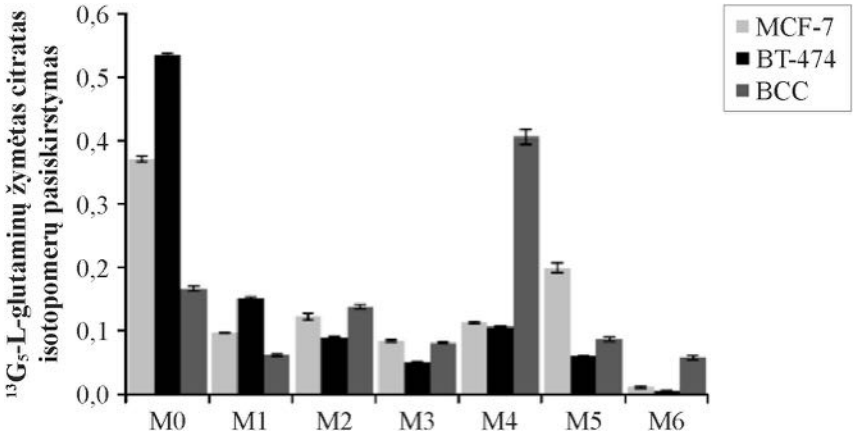

3.4.2 pav. *Pilnai pažymėto citrato procentinė dalis trijose skirtingose krūties vėžio ląstelių linijose (n = 4)*

Ląstelės buvo inkubuojamos su ^{13}C žymėtu L-glutaminu. BCC turėjo 5 ir 10 kartų labiau paženklinto citrato, nei MCF-7 ir BT-474 ląstelės, atitinkamai, todėl didesnė tikimybė, kad BCC ląstelėse FAS ir FAO vyks vienu metu. Ši dalis nepasikeitė nutildžius bet kurį iš minėtų genų. Taip galėjo būti dėl to, kad šiose ląstelėse riebalų rūgščių sintezė nevyksta vienu metu. Todėl šis metodas nėra tinkamas stebėti lipidų sintezę ir degradaciją šiose ląstelėse.

BCC ląstelėse ~6 proc. citrato buvo pilnai žymėta ^{13}C ir jo kiekis mažėjo, nutildant minėtus genus (3.4.3 pav.).

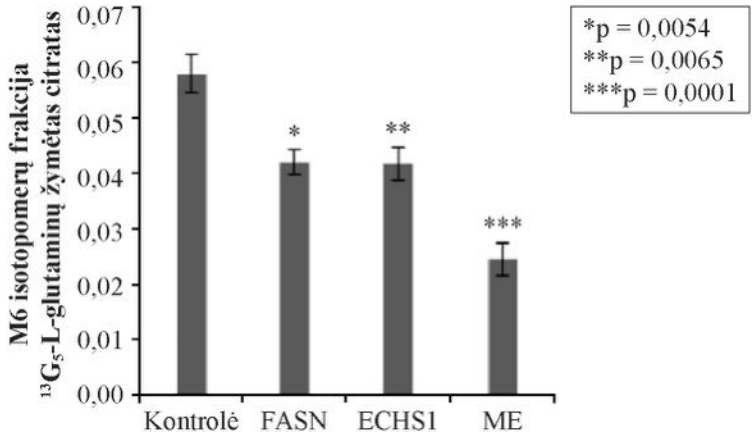

3.4.3 pav. *Eksperimentiniai M6 citrato frakcijos pokyčiai, atsirandantys atitinkamai slopinant FASN, ECHS1 ir ME (n = 4)*

BCC ląstelės buvo transfekuotos siRNR prieš FASN ir ECHS1 genus, kurie atitinkamai dalyvauja FAS ir FAO. Ląstelės taip pat buvo transfekuotos siRNR prieš ME (1–3) genus, siekiant įvertinti ME svarbą visiškai paženklintos citrinos rūgšties susidarymui. SiRNR prieš FASN ir ECHS1 sąlygojo labai panašų M6 frakcijos sumažėjimą, kuris abiem atvejais buvo statistiškai reikšmingas. Kontrolėje M6 frakcija sudarė 5,8 ± 0,3 proc., o siRNR prieš FASN sumažino ją iki 4,2 ± 0,2 proc. (n = 4; p = 0,0054); siRNR prieš ECHS1 – iki 4,2 ± 0,3 proc. (n = 4; p = 0,0065). Tai patvirtina, kad dalis visiškai pažymėto citrato susidaro per hipotetinį FAS ir FAO mechanizmą. Dar didesnį kritimą – iki 2,4 ± 0,3 proc. (n = 4, p = 0,0001) – sukėlė siRNR prieš ME, kas rodo, kad abu visiškai paženklinto citrato susidarymo mechanizmai yra aktyvūs (3.4.3 pav.).

Baltymo raiškai įvertinti buvo atliktas WB tyrimas – transfekavus siRNR prieš FASN, ECHS1 ir ME (1–3) genus ir lyginant su kontroline transfekcija (3.4.4 pav.), baltymo raiška visose ląstelėse sumažėjo.

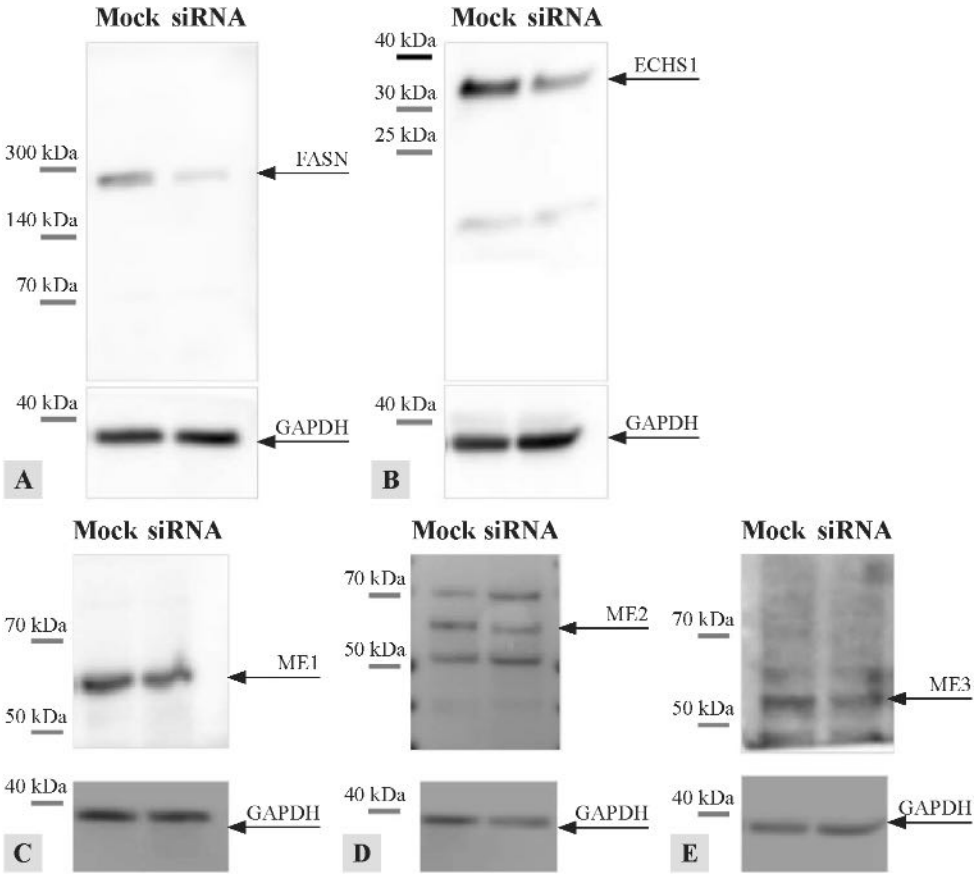

3.4.4 pav. *Baltymo raiška paveikus BCC ląsteles siRNR FASN* ***(A)****, ECHS1* ***(B)****, ME1, ME2, ME3* ***(C–E)***

Gliceraldehido-3-fosfato dehidrogenazė (GAPDH) – kontrolinis baltymas.

3.5. Vienalaikio FAS ir FAO įvertinimas pagal mitochondrijų membranos potencialo pokyčius (Δψm)

FAS ir FAO pasireiškia redukcinio potencialo perkėlimu iš citozolio (NADPH) į mitochondrijas (NADH ir $FADH_2$). Nuo citozolinio NADPH priklauso biomasės komponentų sintezė ir atsparumas oksidaciniam stresui, kuris susijęs su glutationo reduktaze ir glutationo peroksidaze. Dėl padidėjusios ROS gamybos turi sumažėti citozolinio NADPH kiekis ir sustoti FAS bei kiti procesai, kuriems reikia NADPH. BCC ląsteles paveikus staurosporinu, kuris smarkiai padidina ROS lygį, smarkiai sumažėja pilnai žymėto citrato dėl sustabdytos FAS. Reiškia, normos sąlygomis BCC ląstelės gamina daugiau citozolinio NADPH, negu reikia biosintezės procesams. Nedidelio oksidaci-

nio streso metu redukcinio potencialo perteklius perduodamas mitochondrijoms, kur panaudojamas ATP gamybai, o didelio oksidacinio streso metu sunaudojamas citozolinio ROS pašalinimui.

FAS citozolyje metu iš acetil-KoA metu oksiduojamos dvi NADPH molekulės. Kita vertus, FAO metu mitochondrijose susidaro acetil-KoA ir po vieną NADH ir $FADH_2$ molekulę, kurios abi gali būti naudojamos kvėpavimo grandinei maitinti. Tai lemia redokso potencialo perkėlimą iš citozolio į mitochondrijas, kuris gali būti naudojamas išlaikyti didesnį mitochondrijų membranos potencialą. ME katalizuoja NADPH gamybos reakciją, kuri negali vykti kvėpavimo grandinėje. Todėl, jei tuo pat metu vyksta FAS ir FAO, galima tikėtis, kad nutildžius FASN arba ECHS1, sumažės $\Delta\psi m$, tuo tarpu, ME nutildymas neturėtų paveikti $\Delta\psi m$. Mitochondrijų potencialas buvo įvertintas tėkmės citometrija, naudojant JC-1 dažus. Ląstelėse, transfekuotose siRNR prieš FASN ir ECHS1, pastebimas reikšmingas R/G santykio, atspindinčio $\Delta\psi m$, kritimas nuo $10,9 \pm 0,7$ atitinkamai iki $6,9 \pm 0,7$ ($n = 3$; $p = 0,014$) ir $7,5 \pm 0,1$ ($n = 3$; $p = 0,009$) (3.5.1 pav.). Ląsteles paveikus siRNR prieš ME, R/G santykis išliko artimas kontroliniam ($9,2 \pm 0,8$; $n = 3$; $p = 0,19$). Tokiu būdu, FASN ir ECH1, bet ne ME, mažino BCC mitochondrijų potencialą.

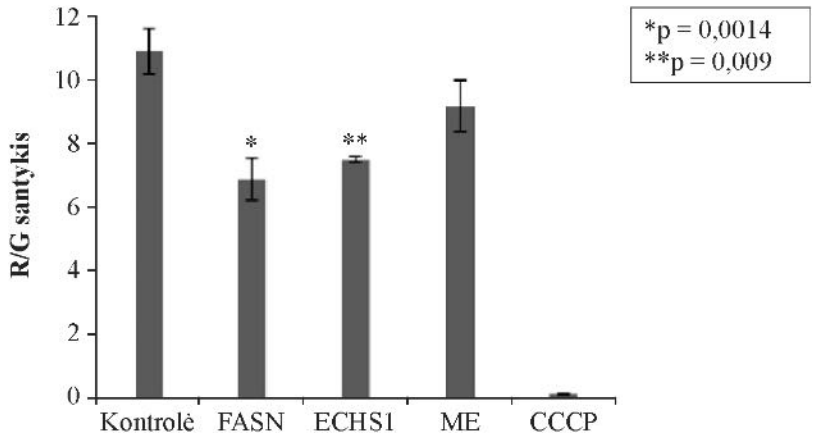

3.5.1 pav. *FASN, ECHS1 ir ME nutildymo poveikis mitochondrijų membranos potencialui (n = 3). CCCP yra oksidacinio fosforilinimo slopiklis, naudojamas Δψm pokyčio kontrolei*

3.6. BCC ląstelių metabolinių srautų analizė

Metabolinių srautų analizė kontrolėje ir panaudojus siRNR prieš FASN, ECHS1 ir ME pateikta 3.6.1 pav., o eksperimentiniai ir sumodeliuoti malato ir citrato izotopomerų pasiskirstymai kontrolėje ir paveikus tomis pačiomis

siRNR pateikti 3.6.2 pav. Citrato ir malato ženklinimo būdai buvo naudojami koreguoti metabolinio srauto pasiskirstymą centrinėje anglies apykaitoje. Metabolinio srauto pasiskirstymas buvo apskaičiuotas naudojant modelį, kuriame dalyvauja TCA ciklas, FAS, FAO, glutaminolizė, redukuojantis α-ketoglutarato karboksilinimas, malato dehidrogenazės, piruvato karboksilazė ir PDH. Mitochondriniai ir citozoliniai citratai bei α-ketoglutaratai buvo laikomi laisvai per mitochondrijų membraną pernešamais junginiais. Manoma, kad citrato lipazės pagamintas citozolio oksaloacetatas pernešamas atgal į mitochondrijas. Izotopų pasiskirstymui modeliuoti buvo naudojama EMU sistema. Pritaikymas buvo atliktas santykinių paklaidų tarp eksperimentinio ir numatomo ženklinimo pavyzdžių minimizavimu. Srauto pasiskirstymas išreiškiamas santykinai su PDH greičiu. Metabolinio srauto pasiskirstymas stebimas naudojant kontrolinį eksperimentą ir eksperimentus su siRNR (FASN, ECHS1 ir ME) (3.6.1 pav.). Kontrolėje FAS ir FAO metabolinis srautas yra 0,69, kaip ir PDH, o ME reakcijoje – 0,48. Ląstelėse, transfekuotose siRNR prieš FASN ar ECHS1, santykinis izotopomerų pasiskirstymas atitiko nulinį srautą FAO reakcijoje. Vienu metu transfekuojant siRNR prieš ME genus, apskaičiuotas ME reakcijos srautas buvo 0,03. Eksperimentiniai ir sumodeliuoti malato ir citrato izotopomerų pasiskirstymai kontrolėje ir paveikus siRNR atitinkamai pateikti 3.6.2 pav.

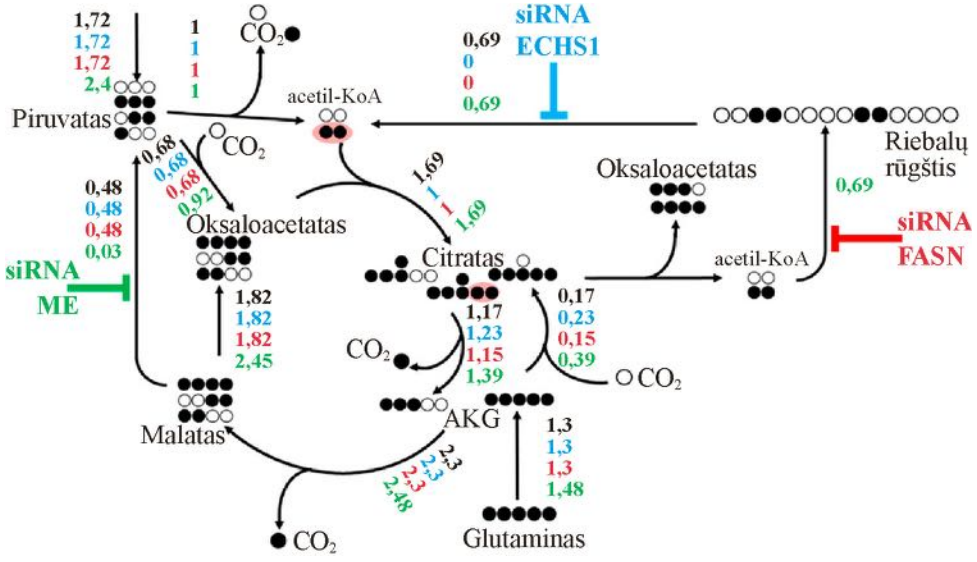

3.6.1 pav. *Apskaičiuoti BCC ląstelių metaboliniai srautai kontrolėje ir panaudojus siRNR prieš FASN, ECHS1 ir ME*

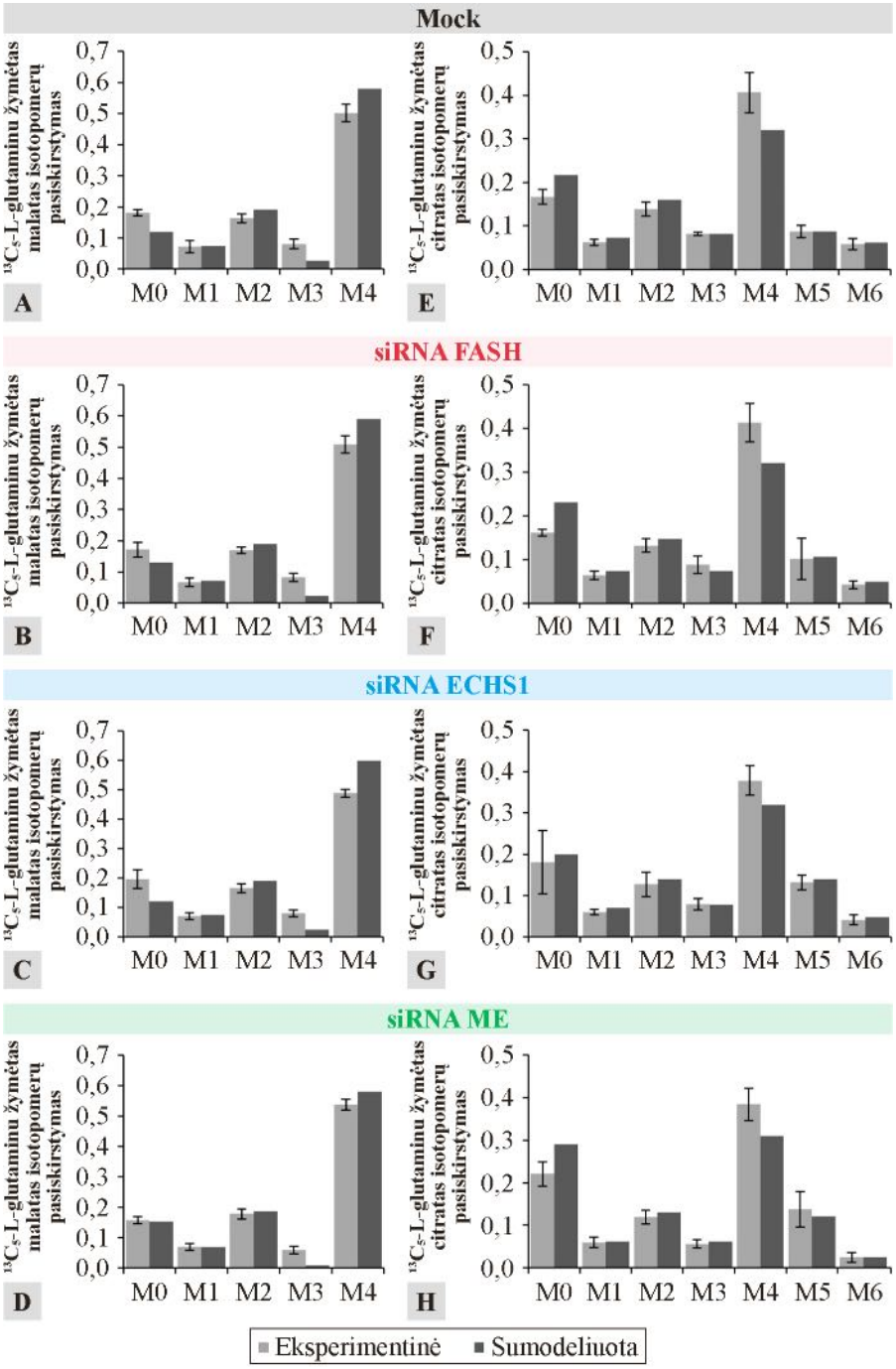

3.6.2 pav. *Eksperimentiniai ir sumodeliuoti malato (A–D) ir citrato (E–H) izotopomerų pasiskirstymai kontrolėje ir paveikus siRNR prieš FASN, ECHS1 ir ME (n = 4)*

Sumažėjusi citrato M6 izotopomerų frakcija atspindi sumažėjusį FAS, FAO ar ME aktyvumą. Tuo tarpu malato izotopomerų pasiskirstymus daugiausia lemia glutaminolizės greitis, todėl FAS, FAO ir ME aktyvumai jiems įtakos neturi. Diagramos rodo citrato ir malato frakcijas, paženklintas nuo nulio (M0) iki šešių (M6) anglies atomų.

3.7. Oksidacinio streso poveikis metaboliniams srautams

FAS ir FAO metabolinis ciklas pasireiškia redukcinio potencialo perkėlimu iš citozolio (NADPH) į mitochondrijas (NADH ir $FADH_2$). Nuo citozolinio NADPH priklauso biomasės komponentų sintezė ir atsparumas oksidaciniam stresui, kuris susijęs su glutationo reduktaze ir glutationo peroksidaze. Dėl padidėjusios ROS gamybos turi sumažėti citozolinio NADPH kiekis ir sustoti FAS bei kiti procesai, kuriems reikia NADPH. BCC paveikus staurosporinu, kuris smarkiai padidina ROS lygį, smarkiai sumažėjo pilnai žymėto citrato kiekis (3.7.1 ir 3.7.2 pav.), ko ir buvo galima tikėtis dėl sustabdytos FAS. Reiškia, normos sąlygomis BCC ląstelės gamina daugiau citozolinio NADPH negu reikia biosintezės procesams. Nedidelio oksidacinio streso metu redukcinio potencialo perteklius perduodamas mitochondrijoms, kur panaudojamas ATP gamybai, o didelio oksidacinio streso metu sunaudojamas citozolinio ROS eliminavimui.

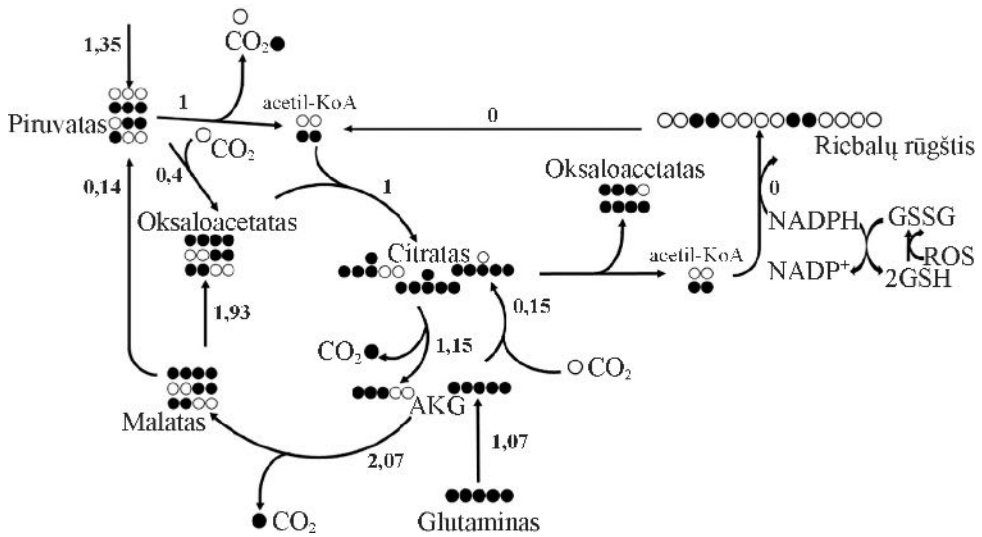

3.7.1 pav. *Malato ir citrato metabolinio srauto pasiskirstymas BCC paveikus staurosporinu*

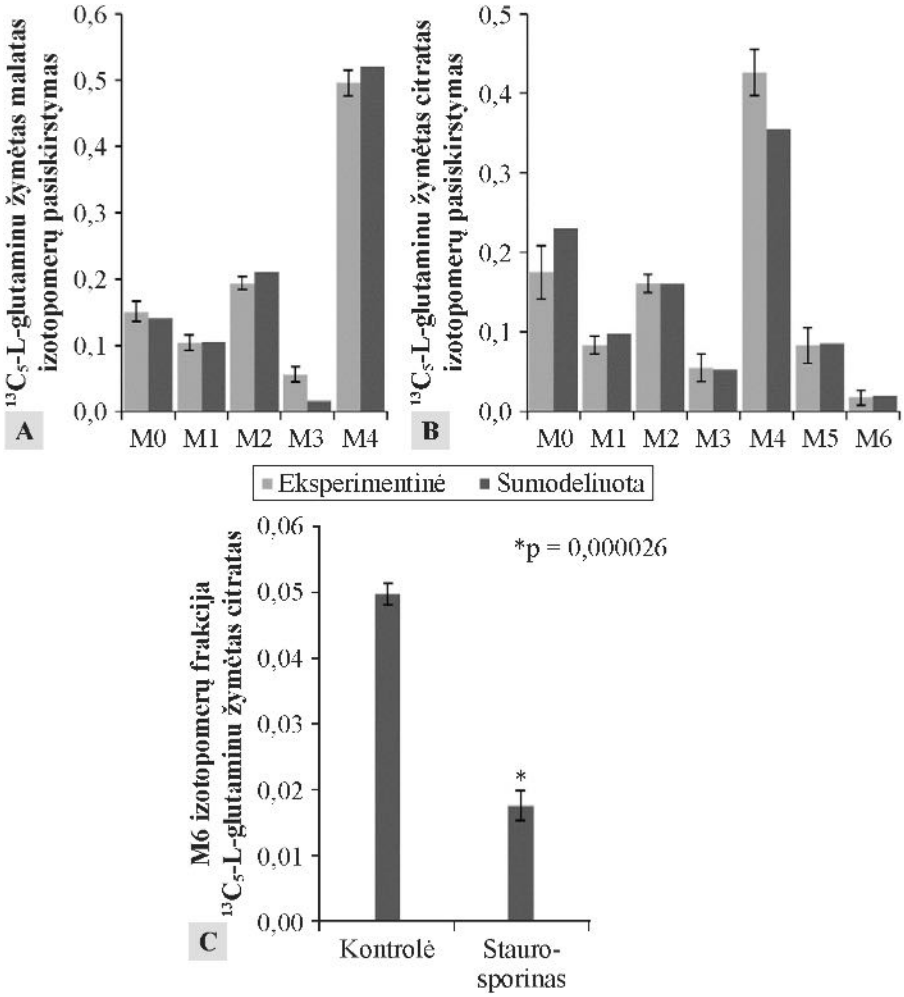

3.7.2 pav. *Staurosporinu paveiktų BCCC malato* ***(A)*** *ir citrato* ***(B)*** *izotopomerų pasiskirstymas (n = 4). Staurosporino poveikis M6 citrato frakcijos dydžiui* ***(C)*** *(n = 4). *p<0,001.*

3.8. BCC ir BT-474 ląstelių atsparumas oksidaciniam stresui

Ląstelės, kuriose vienu metu vyksta FAS ir FAO, turi daug NADPH ir todėl gali slopinti oksidacinį stresą. Palyginome staurosporino sukeltą oksidacinio streso poveikį BCC ir BT-474 ląstelėms, nes pastarosios turėjo 10 kartų mažiau M6 citrato (3.8.2 pav.), o tai reiškia, jog jose vienu metu nevyksta FAS ir FAO, ką patvirtina ir ^{13}C tyrimas, parodęs, kad FAO srauto greitis lygus nuliui (3.8.1 pav.).

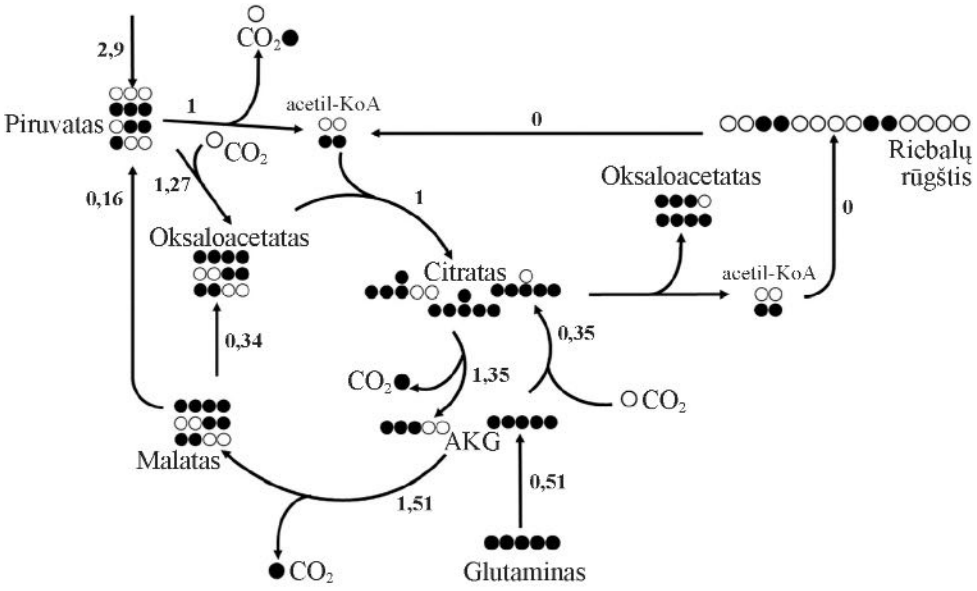

3.8.1 pav. *Malato ir citrato metabolinio srauto pasiskirstymas BT-474 ląstelių linijoje*

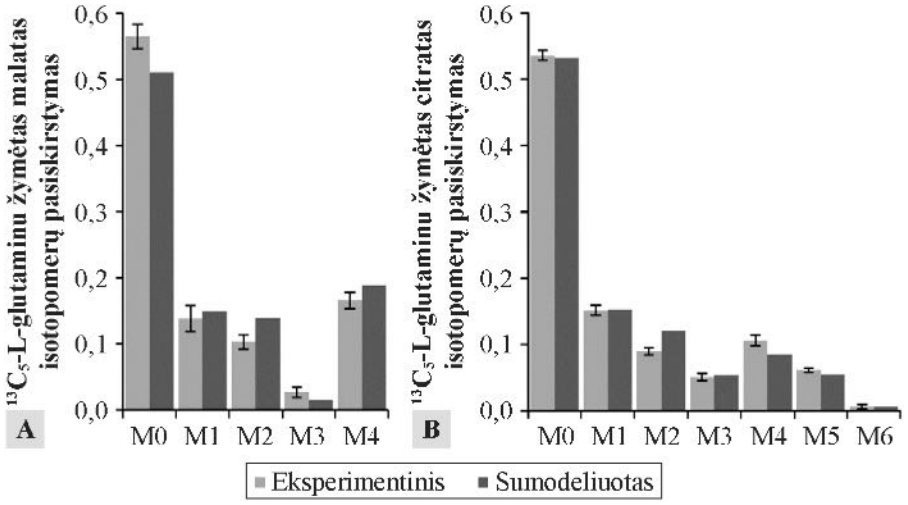

3.8.2 pav. *Sumodeliuotas ir eksperimentinis malato* ***(A)*** *ir citrato* ***(B)*** *izotopomerų pasiskirstymas BT-474 ląstelėse (n = 4)*

Staurosporinas sukėlė žymiai didesnę mitochondrijų membranos potencialo depoliarizaciją BT-474 ląstelėse, negu BCC – R/G santykis atitinkamai pasikeitė 3,4 ± 0,4 ir 1,8 ± 0,05 karto ($p<0,001$) (3.8.3 pav.). Šie rezultatai patvirtina mūsų hipotezę, kad BCC yra atsparesnės oksidaciniam stresui, o FAO galėtų būti vaistų taikiniu kai kurių tipų navikuose.

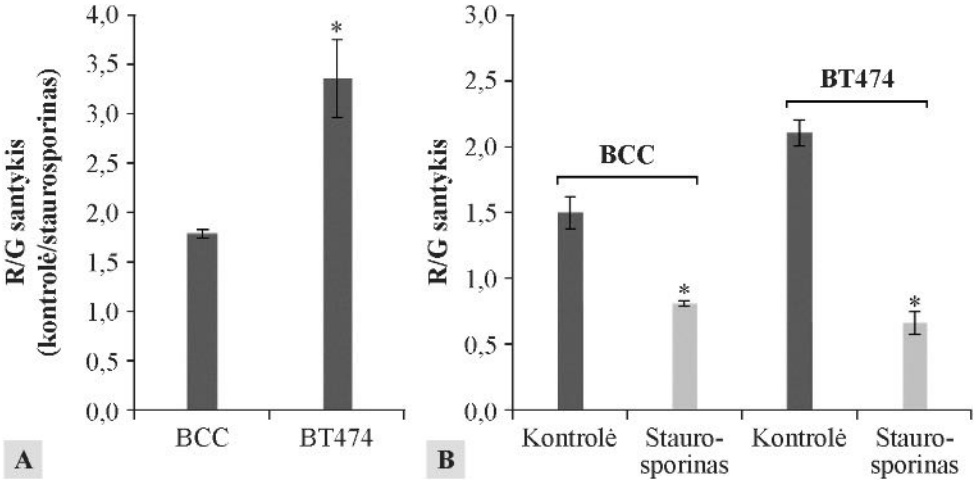

3.8.3 pav. *R/G santykio pokytis BCC ir BT-474 ląstelėse po gydymo staurosporinu* ***(A)*** *ir staurosporino poveikis BCC ir BT-474 ląstelių mitochondrijų potencialui* ***(B)****, vertinant pagal JC-1 dažų R/G santykį (n = 4). *p<0,001.*

4. REZULTATŲ APTARIMAS

Navikinių susirgimų daugėja, todėl labai svarbus savalaikis ir adekvatus naviko gydymas. Šiuo metu intensyviai ieškoma naujų prognozinių veiksnių bei diagnostikos ir gydymo galimybių. Kuo daugiau žinosime apie naviko metabolizmą ir jo pokyčius, tuo tiksliau galėsime panaudoti šias žinias terapijai, nukreiptai į navikines ląsteles, nepažeidžiant sveikų ląstelių.

Prieš atliekant tyrimus, buvo sukurta pirminė krūties vėžio ląstelių kultūra (BCC). Eksperimentuose naudojome vėžines ląstelės, kad nustatytume, ar plačiai naudojamų vėžinių ląstelių linijų tyrimų rezultatus galima pritaikyti realių navikų ląstelėms.

Vaisto panašumas į natūralius metabolinių fermentų substratus (vertinamas naudojant Tanimoto balus) padidina molekulės gebėjimą jungtis prie pasirinkto metabolinio fermento. Vienas iš geriausiai žinomų žmogaus biologinių tinklų yra metabolizmas, nes sukauptos daugiau nei šimtmečio biocheminių tyrimų žinios leidžia tiksliai apibrėžti metabolizmo reakcijas, kurias katalizuoja kiekvienas fermentas, ir šios reakcijos turi gerai žinomą stechiometriją. Visa ši stechiometrinė informacija yra GSMM, kuri apibūdina ląstelės metabolizmą. GSMM ir RNR sekvenavimo duomenimis bei atlikta sveikų ir vėžinių ląstelių metabolinių srautų analize galima nustatyti personalizuotą terapinį langą, kuris leistų priešvėžiniams vaistams preferenciškai veikti vėžines ląsteles, maksimaliai išvengiant nepageidaujamo šalutinio poveikio sveikoms ląstelėms. Eksperimentiniu būdu parodėme, kad lipoamido struktūrinio analogo poveikis gali sumažinti navikinių ląstelių linijos MCF-7 proliferacijos greitį, tuo pačiu neturėdamas reikšmingo poveikio sveikoms ASMC.

Ilgai buvo manoma, kad FAS ir FAO negali vykti ląstelėje tuo pačiu metu. FAO atlieka svarbų vaidmenį navikinių ląstelių išgyvenamume. Kita vertus, FAS taip pat reikalingas navikinių ląstelių augimui ir dauginimuisi. Gali būti, kad FAO padeda ląstelėms išgyventi, esant metaboliniam stresui, kai nėra kitų energijos šaltinių ir redokso kofaktorių. Kita vertus, net jei FAS ir FAO tradiciškai buvo laikomi nesuderinamais dėl malonil-KoA slopinančio poveikio karnitino transporteriui, atsakingam už riebalų rūgščių gabenimą į mitochondrijas, vis daugiau įrodymų patvirtina abiejų reiškinių koegzistavimą navikinėse ląstelėse. Šiame darbe mes parodome, kad taip yra BCC ląstelėse. FAS ir FAO koegzistavimą patvirtina FASN ir ECHS1 genų nutildymo poveikis pilnai pažymėto citrato kiekiui (kai ląstelėms tiekiamas ^{13}C žymėtas glutaminas) ir mitochondrijų membranos potencialui. MCF-7 ir BT-474 ląstelėse labai maža citrato dalis buvo pilnai žymėta (apie 1 proc.), tačiau BCC ląstelėse apie 6 proc. citrato buvo pilnai žymėta ^{13}C ir nutildžius minėtus genus, jo kiekis mažėjo. Atlikus ME genų nutildymą, ^{13}C žymėto

citrato kiekis sumažėjo dar daugiau, tai rodo, kad visiškai paženklinto citrato susidarymo mechanizmai yra aktyvūs. FAS citozolyje metu iš acetil-KoA oksiduojamos dvi NADPH molekulės. Kita vertus, FAO metu mitochondrijose susidaro acetil-KoA ir po vieną NADH ir $FADH_2$ molekulę, kurios abi gali būti naudojamos kvėpavimo grandinei maitinti. Tai lemia redokso potencialo perkėlimą iš citozolio į mitochondrijas, kuris gali būti naudojamas išlaikyti didesnį mitochondrijų membranos potencialą. ME katalizuoja NADPH gamybos reakciją, kuri negali vykti kvėpavimo grandinėje. Todėl, atlikus FASN ir ECHS1 genų nutildymą mitochondrijų membranos potencialas sumažėjo, o ME genų nutildymas mitochondrijų membranos potencialo nemažino. Užblokavus FAS, skirtingai nei blokuojant FAO, labai panašiai sumažėja pilnai žymėto citrato kiekis ir mitochondrijų potencialas. Tai atitinka ankstesnius stebėjimus [133], kuriuose blokuojant lipidų sintezę sumažėjo deguonies suvartojimas.

Galimas fiziologinis šio vienu metu vykstančio FAS ir FAO pasireiškimo vaidmuo yra citozoliniame NADPH esančio redukcinio potencialo perkėlimas į mitochondrijas. Tai leistų ląstelėms perdirbti citozolyje pagaminto NADPH perteklių ir nukreipti jo redukcinį potencialą į kvėpavimo grandinę. Jei ląstelės patiria staigų oksidacinį stresą, ši perteklinė citozolinio NADPH gamyba gali būti nukreipta pašalinti ROS, sustabdant lipidų sintezę. Atrodo, kad šis reiškinys vyksta BCC ląstelėse, kurias paveikus staurosporinu stebimas pilnai pažymėto citrato frakcijos sumažėjimas.

Jau anksčiau mikroorganizmuose buvo pastebėti medžiagų apykaitos ciklai, apimantys perteklinio NADPH oksidaciją [134], kur šį akivaizdų energijos švaistymą galima išnaudoti didinant atsparumą prieš staigų oksidacinį stresą. Mūsų pateiktas atvejis leidžia manyti, kad žmogaus ląstelės taip pat galį naudoti analogišką mechanizmą. Tuo tarpu ląstelės, kuriose tokia FAS ir FAO sąveika nepasireiškia, tokiose kaip BT-474, citozolinio NADPH produktyvumas yra mažesnis, ir dėl to jos yra jautresnės staigiam ROS kiekio padidėjimui. Tai gali būti viena iš stipresnio staurosporino poveikio, pastebėto BT-474 ląstelėse, priežasčių, lyginant su BCC, kuomet sukėlė didesnę mitochondrijų membranos potencialo depoliarizaciją. Tai rodo, kad BCC yra atsparesnės oksidaciniam stresui, lyginat su sveikomis.

Analizuodami 289 mikrogardeles ir 50 RNR sekvenavimo mėginių iš 100 skirtingų navikinių ir 6-ių sveikų besidalijančių ląstelių linijų, pastebėjome, kad navikinių ląstelių linijoms būdingi du skirtingi transkripcinio reguliavimo laukai, apimantys šimtus genų. Pirmasis yra susijęs su EMT ir yra daug intensyvesnis navikinėse ląstelių linijose ir MSC, negu epitelio kamieninėse ląstelėse. Manoma, kad pagrindiniai šio lauko varikliai yra transkripcijos veiksniai SP1, LEF1 ir FOXO4. Jau žinoma, kad SP1 dalyvauja EMT, o mūsų analizė parodė, kad tarp genų, kurių raišką didina SP1, yra 9 Wnt

signalo perdavimo kelio komponentai, kurių aktyvacija lemia β-katenino fosforilinimą, apjungiantį LEF1 ir FOXO4 koduojamus transkripcijos veiksnius, lemiančius tikslinių genų raiškos padidėjimą. Tai rodo teigiamą aktyvavimo grįžtamąjį ryšį, kuris apima SP1, kanoninį Wnt signalo perdavimo kelią ir FOXO4, lemiančius plataus masto transkripcijos pokyčius. Parodyta, kad perėjimą tarp dviejų alternatyvių ląstelių būsenų – epitelinės ir mezenchiminės – reguliuoja transkripcijos veiksnių rinkiniai, sudarantys grįžtamojo ryšio struktūras [135].

Penki fermentai (BCAT2, DBT, DLT, HADHA ir HIBADH), dalyvaujantys leucino, valino ir izoleucino degradacijoje, priklauso transkripcinio reguliavimo laukui, susijusiam su EMT, nors jų pačių SP1 tiesiogiai nereguliuoja. Šis pastebėjimas genų raiškos lygyje buvo patvirtintas fermento BCAT2 baltymo lygyje navikinių ląstelių linijoje MCF-7 ir BCC pirminėje kultūroje (stebėtas aukštas BCAT2 lygis) bei ASM ir MCF-10A ląstelėse, kuriose stebėtas žemas BCAT2 lygis. Navikinės ląstelės didelę dalį ATP (nuo 12 iki 55 proc.) gauna BCAA degradacijos metu. Tai apskaičiuota panaudojus GSMM ir eksperimentinius NCI-60 bibliotekos ląstelių metabolitų įsisavinimo duomenis. BCAT2 geno nutildymas reikšmingai sumažino MCF-7 ir BCC proliferaciją, tačiau neturėjo įtakos ASMC proliferacijai. Taip pat neturėjo poveikio nei navikinių, nei sveikų ląstelių gyvybingumui. Tai rodo, kad BCAT2 veikia selektyviai ir kad egzistuoja terapinis langas, kurį būtų galima panaudoti, kuriant citostatinius vaistus, nukreiptus į navikines ląsteles, ir tikintis mažesnio poveikio sveikoms besidalijančioms ląstelėms.

Mūsų eksperimentai su BCAT2 parodo, kaip aprašyti transkripcijos požymiai gali būti panaudoti kaip terapinis langas, selektyviai nukreipiant į navikines ląsteles, išlaikant nepažeistas sveikas besidalijančias ląsteles.

IŠVADOS

1. Ląstelės, išskirtos iš pirminio naviko, pasižymėjo navikinėms ląstelėms būdingomis sąvybėmis – aukšta proliferacija ir gyvybingumu, atsparumu oksidaciniam stresui – bei leido plačiai naudojamų navikinių ląstelių linijose gautas išvadas pritaikyti realių navikų ląstelėms.

2. Panaudojant GSMM ir RNR sekvenavimo duomenis bei atliekant sveikų ir navikinių ląstelių metabolinių srautų analizę, galima nustatyti personalizuotą terapinį langą, kuris leistų priešvėžiniams vaistams preferentiškai veikti navikines ląsteles, maksimaliai išvengiant nepageidaujamo šalutinio poveikio sveikoms ląstelėms. Lipoamido struktūrinis analogas Amb19149142 buvo naudojamas kaip susintetintas junginys įvertinti terapinį langą. Junginys MCF-7 ląstelių proliferaciją mažino, tačiau ASMC reikšmingo poveikio neturėjo.

3. SP1 transkripcijos veiksnio ir Wnt signalinio kelio sąveika turi įtakos vėžinių ląstelių EMT. EMT taip pat yra susijusi su fermentų, dalyvaujančių BCAA degradacijoje, raiškos padidėjimu. Vieno iš šių fermentų – BCAT2 – nutildymas selektyviai veikė navikinių MCF-7 ir BCC proliferaciją ir neturėjo poveikio sveikoms ASMC ir MCF-10A ląstelėms. BACAT2 nutildymas neturėjo įtakos ląstelių gyvybingumui.

4. Eksperimentiškai patvirtinome, kad ^{13}C žymėjimo eksperimentai tinka riebalų rūgščių oksidacijos pokyčiams matuoti. BCC ląstelėse ~6 proc. citrato buvo pilnai žymėta ^{13}C ir jo kiekis mažėjo, nutildant minėtus genus prieš FASN ir ECHS1 kurie atitinkamai dalyvauja FAS ir FAO. Tai patvirtina, kad dalis visiškai pažymėto citrato susidaro per hipotetinį FAS ir FAO mechanizmą.

SUMMARY

ABBREVIATIONS

7-AAD	–	7-aminoactinomycin D
ASMCs	–	Airway smooth muscle cells
ATP	–	Adenosine-5'-triphosphate
BCAAs	–	Branched-chain amino acids
BCAT2	–	Mitochondrial branched-chained amino acid transferase 2
BCCs	–	Breast cancer cells
BT-474	–	Human breast ductal carcinoma cell line
CD24/44	–	cluster of differentiation
DBT	–	Dihydrolipoamide branched-chain transacylase
DLT	–	Dihydrolipoyl transacetylase
DMEM	–	Dulbecco's Modified Eagle Medium
DNA	–	Deoxyribonucleic acid
ECHS1	–	Enoyl-CoA hydratase
EMT	–	Epithelial-mesenchymal transition
ER	–	Estrogen receptor
FADH	–	Reduced form of flavin adenine dinucleotide
FAO	–	Fatty acid oxidation
FAS	–	Fatty acid synthesis
FASN	–	Fatty acid synthase
FBS	–	Fetal bovine serum
FOXO4	–	Forkhead box protein O
GSMM	–	Genome Scale Metabolic Model
HADHA	–	Hydroxyacyl-CoA dehydrogenase trifunctional multienzyme complex subunit alpha
HER2	–	Human epidermal growth factor receptor 2
HIBADH	–	3-hydroxyisobutyrate dehydrogenase
Ki-67	–	Cell proliferation marker
LEF1	–	Lymphoid enhancer-binding factor 1
MCF-7	–	Human breast adenocarcinoma cell line
ME	–	Malic enzyme
NADH	–	Reduced form of nicotinamide adenine dinucleotide
NADPH	–	Reduced form of nicotinamide adenine dinucleotide phosphate
PR	–	Progesterone receptor
PDH	–	Pyruvate dehydrogenase
RNA	–	Ribonucleic acid
ROS	–	Reactive oxygen species
siRNA	–	Small interfering RNA
SP1	–	Specificity protein 1
TCA	–	Tricarboxylic acid
Tp53	–	Tumor protein p53

INTRODUCTION

Side effects caused by chemotherapy are one of the biggest problems. Most drugs used in chemotherapy target DNA replication or key regulators of the cell cycle, which adversely affects not only malignant cells, but also healthy proliferating cells (including stem cells), resulting in impaired regeneration and healthy tissue function [136]. To avoid or reduce side effects, it is necessary to identify systemic differences between tumor and healthy cells and to calculate therapeutic windows for potential drugs. Genomics, transcription, proteomics, and metabolomics research technologies, such as cDNA microarrays and RNA sequencing, have accumulated large amounts of information in databases that can be used to identify systemic differences between healthy and tumor cells. Transcriptional differences are expected to provide a basis for targeted therapy that uses drugs designed to "target" cancer cells without affecting normal cells.

Tumors originate from the transformation of normal cells through the accumulation of genetic modifications [2, 3]. Studies on the RNA sequence of human tumors have revealed hundreds of mutations associated with tumor occurrence [4], but very few mutated genes have been repeated in large fractions of test samples. Specifically, in each cancer type about 4 genes were altered in more than 20% of the tumors analyzed [5]. The TP53 tumor suppressor and DNA damage checkpoint gene was among the most frequently mutated genes in all tumour types examined [6]. Despite the high heterogeneity of genes that cause malignant transformations, cancer can be characterized by basic hallmark capabilities, distinct and supplementary: sustaining proliferative signaling, evading growth suppressors, enabling replicative immortality, activating invasion and metastasis, inducing angiogenesis and resisting cell death [7]. These signs are associated with transcriptional changes that do not exist in healthy cells. To assess these differences we analyzed large amounts of gene expression data from healthy and tumor cells and experimentally demonstrated that inhibition of branched chain amino acid transaminase 2 (BCAT2) can be used as a therapeutic window to provide a selective action on tumor cells.

Cytosolic fatty acid synthesis (FAS) and fatty acid oxidation (FAO) have been shown to play a role in the survival and proliferation of cancer cells. Further studies using ^{13}C-labeled glutamine sought to determine whether these two processes coexisted in breast tumor cells.

Aim of the study

Analysis of metabolic and transcriptional differences in healthy and tumor cells and search of antitumor targets using fluxomic methods.

Objectives of the study

1. To develop the primary breast cancer cell culture.
2. To identify a therapeutic window by performing analysis of transcriptional differences between healthy and tumor cells.
3. To experimentally evaluate the therapeutic window by the inhibition of branched-chain amino acid transaminases 2 in healthy and tumor cells.
4. To determine the influence of the interaction of fatty acid synthesis and oxidation on the viability of tumor cells using ^{13}C-labeled glutamine.

Novelty of the study

Cancer cells are characterized by the Warburg effect. The Warburg effect consists in the lactic fermentation of glucose even at high oxygen concentrations. This effect was initially believed to be due to defects in cancer cell mitochondria; however, this hypothesis has proven to be wrong, as mitochondria have been shown to be functional and cancer cells cannot survive in fully anaerobic conditions, which proves that they are still dependent on oxidative phosphorylation. Recent studies have shown that the mitochondria of cancer cells function well and both oxidative phosphorylation and lactic fermentation are important for energy production [8].

We hypothesized that in cancer cells, most of the adenosine triphosphate (ATP) is obtained using alternative substrates that are amino acids. We used Genome Scale Metabolic Model (GSMM) in order to quantify the impact of alternative energy source. Based on the results of this analysis, we found that 50% of ATP in the MCF-7 cell line is derived from branched-chain amino acids (BCAAs): valine, leucine, and isoleucine.

We used siRNA that inhibits the expression of enzyme BCAT2, which catalyzes the first stage of degradation of valine, leucine, and isoleucine. We found that silencing of this gene reduced tumor cell proliferation. There are two main interpretations of the functions of FAO in cancer cells. The first is that FAO can only have a protective function in the presence of metabolic stress, when the loss of adhesion to the extracellular matrix impairs glucose uptake and catabolism [9].

Under such conditions, FAO would work as an alternative source of ATP [10] or NADPH [11] and FAS would have negative effects on cell survival as it would increase ATP and NADPH consumption [11]. Alternatively, FAO and FAS have been suggested to occur simultaneously and support each other. This hypothesis is also supported by the fact that the treatment of cells with orlistat, an inhibitor of lipid synthesis, resulted in decreased oxygen

consumption rates [13], which was explained by the simultaneous lipid synthesis and oxidation in cells. However, the available evidence is still circumstantial. In this work, we aimed to directly verify the existence of FAS and FAO by performing metabolic flow analysis using ^{13}C-labeled glutamine and gene silencing using siRNA. We also demonstrated that cells that undergo FAO and FAS simultaneously were less sensitive to oxidative stress.

METHODS

Cell isolation

Breast cancer cells (BCCs) were isolated from a solid block of tissue. Data were obtained from patients' medical records.

The approval to conduct the study was issued by Kaunas Regional Biomedical Research Ethics Committee (permission No. P2-137 / 2006; date of issue: December 8, 2017).

BCCs were prepared from part of the tumor tissue sample taken from a female patient suffering from invasive ductal carcinoma (T1 N0 M0 G2, ER(+), PR(+), HER2(3+)) during lumpectomy and sentinel lymph node biopsy.

The carcinoma tissue sample was cut with scissors into smaller pieces with 2 ml phosphate buffer. Cells were treated with 0.025% trypsin or with 0.025% trypsin and 150 U/mL collagenase (type III) or with the following enzymes: 0.05% trypsin, 125 U/mL collagenase type (III) and 8 U/mL proteinase K or 125 U/mL collagenase type (III) and 408 U/ml hyaluronidase (IV-S). Then they were shaken at 37 °C for 1 h at 350 rpm and centrifuged (420 g) for 5 min. After washing with the Dulbecco's Modified Eagle Medium (DMEM), BCCs were seeded into flasks with a growth medium and incubated at 37°C in a humidified atmosphere of 5% CO_2.

Primary cell cultures were isolated from samples treated with 0.025% trypsin, 0.05% trypsin, or 150 U/mL collagenase (type III). BC4 cells (infiltrative ductal carcinoma ER(+) PER(+) HER2(+)), hereinafter referred to as BCC line, were used for further experiments.

Freezing of cells

The medium was discarded from the cells, washed twice with PBS, and added to 0.05% trypsin solution. The cells were then transferred to a tube and centrifuged at 420 g for 5 min. The supernatant was discarded, and the cells were added to a cooling medium consisting of 75% DMEM/Ham's F12, 15% fetal bovine serum (FBS) and 10% dimethyl sulfoxide. The cells were suspended in a cooling medium, and the suspension was transferred to a cryotube, which was kept at –20°C, and when ice crystals formed, was transferred to –80°C.

Cell lines and culture medium

BCC, BT-474 (human breast ductal carcinoma cell line; ATCC HTB-20, Manassas, VA, USA), and MCF-7 (human breast adenocarcinoma cell line; CLS-Cell Lines Service, Eppelheim, Germany) were cultivated in DMEM/F12 medium with 10% FBS and 1% antibiotics (100 U/ml penicillin/streptomycin). Immortalized human airway smooth muscle cells (ASMCs) were grown in a DMEM medium supplemented with 10% FBS and mix of antibiotics (100 U/ml penicillin/streptomycin). MCF-10A cells (ATCC, Wesel, Germany) were grown in DMEM/F-12 medium supplemented with 5% horse serum (GE Healthcare Life Sciences, Logan, USA), 20 ng/ml EGF (Life technologies, Carlsbad, CA, USA),10 μg/mL insulin (Life technologies, Carlsbad, CA, USA), 0.5 μg/mL hydrocortisone, and 100 ng/mL cholera, toxin and penicillin/streptomycin mix. Cells were maintained in a 5% CO2 humidified incubator at 37°C.

For treatment with staurosporine (Calbiochem, Darmstadt, Germany), cells were incubated for 4 h with 0.25 μM of the latter compound.

Cell proliferation assay by Trypan blue test

Cells (1.5×10^4) were seeded in 6-well plates. Cells were supplemented with various concentrations of Amb19149142 (20, 50, 100 μM) (GreenPharma, France) dissolved in 0.1% ethanol solvent. A volume of 50 μl 0.4% trypan blue dye dissolved in saline (Life technologies, Carlsbad, CA, USA) was added to a tube with 50 μl of cell suspension. Cell suspension with the dye (10 μl) was pipetted into a hemocytometer chamber (Neubauer), (Sigma-Aldrich, Steinheim, Germany). Measurements were taken after 120 h.

siRNA transfection

We used a jetPRIME transfection reagent (Polyplus-transfection® SA, France) and siRNAs for gene silencing according to the manufacturer's instructions. Final concentrations of 10 nM ECHS1 siRNA (ATGATGTGTG ATATCATCTAT; Qiagen, Germantown, MD, USA) or fatty acid synthase (FASN) siRNA (CAGGCTTCAGCTCAACGGGAA; Qiagen) were used. Cells were simultaneously transfected with three different siRNAs against the different malic enzyme (ME1, ME2, and ME3) genes: 4 nM ME1 (UGCCAU GACUCAGCGUUCtt; Ambion, Waltham, MA, USA), 4 nM ME2 (GGGUG UCUAUGGAAUGGGAtt; Ambion), and 4 nM ME3 (GCCUUUACCCUU GAAGAAAtt; Ambion). All following procedures were performed 24 h after siRNA transfection. Mock transfection was used as control.

^{13}C labeling

Cells were incubated in DMEM without glucose, L-glutamine, and pyruvate (Sigma, Schnelldorf, Germany), supplemented with 10% FBS and antibiotics. L-Glutamine-$^{13}C_5$ (Aldrich, Hamburg, Germany) was added to the final concentration of 4 mM. Cells were incubated for 24 h.

Metabolic flux distribution

We used the elementary metabolic units (EMU) system to distribute the metabolic flow [126]. Seven independent reaction rates were indicated in the model. One of them – pyruvate dehydrogenase (PDH) rate – was detected at 1 and all other reactions were compared to the amount of PDH. The remaining independent reactions were rates of fatty acid oxidation; malate dehydrogenase; α-ketoglutarate formation derived from glutaminolysis; α-ketoglutarate carboxylation; pyruvate carboxylase; and pyruvate import into the mitochondria. All parts by weight of the labeled malate and citrate were measured from M0 to M6, and the sum of the relative differences between the model and the experimental results was reduced. Before determination, identifycation analysis was performed by calculating the value of the Jacobo matrix of the system to measure how linearly the columns of this calculator are. A minimum single value of zero would mean that there are many different distributions of metabolic flow resulting in the same labeling patterns; therefore, so the system cannot be determined. In order to evaluate the contribution of each metabolic flow to the system identifiable, new Jacobo matrices were calculated by subtracting the column corresponding to the verified change in the metabolic flow and performing the decomposition of the individual values of the new matrix. The higher the new minimum value, the more difficult it was to determine the value deducted. The FAO (the most interesting in this work) was the most difficult to identify. To avoid this problem, we performed a global optimization of experiments corresponding to mock transfection and FASN and ECHS1 silencing. This approach is based on the assumption that siRNA does not affect all independent effects except FAO. The rate of α-ketoglutarate carboxylation also allowed us to change our conditions, as this change in metabolic flow was reported to be very sensitive to small perturbations in α-ketoglutarate and citric acid concentrations.

The determination of the values corresponding to the silencing of ME was performed by fixing the FAO indicator and allowing the modification of all other parameters. After treatment with staurosporine, there was a distribution that allowed for an exchange of all independent reactions. For each presentation, the values of all metabolic flow values were sequentially increased or decreased by 0.001 (preventing them from taking negative values). If

this increase resulted in a decrease in the objective function, the new values were considered and the process was repeated. Different initial size distribution sets and retention were used to determine the minimum relative error.

UPLC-ESI-MS conditions

Mass spectrometry (MS) analysis of metabolites labeled with L-glutamine-$^{13}C_5$ was performed by tandem mass spectrometry. Separation of organic acids in the samples was performed using an Acquity Class H UPLC system (Waters, Milford, MA, USA) with a YMC-Triart C18 (100 × 2.0 mm, 1.9 μm) column (YMC, Kyoto, Japan). A Xevo TQD triple quadrupole tandem mass spectrometer (Waters, Milford, MA, USA) with an electrospray ionization (ESI) source was used to obtain MS data. The column temperature was maintained at 40°C. The gradient elution was performed with a mobile phase consisting of 0.1% aqueous formic acid solution (solvent A) and acetonitrile (solvent B) at an air flow rate of 0.4 mL/min. Initial conditions were set at 95% solvent A. The linear gradient profile was adjusted in the following proportions of solvent A: 0–0.2 min was found to be 95%; 0.2–1.5 min, 10%; and 1.5–1.8 min, 90%, and returned to the original conditions. The total time for equilibrium analysis was 3 min. Negative ionization of electric spraying was performed by using the following parameters: capillary voltage was set to negative 2 kV; source temperature, at 150°C; desulfurization temperature of supplied nitrogen gas, at 400°C; desolvation gas flow, 700 L/h; and gas turnover, 20 L/h. The cone voltage was set at 25 V. MS data were collected in a full scan mode from 50 m/z to 250 m/z. The obtained mass spectra were used to determine the distribution of metabolic flows using the EMU method [126]. This was done through programming in Python.

Flow cytometry assay

Initially, 5×10^4 cells were seeded in 35 mm dishes in 2 mL of full media. Mock-transfected and siRNA-transfected cells were incubated with media containing 1 mg/L JC-1 dye (Biotium, Fremont, CA, USA) for 20 min at room temperature. Afterwards, cells were washed with PBS, trypsinized, and collected using centrifugation. Then cells were resuspended in PBS with 5 mg/L 7-aminoactinomycin D (7-AAD) dye (Millipore, Burlington, MA, USA) and incubated for 10 min. For positive control, 10 μM of carbonyl cyanide m-chlorophenylhydrazone was used. Samples were quantified using a Guava PCA flow cytometer (Millipore). The data were analyzed by the GuavaSoft 2.7 InCyte software. Mitochondrial membrane potential was expressed as the ratio of JC-1 aggregates (red fluorescence) to monomers (green fluorescence) (R/G).

Western blot analysis

Primary antibodies were used for immunocytochemistry and immune-blotting analysis: rabbit anti-PPAR delta (ThermoFisher Scientific, cat # PA1-823A), rabbit anti-histone H3 (ThermoFisher Scientific, cat # 702023), mouse anti-beta-catenin (ThermoFisher Scientific, cat # CAT-5H10), mice against GAPDH (Ambion, cat # AM4300), rabbit against BCAT2 (Abcam, cat # ab95976). Secondary donkey anti-rabbit IgG H&L antibody was conjugated to Alexa Fluor 488 (Life technologies, cat # A21206).

For Western blot, BCCs (3×10^6) were lysed in ice-cold cell extraction buffer (Invitrogen, Carlsbad, CA, USA) supplemented with a 20 µl/mL protease inhibitor cocktail (Sigma-Aldrich, Germany) and 1 mM PMSF (Abcam, Cambridge, JK) for 30 min. The lysates were centrifuged at 13,000 rpm for 10 minutes at 4°C. The Qubit® protein assay kit (Invitrogen) was used to determine the total protein concentration with a Qubit 3.0 fluorometer (Invitrogen). Cell lysates (30 µg) were separated by Bolt™ 4%–12% Bis-Tris and gels (Invitrogen) in MES SDS flowing buffer and transferred to 0.45 polyvinylidene fluoride (PVDF) membranes (GEHealthcare, UK). Proteins were detected using primary antibodies in ECHS1 (ab174312), FASN (ab99359) and BCAT2 (ab95976) (Abcam), PPAR-δ (PA1-823A), ME1 (MA5-23524), ME2 (PA5-38007), ME3 (PA5-36494) and GAPDH (AM43) (Fisher Science, USA) and WesternBreeze®chemiluminescence kits (Invitrogen) according to the manufacturer's instructions. The bands were visualized using the G: Box Chemi Gel documentation system (Syngene, Frederick, MD, USA).

Statistical analysis

All experiments with cells were performed in at least 3 replicates (n = 3). In the simulation experiments, the error bars correspond to the standard errors when the two experiments were compared to each other. When the predicted isotopomer distributions were compared with the calculated ones, the error bands for the experimental values correspond to 95% confidence intervals. A comparison of the two values was performed using the Student's t test. The level of significance was set at $P<0.05$. Statistical analysis was performed using Excel and the scipy.stats library.

RESULTS

Development and characterization of primary culture of breast cancer cells

Cells were isolated as described in Methods using the standard protocols [128]. CD44 and CD24 are transmembrane glycoproteins. CD24 expression is observed in tumor cells and this marker acts as a specific hyaluronic acid receptor that promotes the movement of malignant cells. The CD44 marker in BCCs is in active form and is involved in many intracellular signaling cascades as well as in cell proliferation, differentiation, and motility. Ki-67, a cell proliferation marker, is a non-histone nuclear protein used as a marker of cell proliferation. High levels of Ki-67 are characteristic of tumor cells and are associated with poor disease prognosis and good response to chemotherapy.

Lipoamide structural analog

We experimentally showed how Genome Scale Metabolic Models (GSMMs) can be used as tools for drug design. New metabolite-like inhibitors can be searched in available metabolite databases. New inhibitors are molecules that bind to a biological target and inhibit its biological function. The Tanimoto score is a numerical similarity between so-called fingerprints of molecules. The Tanimoto score is expressed from 0 (no similarity) to 1 (high similarity). After calculating and evaluating the Tanimoto score, a new inhibitor similar to one of the metabolites was found to bind to the target whose substrate is a said metabolite.

We compared the chemical structures and compounds of human metabolites (derived from their KEGG indices) in the DrugBank database. Compounds with a Tanimoto score greater than 0.9 increase 29.5-fold the likelihood that the analyte will bind to the same target as a similar metabolite rather than a randomly selected molecule. Using RNA-seq data and human GSMM, it is possible to estimate the distribution of metabolic fluxes and measure changes in metabolic fluxes (e.g., using a drug that inhibits catalytic enzymes). This method allowed predicting the different effects of lipoamide analogs on the proliferation of MCF-7 (breast cancer cell line) and ASMCs (airway smooth muscle cells) [129]. The experiments required a synthesized compound that could be obtained. Lipoamide is an intermediate product in the degradation of valine, leucine, and isoleucine, which produces a large proportion of the ATP required by tumor cells.

Degradation of branched-chain amino acids (valine, leucine and isoleucine)

Tumor cells produce a large proportion of ATP during BCAA degradation. To quantify this method, we used GSMM and experimental data on the uptake of cellular metabolites by the NCI-60 library [130, 131]. For each cell line, we calculated a flow distribution that satisfies the observed uptake and secretion rates, minimizing the sum of all metabolic flows. From the obtained flow distribution, we estimated the total production of ATP. Experimental lactic acid production rates and consumption rates of each BCAA were used to compare ATP production during these processes. It was found that 12% to 55% of the total ATP was formed by the degradation of BCAAs.

Tumor cells differ from healthy ones by increased expression of 5 enzymes involved in valine degradation (BCAT2, dihydrolipoamide branched-chain transacylase (DBT), dihydrolipoyl transacetylase (DLT), hydroxyacyl-CoA dehydrogenase trifunctional multienzyme complex subunit alpha (HADHA), and -hydroxyisobutyrate dehydrogenase (HIBADH)); 4 of them, in isoleucine degradation (BCAT2, DBT, DLT, and HADHA); and 3, in leucine degradation (BCAT2, DBT, and DLT). The five enzymes mentioned are not directly regulated by specificity protein 1 (SP1), but their mode of expression is identical to that of EMT-associated genes, suggesting that BCAA cleavage is promoted by regulatory cascades associated with EMT.

The results of the analysis of 289 microarrays showed that tumor cells showed two significant transcriptional changes compared to healthy cells: an increase in the expression of Wnt-regulated genes and a decrease in the expression of activator protein 1 (AP-1)-regulated genes. The EMT of tumor cells is affected by the interaction of the SP1 transcription factor and the Wnt signaling pathway. EMT is also associated with an increase in the expression of enzymes involved in the degradation of BCAAs (valine, leucine and isoleucine). We investigated the effect of silencing one of these enzymes, i.e., BCAT2.

BCAT2 catalyzes the first step of degradation of valine, leucine, and isoleucine. An increase in BCAT1 and BCAT2 expression is documented in a variety of tumor cells, but an increase in BCAT2 expression and effects in BCCs remain unclear. We included BCCs in our experimental design to determine if the findings obtained in widely used tumor cell lines could be extrapolated to real tumor cells. ASMC and MCF-10A cell lines were selected as healthy cells. An immunofluorescence study showed that BCAT2 levels were significantly higher in tumor cells than healthy cells.

SiRNA against BCAT2 reduced tumor cell proliferation, but did not affect the proliferation of healthy cells. MCF-7 and BCC counts decreased by

16.6% ± 2.1% and 11.3% ± 1.5%, respectively. The number of ASMCs and MCF-10A cells did not change (99% ± 0.8% and 106% ± 3.4%, respectively).

Flow cytometry using annexin V-PE/7-AAD showed that siRNA against BCAT2 had no effect on the viability of tumor or healthy cells.

These results suggest that BCAT2 may be a suitable target for new drugs to achieve cytostatic effects on cancer cells.

Assessment of simultaneous fatty acid synthesis and oxidation using ^{13}C labeling

Tumor cell viability and proliferation are affected by cytosolic FAS and mitochondrial FAO. To test the hypothesis that FAS and FAO occur simultaneously in tumor cells, we used ^{13}C-labeled glutamine to assess their oxidation level. Fatty acids are synthesized from cytosolic acetyl-CoA, which itself is mainly derived from citric acid. Citric acid is derived from the tricarboxylic acid (TCA) cycle and transported to the cytosol, but also can be obtained from glutamine by reducing the carboxylation of α-ketoglutarate. FAO occurs in mitochondria (fatty acids are transported from the cytosol via a transporter) to produce mitochondrial acetyl-CoA, which feeds the TCA cycle. In a combination of these processes, part of the acetyl-CoA that feeds the TCA cycle is derived from citrate. Labeled ^{13}C glutamine through reductive carboxylation marks five carbon atoms in citrate and labels cytosolic acetyl-CoA in further lipid synthesis. If these lipids are being simultaneously degraded at the same time, labeled acetyl-CoA will enter the TCA cycle to form fully labeled citric acid molecules (M6 isotopomer).

A metabolic model with atomic transitions, showing how fatty acids are degraded by glutamate or ME activity, can form the M6 citrate isotopomers. The scheme depicts the jump of redox potential from cytosolic NADPH to mitochondria resulting from the simultaneous occurrence of FAS and FAO.

A stronger FAO should correspond to a higher citrate fraction with 6 labeled carbon atoms. To test whether the rate of beta fatty acid oxidation can be assessed by citrate labeling, we silenced FASN, acetyl-CoA hydratase (ECHS1), which is involved in beta oxidation, and malate dehydrogenase (ME), which atoms are labeled independently of lipid metabolism. MCF-7, BT-474, and BCCs were used for the assays. Labeled pyruvate derived from malate under the action of ME forms a fully labeled citrate.

Therefore, to assess whether lipid metabolism actually plays an important role in the formation of fully labeled citrate, we additionally performed gene silencing using siRNA. To verify the existence of FAS and FAO, a BCC line was selected at the same time because the other two cell lines, MCF-7 and BT-474, had significantly lower levels of fully labeled citrate. The

percentage of M6 citrate in MCF-7 and BT-474 was 1.15% and 0.5%, respectively.

Cells were incubated with ^{13}C-labeled L-glutamine. BCCs had 5 and 10 times more labeled citrate than MCF-7 and BT-474 cells, respectively, making FAS and FAO more likely to occur simultaneously in BCCs.

BCCs were transfected with siRNA against the FASN and ECHS1 genes involved in FAS and FAO, respectively. Cells were also transfected with siRNA against the ME (1–3) genes to assess the importance of ME for the formation of fully labeled citric acid. SiRNA against FASN and ECHS1 resulted a very similar decrease in M6 fraction, which was statistically significant in both cases (from 5.8% ± 0.3% to 4.2% ± 0.2%, n = 4, $P = 0.0054$; and 4.2% ± 0.3%, n = 4, $P = 0.0065$; respectively). This confirms that part of the fully labeled citrate was formed through the hypothetical mechanism of FAS and FAO. siRNA against ME induced an even greater drop to 2.4% ± 0.3% (n = 4, $P = 0.0001$), which suggests that both mechanisms of fully labeled citrate formation are active. In BCCs, ~6% of citrate was fully ^{13}C-labeled and decreased by silencing the aforementioned genes. To assess protein expression, a WB assay was performed after transfection of siRNA against FASN, ECHS1, and ME (1–3) genes and a decrease in protein expression in all cells compared to control transfection was documented.

Assessment of simultaneous FAS and FAO using measurements of mitochondrial membrane potential

FAS and FAO are manifested by the transfer of reducing potential from cytosol (NADPH) to mitochondria (NADH and FADH2). The synthesis of biomass components and resistance to oxidative stress associated with glutathione reductase and glutathione peroxidase depend on cytosolic NADPH. Increased ROS production should result in a decrease in cytosolic NADPH and a halt in FAS and other processes that require NADPH. Exposure of BCCs to staurosporine, which significantly increases ROS levels, results in a significant decrease in fully labeled citrate due to arrested FAS. This means that under normal conditions, BCCs produce more cytosolic NADPH than is required for biosynthesis processes. During low oxidative stress, excess reductive potential is transferred to mitochondria, where it is used for ATP production, and during high oxidative stress, it is used to eliminate cytosolic ROS.

During FAS, fatty acids are created from acetyl-CoA and two NADPH molecules. Mitochondrial FAO results in the generation of one NADH and one FADH2 molecule per acetyl-CoA, both of which can be used to feed the respiratory chain. This results in a transfer of redox potential from the cytosol

to mitochondria, which can be used to maintain a higher mitochondrial membrane potential. ME catalyzes the reaction of NADPH production that cannot take place in the respiratory chain. Therefore, if FAS and FAO occur simultaneously, silencing of FASN or ECHS1 can be expected to decrease $\Delta\psi m$, while after silencing of ME, $\Delta\psi m$ should not be affected. Mitochondrial potential was assessed by flow cytometry using JC-1 staining. Cells transfected with siRNA against FASN and ECHS1 showed significant drops in the mitochondrial membrane potential from 10.9 ± 0.7 to 6.9 ± 0.7 ($n = 3$, $P = 0.014$) and 7.5 ± 0.1 ($n = 3$, $P = 0.009$), respectively. Cells transfected with siRNA targeting ME did not show a significant drop in the membrane potential (9.2 ± 0.8; $n = 3$; $P = 0.19$). FASN and ECHS1, but not ME, reduced the mitochondrial potential in BCCs.

Metabolic flux analysis of breast cancer cells

Citrate and malate labeling techniques were used to adjust the distribution of metabolic flow in the central carbon metabolism. Metabolic flux distribution was calculated using a model involving the TCA cycle, FAS, FAO, glutaminolysis, reducing α-ketoglutarate carboxylation, malate dehydrogenase, pyruvate carboxylase, and PDH. The mitochondrial and cytosolic pools of citrate and α-ketoglutarate were treated as if these compounds were freely transferred across the mitochondrial membrane. Cytosolic oxaloacetate produced by citrate lyase is thought to be transported back to mitochondria. An EMU approach was used to model isotope distribution. The adaptation was performed by minimizing the relative errors between the experimental and predicted labeling samples. The flow distribution is expressed relative to the rate of PDH flow. The distribution of metabolic flow is monitored using a control experiment and experiments with siRNA (FASN, ECHS1, and ME). The metabolic flux of FAS and FAO in the control is 0.69, as in that of pyruvate dehydrogenase, and 0.48 in the ME reaction. In cells transfected with siRNA against FASN or ECHS1, the relative distribution of isotopomers corresponded to zero flux in the FAO reaction. When transfecting siRNA against ME genes, the calculated flux of the ME reaction was 0.03. The reduced fraction of M6 citrate isotopomers indicates reduced FAS, FAO, or ME activity. Distributions of malate isotopomers are mainly determined by the rate of glutaminolysis and are not expected to be modified by changes in FAS, FAO, and ME.

Effects of oxidative stress on metabolic fluxes

The metabolic cycle of FAS and FAO is manifested by the transfer of reducing potential from cytosol (NADPH) to mitochondria (NADH and $FADH_2$). The synthesis of biomass components and the resistance to oxidative stress associated with glutathione reductase and glutathione peroxidase depend on cytosolic NADPH. Increased ROS production is expected to result in the depletion of cytosolic NADPH and, subsequently, in the termination FAS and other processes that require NADPH. BCCs treated with staurosporine, which significantly increases ROS levels, resulted in a significant decrease in fully labeled citrate, which is consistent with the expected arrest of FAS. Under normal conditions, BCCs produce more cytosolic NADPH than it is necessary for their biosynthesis needs. Under conditions of low oxidative stress, the excess redox potential is transferred to mitochondria, where it is used for ATP production, while under conditions of high oxidative stress, it is used to eliminate cytosolic ROS.

Resistance of BCCs and BT-474 cells to oxidative stress

Cells in which FAS and FAO occur simultaneously have high cytosolic NADPH production rates and can inhibit oxidative stress. We compared the effects of staurosporine-induced oxidative stress on BCCs and BT-474 cells. BT-474 cells were used for the comparison as they had 10-times lower amount of M6 citrate than BCCs, which suggests that the loop formed by simultaneous FAS and FAO is not active in this cell line as confirmed by 13C experiments showing that the FAO flow rate is zero.

Staurosporine induced significantly stronger depolarization of mitochondrial membrane potential in BT-474 cells than BCCs: the R/G ratio changed 3.4 ± 0.4 and 1.8 ± 0.05 times, respectively ($P<0.001$). These results are consistent with our hypothesis that BCCs are more resistant to oxidative stress and that FAO could be a drug target in some types of tumors.

DISCUSSION

It has been shown that drug similarity to the natural substrates of metabolic enzymes (measured using Tanimoto scores) is a good predictor of the ability of a ligand to bind the chosen metabolic enzymes. One of the best known human biological networks is metabolism, as the knowledge accumulated from more than a century of biochemical research allows the precise definition of metabolic reactions catalyzed by each enzyme, and these reactions have a well-known stoichiometry. All of this stoichiometric information is in the GSMM, which describes metabolic capabilities of a cell. GSMM and RNA sequencing data and analysis of metabolic flows in healthy and tumor

cells have an important practical application. It is important to determine therapeutic windows that would allow affecting the metabolic capabilities of malignant cells while having milder effects on healthy cells. As a proof of concept, we have experimentally shown that the effect of a structural analogue of lipoamide can reduce the proliferation rate of the MCF-7 cell line without having a significant effect on healthy ASMCs.

It has long been thought that FAS and FAO cannot take place in a cell at the same time. FAO plays an important role in tumor cell survival. On the other hand, FAS is also necessary for tumor cell growth and proliferation. It is possible that FAO helps cells survive under metabolic stress in the absence of other energy sources and redox cofactors. Despite FAS and FAO have been traditionally considered incompatible due to the inhibitory effect of malonyl-CoA on the carnitine shuttle responsible for transporting fatty acids to the mitochondria, there is growing evidence to support the coexistence of both phenomena in tumor cells. In this work, we have shown that this phenomenon coexists in BCCs. The coexistence of FAS and FAO is confirmed by the effect of FASN and ECHS1 gene silencing on the amount of fully labeled citrate (when cells are supplied with ^{13}C-labeled glutamine) and mitochondrial membrane potential. Very small proportion of citrate was fully labeled (about 1%) in MCF-7 and BT-474 cells, but about 6% of citrate was completely ^{13}C-labeled and decreased after silencing of the above genes in BCCs. After the silencing of ME genes, the amount of ^{13}C-labeled citrate decreased even more, which indicates that the mechanisms of fully labeled citrate formation are active. Two NADPH molecules are oxidized from acetyl-CoA in the cytosol FAS. On the other hand, during FAO, acetyl-CoA and one molecule of NADH and $FADH_2$ are formed in mitochondria, both of which can be used to feed the respiratory chain. This results in a transfer of redox potential from the cytosol to mitochondria, which can be used to maintain a higher mitochondrial membrane potential. ME catalyzes a NADPH production reaction that cannot take place in the respiratory chain. Therefore, silencing of the FASN and ECHS1 genes decreased the mitochondrial membrane potential, and silencing of ME genes did not have any impact on the mitochondrial membrane potential. Blocking FAS, unlike blocking FAO, reduces the amount of fully labeled citrate and the mitochondrial potential in a very similar way. This is consistent with previous observations [132] in which the inhibition of lipid synthesis reduced oxygen consumption. A possible physiological role for this simultaneous occurrence of FAS and FAO is the shuttling of the reducing potential from cytosolic NADPH to mitochondria. This would allow cells to process the excess NADPH produced in the cytosol and direct its reducing potential into the respiratory chain. If cells are challenged by sudden increases of oxidative stress, this excess production of cytosolic

NADPH can be directed to eliminate ROS by stopping lipid synthesis. This phenomenon appears to occur in BCCs treated with staurosporine when a decrease in the fraction of fully labeled citrate is observed compared to the untreated cells. Metabolic cycles involving the oxidation of overproduced NADPH have been observed in microorganisms [133], where this apparent waste of energy can be exploited to increase resistance against sudden oxidetive stress. The case we present suggests that human cells may also use a similar mechanism. Meanwhile, cells such as BT-474 in which such an interaction between FAS and FAO does not occur, have lower production rate of cytosolic NADPH and are more sensitive to sudden increases in ROS. This may be one of the reasons for the stronger exposure to staurosporine observed with BT-474 compared to BCCs, which resulted in greater depolarization of mitochondrial membrane potential. This suggests that BCCs are more resistant to oxidative stress compared to healthy ones.

Analyzing 289 microarrays and 50 RNA sequencing samples from 100 different tumor and 6 healthy, dividing cell lines, we found that tumor cell lines are characterized by two distinct regulatory events involving hundreds of genes. The first is related to EMT and is much more intense in tumor cell lines and mesenchymal stem cells than in epithelial stem cells. The major drivers of this large-scale transcriptional pattern are thought to be the transcription factors such as SP1, lymphoid enhancer-binding factor 1 (LEF1), and forkhead box protein O (FOXO4). SP1 is already known to be involved in EMT, and our analysis revealed that among the genes up-regulated by SP1, there are 9 Wnt signaling pathway components whose activetion results in β-catenin phosphorrylation, which combines LEF1 and FOXO4 encoded transcription factors leading to up-regulation of their target genes. This suggests positive activation feedback, which includes SP1, canonical Wnt signaling pathway, and FOXO4, resulting in large-scale transcriptional changes. The transition between two alternative cell states, epithelial and mesenchymal, has been shown to be regulated by sets of transcription factors that form feedback structures [134].

Five enzymes (BCAT2, DBT, DLT, HADHA, and HIBADH) involved in the degradation of leucine, valine, and isoleucine belong to the transcriptional regulation associated with EMT, although they are not directly regulated by SP1. This observation at the gene expression level was confirmed at the level of the enzyme BCAT2 protein in the MCF-7 cell line and BCCs where high BCAT2 levels were observed as well as ASMCs and MCF-10A cells with low BCAT2 expression. Tumor cells receive a high proportion of ATP (12% to 55%) during BCAA degradation. This was calculated using GSMM and experimental NCI–60 library cell metabolite uptake data. Silencing of the BCAT2 gene significantly reduced MCF-7 and BCC proliferation, but did not affect ASMC proliferation. It also had no effect on the viability of

either tumor or healthy cells. This indicates that BCAT2 acts selectively. This suggests that there is a therapeutic window that could be potentially exploited to develop cytostatic drugs that target tumor cells selectively while keeping unaffected healthy dividing cells.

Our experiments with BCAT2 show how the described transcriptional traits can be used as a therapeutic window for selectively targeting tumor cells while maintaining intact healthy dividing cells.

CONCLUSIONS

1. The cells isolated from the primary tumor were characterized by high proliferation and viability as well as resistance to oxidative stress and allowed to extrapolate the findings obtained in widely used tumor cell lines to real tumor cells.

2. Using GSMM and RNA sequencing data and analyzing metabolic flows in healthy and tumor cells, a personalized therapeutic window can be identified. This is the possibility of inflicting damage on a particular cell type (such as tumor cells) while minimizing the negative effects on healthy cells. Amb19149142, a lipoamide structural analogue, was used as a synthesized compound to evaluate the therapeutic window. The compound reduced the proliferation of MCF-7 cells, but had no significant effect on ASMCs.

3. The EMT of cancer cells is affected by the interaction of the SP1 transcription factor and the Wnt signaling pathway. EMT is also associated with increased expression of enzymes involved in BCAA degradation. Silencing one of these enzymes, BCAT2, selectively affected the proliferation of MCF-7 and BCCs and had no effect on healthy ASMCs and MCF-10A cells. Silencing of BCAT2 did not affect cell viability.

4. We experimentally confirmed that ^{13}C labeling experiments are suitable for measuring changes in fatty acid oxidation. About 6% of the citrate was fully ^{13}C-labeled and decreased by silencing the genes against FASN and ECHS1 involved in FAS and FAO, respectively, in BCCs. This confirms that some of the fully labeled citrate is formed through the hypothetical mechanism of FAS and FAO.

BIBLIOGRAFINIS SĄRAŠAS

1. Li YM, Guo YP, Liu Y. Cancer chemotherapy induces cardiotoxicity by targeting cardiac stem cells. Journal of cellular and molecular medicine. 2010;14(11):2630-2.
2. Stuelten CH, Mertins SD, Busch JI, Gowens M, Scudiero DA, Burkett MW, et al. Complex display of putative tumor stem cell markers in the NCI60 tumor cell line panel. Stem cells (Dayton, Ohio). 2010;28(4):649-60.
3. Reya T, Morrison SJ, Clarke MF, Weissman IL. Stem cells, cancer, and cancer stem cells. Nature. 2001;414(6859):105-11.
4. Comprehensive genomic characterization defines human glioblastoma genes and core pathways. Nature. 2008;455(7216):1061-8.
5. Negrini S, Gorgoulis VG, Halazonetis TD. Genomic instability—an evolving hallmark of cancer. Nature reviews Molecular cell biology. 2010;11(3):220-8.
6. Petitjean A, Achatz MIW, Borresen-Dale AL, Hainaut P, Olivier M. TP53 mutations in human cancers: functional selection and impact on cancer prognosis and outcomes. Oncogene. 2007;26(15):2157-65.
7. Hanahan D, Weinberg RA. Hallmarks of cancer: the next generation. Cell. 2011;144(5): 646-74.
8. Porporato PE, Filigheddu N, Pedro JMB-S, Kroemer G, Galluzzi L. Mitochondrial metabolism and cancer. Cell Research. 2018;28(3):265-80.
9. Carracedo A, Cantley LC, Pandolfi PP. Cancer metabolism: fatty acid oxidation in the limelight. Nature reviews Cancer. 2013;13(4):227-32.
10. Schafer ZT, Grassian AR, Song L, Jiang Z, Gerhart-Hines Z, Irie HY, et al. Antioxidant and oncogene rescue of metabolic defects caused by loss of matrix attachment. Nature. 2009;461(7260):109-13.
11. Jeon SM, Chandel NS, Hay N. AMPK regulates NADPH homeostasis to promote tumour cell survival during energy stress. Nature. 2012;485(7400):661-5.
12. Caro P, Kishan AU, Norberg E, Stanley IA, Chapuy B, Ficarro SB, et al. Metabolic signatures uncover distinct targets in molecular subsets of diffuse large B cell lymphoma. Cancer cell. 2012;22(4):547-60.
13. Samudio I, Harmancey R, Fiegl M, Kantarjian H, Konopleva M, Korchin B, et al. Pharmacologic inhibition of fatty acid oxidation sensitizes human leukemia cells to apoptosis induction. The Journal of clinical investigation. 2010;120(1):142-56.
14. Schlaepfer IR, Rider L, Rodrigues LU, Gijon MA, Pac CT, Romero L, et al. Lipid catabolism via CPT1 as a therapeutic target for prostate cancer. Molecular cancer therapeutics. 2014;13(10):2361-71.
15. Tirado-Velez JM, Joumady I, Saez-Benito A, Cozar-Castellano I, Perdomo G. Inhibition of fatty acid metabolism reduces human myeloma cells proliferation. PloS one. 2012;7(9):e46484.
16. Cirri P, Chiarugi P. Cancer-associated-fibroblasts and tumour cells: a diabolic liaison driving cancer progression. Cancer metastasis reviews. 2012;31(1-2):195-208.
17. Pietras K, Ostman A. Hallmarks of cancer: interactions with the tumor stroma. Experimental cell research. 2010;316(8):1324-31.
18. O'Brien P, O'Connor BF. Seprase: an overview of an important matrix serine protease. Biochimica et biophysica acta. 2008;1784(9):1130-45.
19. Micke P, Ostman A. Tumour-stroma interaction: cancer-associated fibroblasts as novel targets in anti-cancer therapy? Lung cancer (Amsterdam, Netherlands). 2004;45 Suppl 2:S163-75.

20. Hasebe T, Tamura N, Iwasaki M, Okada N, Akashi-Tanaka S, Hojo T, et al. Grading system for lymph vessel tumor emboli: significant outcome predictor for patients with invasive ductal carcinoma of the breast who received neoadjuvant therapy. Modern Pathology. 2010;23(4):581-92.
21. van Kuijk SJA, Yaromina A, Houben R, Niemans R, Lambin P, Dubois LJ. Prognostic Significance of Carbonic Anhydrase IX Expression in Cancer Patients: A Meta-Analysis. Frontiers in Oncology. 2016;6(69).
22. Utispan K, Thuwajit P, Abiko Y, Charngkaew K, Paupairoj A, Chau-in S, et al. Gene expression profiling of cholangiocarcinoma-derived fibroblast reveals alterations related to tumor progression and indicates periostin as a poor prognostic marker. Molecular cancer. 2010;9:13.
23. Moreno-Bueno G, Portillo F, Cano A. Transcriptional regulation of cell polarity in EMT and cancer. Oncogene. 2008;27(55):6958-69.
24. Shih J-Y, Yuan A, Chen JJ-W, Yang P-C. Tumor-associated macrophage: its role in cancer invasion and metastasis. J Cancer Mol. 2006;2(3):101-6.
25. Zamarron BF, Chen W. Dual Roles of Immune Cells and Their Factors in Cancer Development and Progression. International Journal of Biological Sciences. 2011;7(5): 651-8.
26. Lin S-C, Chu P-Y, Liao W-T, Wu M-Y, Tsui K-H, Lin L-T, et al. Glycyrrhizic acid induces human MDA-MB-231 breast cancer cell death and autophagy via the ROS-mitochondrial pathway. Oncology reports. 2018;39(2):703-10.
27. Motofei IG. Biology of Cancer; From Cellular Cancerogenesis to Supracellular Evolution of Malignant Phenotype. Cancer investigation. 2018;36(5):309-17.
28. Hao Y, Baker D, ten Dijke P. TGF-β-mediated epithelial-mesenchymal transition and cancer metastasis. International journal of molecular sciences. 2019;20(11):2767.
29. Micalizzi DS, Ford HL. Epithelial–mesenchymal transition in development and cancer. Future oncology. 2009;5(8):1129-43.
30. Felipe Lima J, Nofech-Mozes S, Bayani J, Bartlett J. EMT in breast carcinoma—a review. Journal of clinical medicine. 2016;5(7):65.
31. Chiu H-C, Li C-J, Yiang G-T, Tsai AP-Y, Wu M-Y. Epithelial to mesenchymal transition and cell biology of molecular regulation in endometrial carcinogenesis. Journal of clinical medicine. 2019;8(4):439.
32. Chiu H-C, Wu M-Y, Li C-H, Huang S-C, Yiang G-T, Yen H-S, et al. Epithelial-mesenchymal transition with malignant transformation leading multiple metastasis from disseminated peritoneal leiomyomatosis. Journal of clinical medicine. 2018;7(8): 207.
33. Kalluri R, Weinberg RA. The basics of epithelial-mesenchymal transition. The Journal of clinical investigation. 2009;119(6):1420-8.
34. Lamouille S, Xu J, Derynck R. Molecular mechanisms of epithelial–mesenchymal transition. Nature reviews Molecular cell biology. 2014;15(3):178.
35. Makker A, Goel MM. Tumor progression, metastasis, and modulators of epithelial-mesenchymal transition in endometrioid endometrial carcinoma: an update. Endocr Relat Cancer. 2016;23(2):R85-R111.
36. Al Saleh S, Al Mulla F, Luqmani YA. Estrogen receptor silencing induces epithelial to mesenchymal transition in human breast cancer cells. PloS one. 2011;6(6).
37. Brabletz T, Kalluri R, Nieto MA, Weinberg RA. EMT in cancer. Nature Reviews Cancer. 2018;18(2):128.
38. Zhan T, Rindtorff N, Boutros M. Wnt signaling in cancer. Oncogene. 2017;36(11): 1461-73.

39. Perrot-Applanat M, Di Benedetto M. Autocrine functions of VEGF in breast tumor cells: adhesion, survival, migration and invasion. Cell adhesion & migration. 2012;6(6): 547-53.
40. Zaidi Z, Dib HA. The worldwide female breast cancer incidence and survival, 2018. AACR; 2019.
41. Turashvili G, Brogi E. Tumor Heterogeneity in Breast Cancer. Front Med (Lausanne). 2017;4:227-.
42. Fragomeni SM, Sciallis A, Jeruss JS. Molecular Subtypes and Local-Regional Control of Breast Cancer. Surg Oncol Clin N Am. 2018;27(1):95-120.
43. Mavaddat N, Michailidou K, Dennis J, Lush M, Fachal L, Lee A, et al. Polygenic Risk Scores for Prediction of Breast Cancer and Breast Cancer Subtypes. The American Journal of Human Genetics. 2019;104(1):21-34.
44. Tyanova S, Albrechtsen R, Kronqvist P, Cox J, Mann M, Geiger T. Proteomic maps of breast cancer subtypes. Nature Communications. 2016;7(1):10259.
45. Dai X, Xiang L, Li T, Bai Z. Cancer Hallmarks, Biomarkers and Breast Cancer Molecular Subtypes. J Cancer. 2016;7(10):1281-94.
46. Waks AG, Winer EP. Breast Cancer Treatment: A Review. JAMA. 2019;321(3):288-300.
47. Zhan Q-H, Fu J-Q, Fu F-M, Zhang J, Wang C. Survival and time to initiation of adjuvant chemotherapy among breast cancer patients: a systematic review and meta-analysis. Oncotarget. 2017;9(2):2739-51.
48. Helissey C, Vicier C, Champiat S. The development of immunotherapy in older adults: New treatments, new toxicities? Journal of Geriatric Oncology. 2016;7(5):325-33.
49. Sancho-Garnier H, Colonna M. [Breast cancer epidemiology]. Presse Med. 2019;48(10):1076-84.
50. Liu S, Ginestier C, Ou SJ, Clouthier SG, Patel SH, Monville F, et al. Breast cancer stem cells are regulated by mesenchymal stem cells through cytokine networks. Cancer research. 2011;71(2):614-24.
51. Tsuyada A, Chow A, Wu J, Somlo G, Chu P, Loera S, et al. CCL2 mediates cross-talk between cancer cells and stromal fibroblasts that regulates breast cancer stem cells. Cancer research. 2012;72(11):2768-79.
52. Sherwood V. WNT signaling: an emerging mediator of cancer cell metabolism? Mol Cell Biol. 2015;35(1):2-10.
53. Plaks V, Kong N, Werb Z. The cancer stem cell niche: how essential is the niche in regulating stemness of tumor cells? Cell stem cell. 2015;16(3):225-38.
54. Yang J, Liao D, Chen C, Liu Y, Chuang TH, Xiang R, et al. Tumor-associated macrophages regulate murine breast cancer stem cells through a novel paracrine EGFR/Stat3/Sox-2 signaling pathway. Stem cells (Dayton, Ohio). 2013;31(2):248-58.
55. Okuda H, Kobayashi A, Xia B, Watabe M, Pai SK, Hirota S, et al. Hyaluronan synthase HAS2 promotes tumor progression in bone by stimulating the interaction of breast cancer stem-like cells with macrophages and stromal cells. Cancer research. 2012; 72(2):537-47.
56. Seo A, Lee H, Kim E, Kim H, Jang M, Lee H, et al. Tumour-infiltrating CD8+ lymphocytes as an independent predictive factor for pathological complete response to primary systemic therapy in breast cancer. British journal of cancer. 2013;109(10):2705-13.
57. Wolfson B, Eades G, Zhou Q. Adipocyte activation of cancer stem cell signaling in breast cancer. World journal of biological chemistry. 2015;6(2):39.

58. Goto H, Shimono Y, Funakoshi Y, Imamura Y, Toyoda M, Kiyota N, et al. Adipose-derived stem cells enhance human breast cancer growth and cancer stem cell-like properties through adipsin. Oncogene. 2019;38(6):767-79.
59. Ghiabi P, Jiang J, Pasquier J, Maleki M, Abu-Kaoud N, Rafii S, et al. Endothelial cells provide a notch-dependent pro-tumoral niche for enhancing breast cancer survival, stemness and pro-metastatic properties. PloS one. 2014;9(11).
60. Wu W, Zhao S. Metabolic changes in cancer: beyond the Warburg effect. Acta Biochimica et Biophysica Sinica. 2013;45(1):18-26.
61. Warburg O. On the origin of cancer cells. Science (New York, NY). 1956;123(3191): 309-14.
62. Koppenol WH, Bounds PL, Dang CV. Otto Warburg's contributions to current concepts of cancer metabolism. Nature reviews Cancer. 2011;11(5):325-37.
63. Corbet C, Feron O. Emerging roles of lipid metabolism in cancer progression. Current Opinion in Clinical Nutrition & Metabolic Care. 2017;20(4):254-60.
64. Munir R, Lisec J, Swinnen JV, Zaidi N. Lipid metabolism in cancer cells under metabolic stress. British journal of cancer. 2019:1.
65. Ippolito L, Morandi A, Giannoni E, Chiarugi P. Lactate: A Metabolic Driver in the Tumour Landscape. Trends in Biochemical Sciences. 2019;44(2):153-66.
66. Yizhak K, Le Dévédec SE, Rogkoti VM, Baenke F, de Boer VC, Frezza C, et al. A computational study of the Warburg effect identifies metabolic targets inhibiting cancer migration. Molecular systems biology. 2014;10(11):765.
67. Paolicchi E, Gemignani F, Krstic-Demonacos M, Dedhar S, Mutti L, Landi S. Targeting hypoxic response for cancer therapy. Oncotarget. 2016;7.
68. Hall A, Meyle KD, Lange MK, Klima M, Sanderhoff M, Dahl C, et al. Dysfunctional oxidative phosphorylation makes malignant melanoma cells addicted to glycolysis driven by the (V600E)BRAF oncogene. Oncotarget. 2013;4(4):584-99.
69. Parmenter TJ, Kleinschmidt M, Kinross KM, Bond ST, Li J, Kaadige MR, et al. Response of BRAF-mutant melanoma to BRAF inhibition is mediated by a network of transcriptional regulators of glycolysis. Cancer discovery. 2014;4(4):423-33.
70. Son J, Lyssiotis CA, Ying H, Wang X, Hua S, Ligorio M, et al. Glutamine supports pancreatic cancer growth through a KRAS-regulated metabolic pathway. Nature. 2013;496(7443):101-5.
71. Munoz-Pinedo C, El Mjiyad N, Ricci JE. Cancer metabolism: current perspectives and future directions. Cell death & disease. 2012;3:e248.
72. Farnie G, Sotgia F, Lisanti MP. High mitochondrial mass identifies a sub-population of stem-like cancer cells that are chemo-resistant. Oncotarget. 2015;6(31):30472-86.
73. Song IS, Jeong JY, Jeong SH, Kim HK, Ko KS, Rhee BD, et al. Mitochondria as therapeutic targets for cancer stem cells. World journal of stem cells. 2015;7(2):418-27.
74. San-Millán I, Brooks GA. Reexamining cancer metabolism: lactate production for carcinogenesis could be the purpose and explanation of the Warburg Effect. Carcinogenesis. 2016;38(2):119-33.
75. San-Millán I, Brooks GA. Reexamining cancer metabolism: lactate production for carcinogenesis could be the purpose and explanation of the Warburg Effect. Carcinogenesis. 2017;38(2):119-33.
76. Zhou Y, Niu W, Luo Y, Li H, Xie Y, Wang H, et al. p53/Lactate dehydrogenase A axis negatively regulates aerobic glycolysis and tumor progression in breast cancer expressing wild-type p53. Cancer science. 2019;110(3):939-49.

77. Lamb R, Harrison H, Hulit J, Smith DL, Lisanti MP, Sotgia F. Mitochondria as new therapeutic targets for eradicating cancer stem cells: Quantitative proteomics and functional validation via MCT1/2 inhibition. Oncotarget. 2014;5(22):11029.
78. Chiavarina B, Whitaker-Menezes D, Migneco G, Martinez-Outschoorn UE, Pavlides S, Howell A, et al. HIF1-alpha functions as a tumor promoter in cancer-associated fibroblasts, and as a tumor suppressor in breast cancer cells: Autophagy drives compartment-specific oncogenesis. Cell cycle (Georgetown, Tex). 2010;9(17):3534-51.
79. Chiavarina B, Martinez-Outschoorn UE, Whitaker-Menezes D, Howell A, Tanowitz HB, Pestell RG, et al. Metabolic reprogramming and two-compartment tumor metabolism: opposing role (s) of HIF1α and HIF2α in tumor-associated fibroblasts and human breast cancer cells. Cell cycle (Georgetown, Tex). 2012;11(17):3280-9.
80. Pavlides S, Whitaker-Menezes D, Castello-Cros R, Flomenberg N, Witkiewicz AK, Frank PG, et al. The reverse Warburg effect: aerobic glycolysis in cancer associated fibroblasts and the tumor stroma. Cell cycle (Georgetown, Tex). 2009;8(23):3984-4001.
81. Sanità P, Capulli M, Teti A, Galatioto GP, Vicentini C, Chiarugi P, et al. Tumor-stroma metabolic relationship based on lactate shuttle can sustain prostate cancer progression. BMC cancer. 2014;14(1):154.
82. Ryan DG, Murphy MP, Frezza C, Prag HA, Chouchani ET, O'Neill LA, et al. Coupling Krebs cycle metabolites to signalling in immunity and cancer. Nature metabolism. 2019;1(1):16-33.
83. Monaco ME. Fatty acid metabolism in breast cancer subtypes. Oncotarget. 2017;8(17): 29487-500.
84. Mashima T, Seimiya H, Tsuruo T. De novo fatty-acid synthesis and related pathways as molecular targets for cancer therapy. Br J Cancer. 2009;100(9):1369-72.
85. Zadra G, Ribeiro CF, Chetta P, Ho Y, Cacciatore S, Gao X, et al. Inhibition of de novo lipogenesis targets androgen receptor signaling in castration-resistant prostate cancer. 2019;116(2):631-40.
86. Lee S, Zhang C. Network analyses identify liver-specific targets for treating liver diseases. 2017;13(8):938.
87. Beckers A, Organe S, Timmermans L, Scheys K, Peeters A, Brusselmans K, et al. Chemical inhibition of acetyl-CoA carboxylase induces growth arrest and cytotoxicity selectively in cancer cells. Cancer research. 2007;67(17):8180-7.
88. Quijano C, Cao L, Fergusson MM, Romero H, Liu J, Gutkind S, et al. Oncogene-induced senescence results in marked metabolic and bioenergetic alterations. Cell cycle (Georgetown, Tex). 2012;11(7):1383-92.
89. Marien E, Meister M, Muley T, Fieuws S, Bordel S, Derua R, et al. Non-small cell lung cancer is characterized by dramatic changes in phospholipid profiles. International journal of cancer. 2015;137(7):1539-48.
90. Feizi A, Bordel S. Metabolic and protein interaction sub-networks controlling the proliferation rate of cancer cells and their impact on patient survival. Scientific reports. 2013;3(1):1-9.
91. Qu Q, Zeng F, Liu X, Wang QJ, Deng F. Fatty acid oxidation and carnitine palmitoyltransferase I: emerging therapeutic targets in cancer. Cell death & disease. 2016;7:e2226.
92. Carracedo A, Weiss D, Leliaert AK, Bhasin M, de Boer VC, Laurent G, et al. A metabolic prosurvival role for PML in breast cancer. The Journal of clinical investigation. 2012;122(9):3088-100.
93. Zaugg K, Yao Y, Reilly PT, Kannan K, Kiarash R, Mason J, et al. Carnitine palmitoyltransferase 1C promotes cell survival and tumor growth under conditions of metabolic stress. Genes & development. 2011;25(10):1041-51.

94. Guan L, Chen Y, Wang Y, Zhang H, Fan S, Gao Y, et al. Effects of carnitine palmitoyltransferases on cancer cellular senescence. 2019;234(2):1707-19.
95. Melone MAB, Valentino A, Margarucci S, Galderisi U, Giordano A, Peluso G. The carnitine system and cancer metabolic plasticity. Cell death & disease. 2018;9(2):228.
96. Livieri AL, Navone L, Marcellin E, Gramajo H, Rodriguez E. A novel multidomain acyl-CoA carboxylase in Saccharopolyspora erythraea provides malonyl-CoA for de novo fatty acid biosynthesis. Scientific Reports. 2019;9(1):6725.
97. Abu-Elheiga L, Matzuk MM, Abo-Hashema KA, Wakil SJ. Continuous fatty acid oxidation and reduced fat storage in mice lacking acetyl-CoA carboxylase 2. Science (New York, NY). 2001;291(5513):2613-6.
98. Ogino S, Kawasaki T, Ogawa A, Kirkner GJ, Loda M, Fuchs CS. Fatty acid synthase overexpression in colorectal cancer is associated with microsatellite instability, independent of CpG island methylator phenotype. Human Pathology. 2007;38(6):842-9.
99. Alò PL, Visca P, Framarino ML, Botti C, Monaco S, Sebastiani V, et al. Immunohistochemical study of fatty acid synthase in ovarian neoplasms. Oncology reports. 2000; 7(6):1383-91.
100. Menendez JA, Ropero S, Mehmi I, Atlas E, Colomer R, Lupu R. Overexpression and hyperactivity of breast cancer-associated fatty acid synthase (oncogenic antigen-519) is insensitive to normal arachidonic fatty acid-induced suppression in lipogenic tissues but it is selectively inhibited by tumoricidal α-linolenic and γ-linolenic fatty acids: A novel mechanism by which dietary fat can alter mammary tumorigenesis. International journal of oncology. 2004;24(6):1369-83.
101. Shah US, Dhir R, Gollin SM, Chandran UR, Lewis D, Acquafondata M, et al. Fatty acid synthase gene overexpression and copy number gain in prostate adenocarcinoma. Human pathology. 2006;37(4):401-9.
102. Takahiro T, Shinichi K, Toshimitsu S. Expression of fatty acid synthase as a prognostic indicator in soft tissue sarcomas. Clinical cancer research. 2003;9(6):2204-12.
103. Grube S, Dünisch P, Freitag D, Klausnitzer M, Sakr Y, Walter J, et al. Overexpression of fatty acid synthase in human gliomas correlates with the WHO tumor grade and inhibition with Orlistat reduces cell viability and triggers apoptosis. Journal of neurooncology. 2014;118(2):277-87.
104. Innocenzi D, Alo P, Balzani A, Sebastiani V, Silipo V, La Torre G, et al. Fatty acid synthase expression in melanoma. Journal of cutaneous pathology. 2003;30(1):23-8.
105. Vander Steen T, Lupu R. Inhibition of FASN induces apoptosis and senescence in breast cancer. AACR; 2018.
106. Lee KH, Lee MS, Cha EY, Sul JY, Lee JS, Kim JS, et al. Inhibitory effect of emodin on fatty acid synthase, colon cancer proliferation and apoptosis. Molecular medicine reports. 2017;15(4):2163-73.
107. Xiao F, Wang C, Yin H, Yu J, Chen S, Fang J, et al. Leucine deprivation inhibits proliferation and induces apoptosis of human breast cancer cells via fatty acid synthase. Oncotarget. 2016;7(39):63679.
108. Zhang Y-K, Qu Y-Y, Lin Y, Wu X-H, Chen H-Z, Wang X, et al. Enoyl-CoA hydratase-1 regulates mTOR signaling and apoptosis by sensing nutrients. Nature Communications. 2017;8(1):464.
109. Ferdinandusse S, Friederich MW, Burlina A, Ruiter JPN, Coughlin CR, Dishop MK, et al. Clinical and biochemical characterization of four patients with mutations in ECHS1. Orphanet Journal of Rare Diseases. 2015;10(1):79.
110. Wen D, Liu D, Tang J, Dong L, Liu Y, Tao Z, et al. Malic enzyme 1 induces epithelial-mesenchymal transition and indicates poor prognosis in hepatocellular carcinoma.

Tumour biology : the journal of the International Society for Oncodevelopmental Biology and Medicine. 2015;36(8):6211-21.
111. Zhu BH, Zhang RH, Lv NN, Yang GP, Wang YS, Pan KH. The Role of Malic Enzyme on Promoting Total Lipid and Fatty Acid Production in Phaeodactylum tricornutum. Frontiers in plant science. 2018;9:826.
112. Gurer-Orhan H, Ince E, Konyar D, Saso L, Suzen S. The role of oxidative stress modulators in breast cancer. Current medicinal chemistry. 2018;25(33):4084-101.
113. Hecht F, Pessoa CF, Gentile LB, Rosenthal D, Carvalho DP, Fortunato RS. The role of oxidative stress on breast cancer development and therapy. Tumour biology : the journal of the International Society for Oncodevelopmental Biology and Medicine. 2016; 37(4): 4281-91.
114. Zorova LD, Popkov VA, Plotnikov EY, Silachev DN, Pevzner IB, Jankauskas SS, et al. Mitochondrial membrane potential. Anal Biochem. 2018;552:50-9.
115. Perry SW, Norman JP, Barbieri J, Brown EB, Gelbard HA. Mitochondrial membrane potential probes and the proton gradient: a practical usage guide. BioTechniques. 2011;50(2):98-115.
116. Bellance N, Lestienne P, Rossignol R. Mitochondria: from bioenergetics to the metabolic regulation of carcinogenesis. Frontiers in bioscience (Landmark edition). 2009;14: 4015-34.
117. Adeva-Andany MM, López-Maside L, Donapetry-García C, Fernández-Fernández C, Sixto-Leal C. Enzymes involved in branched-chain amino acid metabolism in humans. Amino acids. 2017;49(6):1005-28.
118. Nie C, He T. Branched Chain Amino Acids: Beyond Nutrition Metabolism. 2018;19(4).
119. Ananieva EA, Wilkinson AC. Branched-chain amino acid metabolism in cancer. Curr Opin Clin Nutr Metab Care. 2018;21(1):64-70.
120. Nilsson A, Nielsen J. Genome scale metabolic modeling of cancer. Metabolic engineering. 2017;43:103-12.
121. Duarte NC, Becker SA, Jamshidi N, Thiele I, Mo ML, Vo TD, et al. Global reconstruction of the human metabolic network based on genomic and bibliomic data. Proc Natl Acad Sci U S A. 2007;104(6):1777-82.
122. Thiele I, Swainston N, Fleming RM, Hoppe A, Sahoo S, Aurich MK, et al. A community-driven global reconstruction of human metabolism. Nature biotechnology. 2013;31(5):419-25.
123. Katzir R, Polat IH, Harel M, Katz S, Foguet C, Selivanov VA, et al. The landscape of tiered regulation of breast cancer cell metabolism. Scientific reports. 2019;9(1):1-12.
124. Metzker ML. Sequencing technologies—the next generation. Nature reviews genetics. 2010;11(1):31-46.
125. Gosens R, Stelmack GL, Dueck G, McNeill KD, Yamasaki A, Gerthoffer WT, et al. Role of caveolin-1 in p42/p44 MAP kinase activation and proliferation of human airway smooth muscle. American journal of physiology Lung cellular and molecular physiology. 2006;291(3):L523-34.
126. Sellick CA, Hansen R, Stephens GM, Goodacre R, Dickson AJ. Metabolite extraction from suspension-cultured mammalian cells for global metabolite profiling. Nat Protoc. 2011;6(8):1241-9.
127. Antoniewicz MR, Kelleher JK, Stephanopoulos G. Elementary metabolite units (EMU): A novel framework for modeling isotopic distributions. Metabolic Engineering. 2007;9(1):68-86.

128. Sellick CA, Hansen R, Stephens GM, Goodacre R, Dickson AJ. Metabolite extraction from suspension-cultured mammalian cells for global metabolite profiling. Nature Protocols. 2011;6(8):1241-9.
129. Antanavičiūtė I, Mikalayeva V, Ceslevičienė I, Milašiūtė G, Skeberdis VA, Bordel S. Transcriptional hallmarks of cancer cell lines reveal an emerging role of branched chain amino acid catabolism. Scientific reports. 2017;7(1):7820-.
130. Raškevičius V, Mikalayeva V, Antanavičiūtė I, Ceslevičienė I, Skeberdis VA, Kairys V, et al. Genome scale metabolic models as tools for drug design and personalized medicine. PloS one. 2018;13(1).
131. Jain M, Nilsson R, Sharma S, Madhusudhan N, Kitami T, Souza AL, et al. Metabolite profiling identifies a key role for glycine in rapid cancer cell proliferation. Science (New York, NY). 2012;336(6084):1040-4.
132. Dolfi SC, Chan LL-Y, Qiu J, Tedeschi PM, Bertino JR, Hirshfield KM, et al. The metabolic demands of cancer cells are coupled to their size and protein synthesis rates. Cancer & metabolism. 2013;1(1):20.
133. Samudio I, Harmancey R, Fiegl M, Kantarjian H, Konopleva M, Korchin B, et al. Pharmacologic inhibition of fatty acid oxidation sensitizes human leukemia cells to apoptosis induction. The Journal of clinical investigation. 2010;120(1):142-56.
134. Borgos SE, Bordel S, Sletta H, Ertesvåg H, Jakobsen Ø, Bruheim P, et al. Mapping global effects of the anti-sigma factor MucA in Pseudomonas fluorescens SBW25 through genome-scale metabolic modeling. BMC systems biology. 2013;7(1):19.
135. Österlund T, Bordel S, Nielsen J. Controllability analysis of transcriptional regulatory networks reveals circular control patterns among transcription factors. Integrative biology : quantitative biosciences from nano to macro. 2015;7(5):560-8.
136. Chua H, Bhat-Nakshatri P, Clare S, Morimiya A, Badve S, Nakshatri H. NF-κB represses E-cadherin expression and enhances epithelial to mesenchymal transition of mammary epithelial cells: potential involvement of ZEB-1 and ZEB-2. Oncogene. 2007;26(5):711.

STRAIPSNIAI, KURIUOSE PASKELBTI DISERTACINIO DARBO REZULTATAI

1. Mikalayeva V, **Ceslevičienė I,** Žvikas V, Skeberdis VA, Jakštas V, Bordel S. Fatty acid synthesis and degradation interplay to regulate the oxidative stress in cancer cells. *International journal of molecular sciences.* 2019, vol. 20, no. 6, 1348, p. 1-12. [Citav. rod.: 4,183, bendr. cit. rod.: 5,147].
2. Raškevičius V, Mikalayeva V, Antanavičiūtė I, **Ceslevičienė I,** Skeberdis VA, Kairys V, Bordel S. Genome scale metabolic models as tools for drug design and personalized medicine. *PLoS One.* 2018, vol. 13, no. 1, art. no. 0190636, p. 1-14. (Research article). [Citav. rod.: 2,776, bendr. cit. rod.: 5,145].
3. Antanavičiūtė I, Mikalayeva V, **Ceslevičienė I,** Milašiūtė G, Skeberdis VA, Bordel S. Transcriptional hallmarks of cancer cell lines reveal an emerging role of branched chain amino acid catabolism. *Scientific reports.* 2017, vol. 7, no. 1, 7820, p. 1-12. [Citav. rod.: 4,122, bendr. cit. rod.: 5,110].

Kiti straipsniai

Pankratjevaitė L, **Ceslevičienė I**, Poškienė L, Boguševičius A. A Case report of desmoid type fibromatosis of the breast. *Lietuvos chirurgija* 2019, t. 18, Nr. 2, p. 107-111.

MOKSLINĖS KONFERENCIJOS, KURIOSE PRISTATYTI DARBO REZULTATAI

1. Jančiukė G, Ceslevičienė I, Mikalayeva V. The Effect of age-related Wnt signalling on breast cancer cell viability and mitochondrial membrane // Medicina: Abstracts accepted for the International Scientific Conference on Medicine organized within the frame of the 78th International Scientific Conference of the University of Latvia : 20 March, 2020, Riga, Latvia / Editor-in-Chief Edgaras Stankevičius ; English language editor: Andra Damberga. Kaunas ; Basel : LSMU ; MDPI. ISSN 1010-660X. eISSN 1648-9233. 2020, vol. 56, suppl. 1, p. 272.
2. Ceslevičienė I, Mikalayeva V, Sarapinienė I, Skeberdis VA, Žvikas V, Bordel S. Cytosolic fatty acid synthesis and mitochondrial fatty acid oxidation coexist simultaneously in breast cancer cells // FEBS3+ conference of Latvian, Lithuanian and Estonian biochemical societies : abstract book : Riga, Latvia, 17-19 June 2019 / Organizers: Kaspars Tärs, Tiit Lukk, Daumantas Matulis, Zane Kalniņa, Nils Rostoks. Riga : University of Latvia Press, 2019. ISBN 9789934184505. p. 64-64, no. 8.
3. Ceslevičienė I, Antanavičiūtė I, Mikalayeva V, Skeberdis VA, Bordel S. Branched chain amino acid catabolism in breast cancer cells // 1st International doctoral students' conference "Science for Health" : book of abstracts : April 13, 2018, Kaunas, Lithuania / Lithuanian university of health sciences. LSMU Department of Research Affairs. Council of LSMU Doctoral Students ; [Edited by Indrė Šveikauskaitė]. Kaunas : Lietuvos sveikatos mokslų universiteto Leidybos namai, 2018. ISBN 9789955155300. p. 51-52.
4. Mikalayeva V, Antanavičiūtė I, Ceslevičienė I, Skeberdis VA, Bordel S. The Role of transcriptional regulation in lipid oxidation in breast cancer // FEBS Open Bio : Supplement: 43rd FEBS Congress, Biochemistry Forever : Prague, Czech Republic, July 712, 2018 : abstracts / Federation of European Biochemical Societies (FEBS). Hoboken, NJ : FEBS Press and John Wiley & Sons Ltd. ISSN 2211-5463. eISSN 2211-5463. 2018, vol. 8, suppl. 1, July, no. P.10-043-Mon, p. 308-309.
5. Ceslevičienė I, Antanavičiūtė I, Mikalayeva V, Milašiūtė G, Skeberdis VA, Bordel S. Trancriptional regulation of metabolic reaction in breast cancer cells // Acta Physiologica : Special Issue: Joint Meeting of the Federation of European Physiological Societies and the Austrian Physiological Society with Participation of the Czech, French, Italian, Slovak, Slovenian, Swiss and Turkish Physiological Societies : Vienna, Austria, September 13th-15th, 2017 / Scandinavian Physiological

Society. European Physiological Societies. Oxford : John Wiley & Sons Ltd. ISSN 1748-1708. eISSN 17481716. 2017, vol. 221, iss. suppl. S713, p. 179-179, no. C03-8.
6. Mikalayeva V, Antanavičiūtė I, Milaišiutė G, Ceslevičienė I, Skeberdis VA, Bordel S. Sources of mitochondrial Acetyl-CoA in cancer cells // XIVth International conference of the Lithuanian biochemical society : the program and abstract book : Druskininkai, June 27-30, 2016 / Lithuanian Biochemical Society. Kaunas : Vitae Litera, 2016. ISBN 9786094542275. p. 53-53, no. 14.

SCIENTIFIC REPORTS

OPEN

Transcriptional hallmarks of cancer cell lines reveal an emerging role of branched chain amino acid catabolism

Received: 1 March 2017
Accepted: 7 July 2017
Published online: 10 August 2017

Ieva Antanavičiūtė[1], Valeryia Mikalayeva[1], Ieva Ceslevičienė[1], Gintarė Milašiūtė[1], Vytenis Arvydas Skeberdis[1] & Sergio Bordel[1,2]

A comparative analysis between cancer cell lines and healthy dividing cells was performed using data (289 microarrays and 50 RNA-seq samples) from 100 different cancer cell lines and 6 types of healthy stem cells. The analysis revealed two large-scale transcriptional events that characterize cancer cell lines. The first event was a large-scale up-regulation pattern associated to epithelial-mesenchymal transition, putatively driven by the interplay of the SP1 transcription factor and the canonical Wnt signaling pathway; the second event was the failure to overexpress a diverse set of genes coding membrane and extracellular proteins. This failure is putatively caused by a lack of activity of the AP-1 complex. It was also shown that the epithelial-mesenchymal transition was associated with the up-regulation of 5 enzymes involved in the degradation of branched chain amino acids. The suitability of silencing one of this enzymes (branched chain amino acid transaminase 2; BCAT2) with therapeutic effects was tested experimentally on the breast cancer cell line MCF-7 and primary cell culture of breast tumor (BCC), leading to lower cell proliferation. The silencing of BCAT2 did not have any significant effect on ASM and MCF10A cells, which were used as models of healthy dividing cells.

Side effects are among the main problems related to chemotherapy. Most of the drugs used in chemotherapy target DNA replication or key regulators of the cell cycle[1], which has a negative impact not only on malignant cells but also on healthy proliferating cells (stem cells and progenitors), leading to stem cell depletion and impaired renewal and function of healthy tissues[2]. Therefore, identifying systematic differences between cancer cells and healthy dividing cells, is fundamental to identify therapeutic windows that could be exploited to target cancer cells while minimizing side effects. The development of high throughput omics technologies such as cDNA microarrays and more recently, RNA-sequencing, has led to the accumulation of large datasets that constitute rich sources of information allowing us to identify systematic differences that characterize cancer cells. These transcriptional differences are expected to provide keys for the design of therapies targeting cancer cells specifically without damaging healthy dividing cells and therefore to minimize the secondary effects associated with stem cell depletion caused by chemotherapy.

Cancer cell lines have their origin in healthy stem cells or progenitors[3,4] that undergo a series of mutations resulting in a tumorigenic phenotype. Recent high-throughput sequencing studies of human cancers[5–7] have revealed hundreds of somatic mutations associated with cancer; however, very few genes were found to be mutated in large fractions of the studied samples. In each cancer type, only about 4 genes were altered in more than 20% of the studied samples[8]. The TP53 tumor suppressor is the most frequently mutated gene, but it is still far from being present in all sequenced cancers. Despite this large heterogeneity in the mutations that trigger malignant transformations, cancer has been characterized in terms of a small set of hallmarks described by Hannahan and Weinberg[9]. The acquisition of these hallmarks is likely to be associated with well-coordinated large-scale transcriptional changes that are absent in healthy cells (healthy stem cells and progenitors in particular). Here we have analyzed a large set of gene expression data (microarrays and RNA-seq) from cancer cell lines

[1]Institute of Cardiology, Lithuanian University of Health Sciences, 15 Sukilėlių Ave., LT- 50162, Kaunas, Lithuania. [2]Department of Biology and Biological Engineering, Chalmers University of Technology, Kemivägen 10, SE-41296, Göteborg, Sweden. Correspondence and requests for materials should be addressed to S.B. (email: sergio_bordel@hotmail.com)

and healthy proliferating cells, with the aim of identifying transcriptional hallmarks present in cancer cell lines and absent in healthy cells.

Results

Transcriptional hallmarks of cancer cell lines. In order to identify the transcriptional changes that make cancer cell lines different from healthy dividing cells, we analyzed 289 microarrays from the GEO database (the accession numbers are reported in Supplementary Table S1). These microarrays correspond to the cancer cell lines of the NCI-60 collection and 5 types of healthy dividing cells that include: beta cells from pancreatic islets, hematopoietic stem cells, dental pulp stem cells, endothelial progenitor cells, and mesenchymal stem cells. After microarray normalization, a principal component analysis was performed in order to visualize the structure of the data (Fig. 1A,B). It appears that the first principal component discriminates between cells with their origin in the hematopoietic system (hematopoietic stem cells, endothelial progenitor cells and leukemia cell lines) from the rest; however, leukemia cells are strongly displaced toward the proximity of the other cancer cell lines. The second principal component appears to discriminate cancer cell lines from healthy dividing cells. This suggests that it is indeed possible to find a distinct transcriptional pattern that characterizes cancer cell lines.

We used a linear discrimination analysis[10] in order to identify the plane in the gene expression space that best separates cancer cell lines from healthy dividing cells. The vector perpendicular to this plane is described as the characteristic direction (see supplementary material). By projecting the expression profile of each sample on the characteristic direction, we can fully discriminate tumorigenic cells from healthy dividing cells (Supplementary Fig. S1). The genes with statistically significant contributions (negative and positive) to the characteristic direction (with false discovery rates lower than 0.05) are reported in Supplementary File SF2.

In order to assess if the identified expression profile is a general characteristic of tumorigenic cells or just an artifact of our choice of samples, we tested two datasets, each of which contained a stem cell type different from those previously used (colon stem cells and mammary epithelial stem cells) and two different cancer cell lines originated from the same tissue (colon and breast cancer cell lines). The GEO accession numbers and cell lines are reported in the supplementary material (Table S2). Each validation dataset was normalized individually (independently from each other and from the initial microarray set). After normalization, we performed a principal component analysis showing that the cancer cell lines differ from each other in terms of expression as much as they differ from the stem cells of their tissue of origin. However, if we project their expression profiles on the characteristic direction (which was obtained independently using different cell lines), both cancer cell lines get clustered together and clearly separated from the stem cells (Fig. 1C–F). These results suggest that the expression pattern described by the obtained characteristic direction is a general feature that discriminates cancer cell lines from healthy dividing cells.

In order to understand the mechanisms behind the coordinated changes in expression in the identified gene sets, we analyzed the list of genes with significant contributions to the characteristic direction (0.05 false discovery rates) using GeneCodis[11–13] for transcription factor enrichment. The top scoring transcription factors were LEF1 (with p-values of 9.3 e-47 for down-regulated genes and 3.33 e-24 for up-regulated genes), NFAT (p-value of 4.87 e-45 for down-regulated genes), SP1 (p-value of 1.68 e-40 for up-regulated genes), and FOXO4 (p-values of 5.56 e-44 for down-regulated genes and 1.61 e-19 for up-regulated genes). The differentially expressed genes regulated by each of these transcription factors are reported in Supplementary File SF2.

An up-regulation pattern associated with epithelial-mesenchymal transition. The transcription factor coded by LEF1 interacts with β-catenin in the last step of the Wnt signaling pathway. This interaction induces the expression of several key regulators of the cell cycle and results in symmetric division[14,15]. Mutations resulting in the constitutive activation of the Wnt/β-catenin pathway have been reported in many cancer types[16]. It has also been shown that the activation of LEF1 is enough to induce neoplastic transformation in chicken embryo fibroblasts[17].

FOXO proteins have been reported to bind β-catenin[18], and the transcription level of the FOXO targets has been shown to increase when β-catenin binds the FOXO transcription factors[19]. Therefore, the transcriptional changes mediated by LEF1 and FOXO4 could have a common origin in the Wnt/β-catenin pathway.

SP1 is involved in the epithelial-mesenchymal transition[20], and it is necessary to confer metastatic capabilities to tumorigenic cells. Inhibition of SP1 has been shown to have antitumor effects[21]. The results from the enrichment analysis performed with GeneCodis showed that the SP1 gene is among those up-regulated in cancer cell lines and controlled by FOXO4, together with other genes involved in the TGF-β pathway (see Supplementary Files SF2 and SF3). On the other hand, 9 genes (see Supplementary File SF3) belonging to the Wnt signaling pathway are up-regulated in cancer cell lines and controlled by SP1 (according to GeneCodis). This suggests the existence of a positive feedback involving SP1, the Wnt pathway, and FOXO4, resulting in a large-scale transcriptional change. SP1 up-regulation has been recently shown experimentally to activate Wnt/β-catenin signaling in MCF-7 and MCF-10A cells[22], which is consistent with our observations. Inactivation of the Wnt antagonist WTX has been shown to induce β-catenin activation and result in the accumulation of mesenchymal precursor cells in mice[23], which also suggests that β-catenin is indeed involved in epithelial-mesenchymal transition.

The genes identified as up-regulated in cancer cell lines (using the method described in the section Statistical Methods in the supplementary material) and regulated by LEF1, FOXO4, and SP1, respectively (according to GeneCodis[11–13]), are reported in Supplementary File SF2. Among these genes, 197 are regulated by just one of the three transcription factors, while 127 are regulated by two or three (see Venn diagram in Fig. 2A).

The characteristic direction was projected (as described in the supplementary material) on the set of 158 genes putatively regulated by LEF1. This projection was used as an estimation of the activity of the LEF1 transcription factor in each cell line. The characteristic direction was also projected on the set of 128 genes putatively regulated by SP1 excluding the 67 genes that are regulated by SP1 and LEF1. These genes were excluded in order to compare

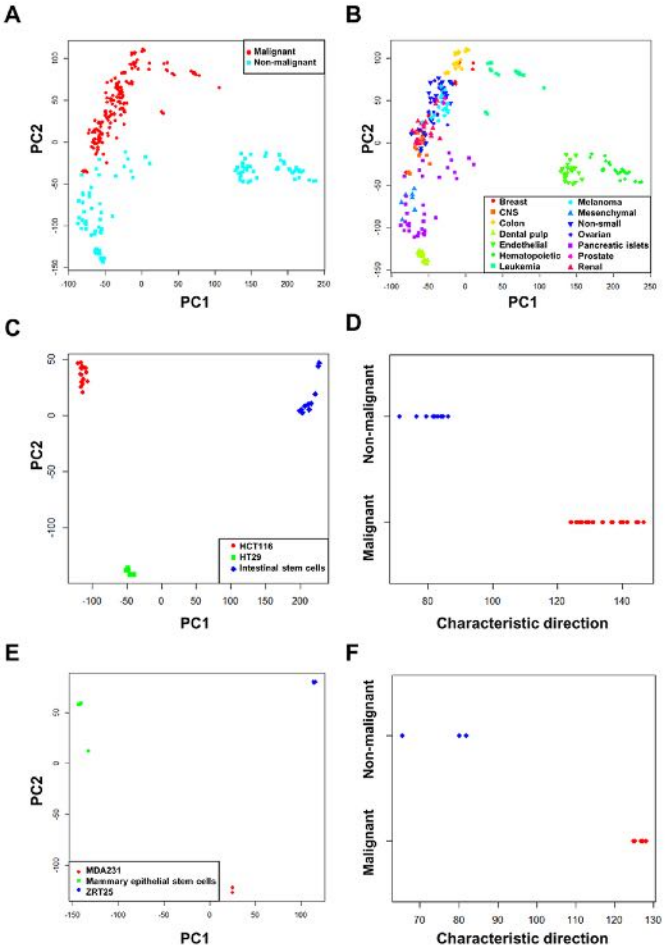

Figure 1. Exploratory analysis of gene expression profiles. The second principal component appears to separate CICs from healthy dividing cells (**A**). The first principal component seems to separate the cells with an origin in the hematopoietic system: hematopoietic stem cells, endothelial progenitor cells, and leukemia (**B**). The colon cancer cell lines HCT116 and HT29 differ strongly between each other and with respect to intestinal stem cells (**C**); however, the projection of their expression profiles along the characteristic direction clusters both cancer cell lines together and separates them from the stem cells (**D**). The same is observed for the breast cancer cell lines MDA231 and ZRT75 (**E**) when compared to mammary epithelial stem cells (**F**).

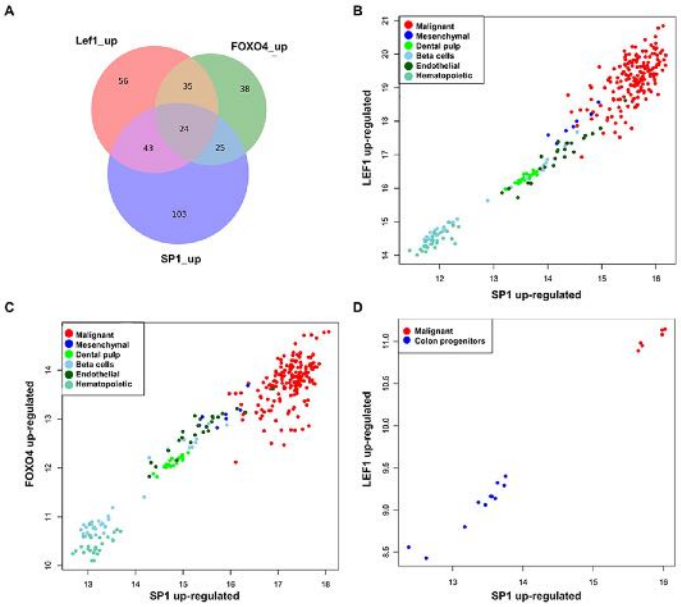

Figure 2. Expression of the SP1, FOXO4, and LEF1 regulated genes. Overlap between genes up-regulated in cancer cell lines and regulated by each of the three transcription factors (according to GeneCodis) (**A**). Correlation between the aggregated expressions of SP1 up-regulated genes and LEF1 up-regulated genes (**B**). Correlation between the aggregated expressions of SP1 up-regulated genes and FOXO4 up-regulated genes (**C**). Correlation between the aggregated expressions of SP1 up-regulated genes and LEF1 up-regulated genes in colon stem cells and the colon cancer cell line HT29 (**D**).

gene sets that do not overlap and to avoid finding spurious correlations. A Pearson correlation coefficient of 0.968 was obtained between the projections on each of the gene sets (Fig. 2B). This confirms that the activities of LEF1 and SP1 are correlated.

The same procedure was repeated using the set of 122 genes putatively regulated by FOXO4 and 146 genes putatively regulated by SP1 and not by FOXO4 (Fig. 2C). In this case, a Pearson correlation coefficient of 0.958 was obtained between the projections on both gene sets, suggesting the existence of correlation between the activities of FOXO4 and SP1.

The cancer cell lines appear in the upper right corner of the correlation plots (Fig. 2B,C) closely situated to the mesenchymal stem cells, which suggests that the transcriptional pattern involving the coordinated up-regulation of genes controlled by SP1, LEF1, and FOXO4 corresponds to the phenomenon of epithelial-mesenchymal transition (SP1 is known to be involved in epithelial-mesenchymal transition[20]). The same pattern is observed on colon stem cells and colon cancer cells HT29, which were not used to compute the characteristic direction and which were normalized independently from the previous dataset (Fig. 2D). This confirms that the observed phenomenon is not restricted to the dataset of 289 microarrays that we used initially.

A down-regulation pattern associated with loss of intercellular communication and attachment to the extra-cellular matrix. The enrichment analysis revealed not only sets of up-regulated genes putatively controlled by LEF1 and FOXO4, but also large sets of down-regulated genes under the putative control of the same two transcription factors. In order to visualize the expression levels of these down-regulated gene sets in different cell lines, we started by plotting the projection of the characteristic direction (see supplementary material) on the genes down-regulated and controlled by LEF1 (noted as LEF1 down-regulated) versus the projection of the characteristic direction on the genes up-regulated and controlled by LEF1 (noted as LEF1 up-regulated) (Fig. 3A). In this case, we observe that the global expression of the down-regulated genes controlled by LEF1 actually increases in mesenchymal stem cells compared to hematopoietic stem cells and a part of the beta

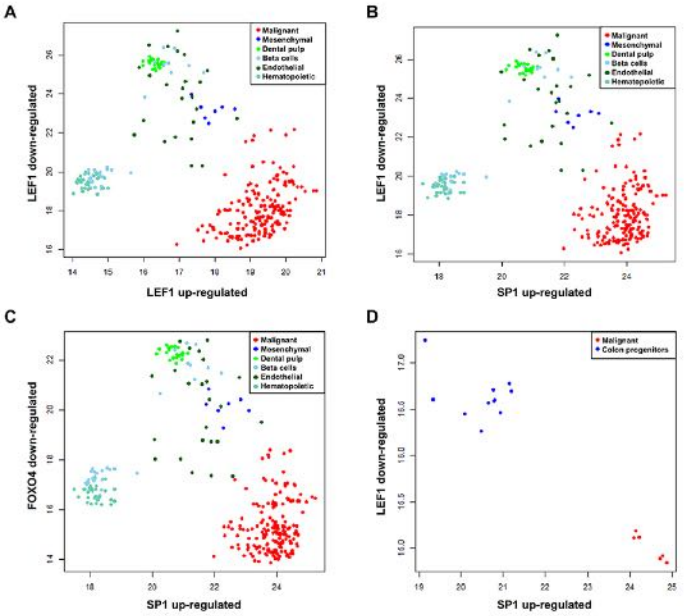

Figure 3. Projections of the characteristic direction on the LEF1 and SP1 regulons. Tumorigenic cells show a consistently higher LEF1 activity, while SP1 activity differentiates epithelial and mesenchymal cells.

cells. The same pattern appears if we plot the global expression of the down-regulated genes controlled by LEF1 and FOXO4 versus the up-regulated genes controlled by SP1 (Fig. 3B,C). This phenomenon is equally observed in the dataset of colon stem cells and colon cancer cells HT29 (Fig. 3D).

The mentioned observations suggest that both sets of genes (LEF1 down-regulated and FOXO4 down-regulated) are actually up-regulated in normal epithelial-mesenchymal transitions, while their expression remains unmodified or decreases in cancer cell lines. Under this interpretation, cancer cell lines would be the result of incomplete epithelial-mesenchymal transition in which large sets of genes that are normally up-regulated, fail to get overexpressed.

The mentioned hypothesis was tested using a different technology to quantify gene expression. RNA-seq data of 44 cancer cell lines from the Human Proteome Atlas (BioProject accession number PRJNA183192) and 6 primary cultures of mesenchymal stem cells (3 from placenta and 3 from bone marrow)[24] were compared. The raw sequence *fastq* files for mesenchymal stem cells were analyzed as described in the methods and a differential expression analysis was carried out in order to identify genes differentially expressed between cancer cell lines and healthy mesenchymal stem cells. The results are shown in the form of a *volcano* plot (Fig. 4A). Among the 1120 genes that appeared to have lower expression in cancer cell lines (based on the previously described microarray analysis), 260 were also down-regulated in the RNA-seq dataset (green points in Fig. 4A. These genes are referred to as consensus down-regulated genes from now on). This is 2.27 times higher than the expected number for a random set of 1120 genes and the p-value of a Fisher exact test is 1.88e-25. In contrast, only 135 of the 977 genes overexpressed in cancer cells were found to be overexpressed in the RNA-seq data (red points in Fig. 4A, further referred to as consensus up-regulated genes), which is only 0.8 times the value expected for a random dataset (statistically significant underrepresentation with a p-value of 0.017). This shows that genes up-regulated in cancer cell lines tend not to be also highly expressed in mesenchymal stem cells. On the other hand, genes with lower expression in cancer cell lines have higher expression in normal mesenchymal stem cells. The sum of the expression levels (measured in RPKM) of all the LEF1 up-regulated genes was plotted versus the sum of expressions of the LEF1 down-regulated genes (Fig. 4B). Remarkably, the same phenomenon as in Fig. 3A is observed. The LEF1 up-regulated genes show comparable levels of expression in cancer cell lines and mesenchymal stem cells, while the LEF1 down-regulated genes show lower expression levels in the cancer cell lines. A significant correlation of 0.72 (Pearson correlation coefficient) is observed between the sum of expressions of LEF1 up-regulated genes

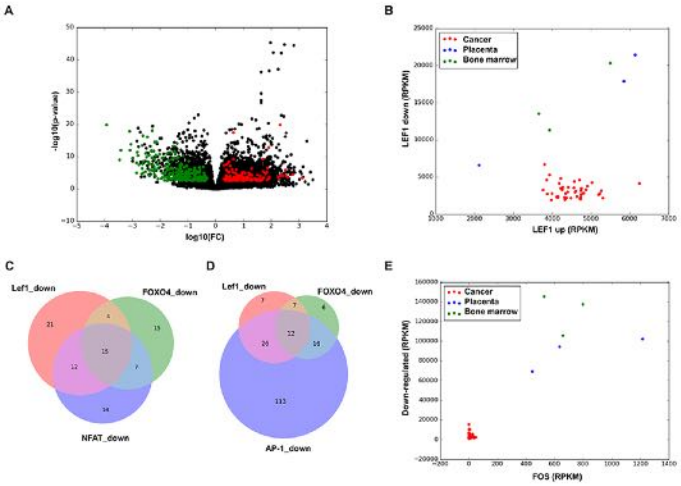

Figure 4. Volcano plot resulting from the differential expression analysis between cancer cell lines and mesenchymal stem cells. Genes found also to be differentially expressed in the microarray analysis are shown in red (up-regulated) and green (down-regulated) (**A**). Plot showing the sums of expression levels of genes regulated by LEF1 (**B**). Overlap between the consensus down-regulated genes controlled by LEF1, FOXO4, and NFAT (**C**). Overlap between the consensus down-regulated genes controlled by LEF1, FOXO4, and AP-1 (**D**). Plot showing the sum of expressions of all the down-regulated consensus genes versus the FOS gene (**E**).

and SP1 up-regulated genes (data not shown), which is in agreement with the previously hypothesized relation between these transcription factors and epithelial-mesenchymal transition.

The reason for the observed failure to overexpress a large number of LEF1 and FOXO4 regulated genes in cancer cell lines could be partially explained by the NFAT transcription factor, which also appeared in the enrichment analysis of down-regulated genes and has been reported to be a Wnt signaling suppressor[25]. This was tested by comparing the overlap between genes regulated by LEF1, FOXO4, and NFAT within the set of consensus down-regulated genes. More than half of the LEF1 and FOXO4 down-regulated genes are not regulated by NFAT (Fig. 4C), which suggests that there should be an extra explanation for their down-regulation.

Two different approaches were used to identify putative transcription factors controlling the expression of the consensus down-regulated genes. Firstly, we performed a new enrichment analysis of the consensus down-regulated genes, this time using DAVID 6.7[26–28]. The top enriched binding motifs corresponded to the transcription factors BACH2 (p-value 6.5e-13), FOXO1 (7.3e-12), AP-1 (3.4e-10), and FOXO4 (4.6e-10). The presence of FOXO binding motifs confirms the identification of FOXO4 by GeneCodis[11–13]. AP-1 complexes and transcription factors from the NFAT family have been reported to act synergistically on certain promoters containing adjacent binding sites[26]; however, the AP-1 regulated genes show a larger overlap with the LEF1 and FOXO4 down-regulated genes (Fig. 4D). Secondly, we used the RNA-seq dataset to compute correlation coefficients between the sum of the expression levels of all the consensus down-regulated genes and each of the genes coding transcription factors (see Table S3). The 8th most correlated transcription factor with a Spearman correlation coefficient of 0.72 and a p-value of 5.64e-8 was FOSL1 and the 10th, with a Spearman correlation coefficient of 0.66 and a p-value of 1.64e-6, was FOSL2, both being the components of the AP-1 complex. The AP-1 transcription factor is a dimeric complex formed by members of the FOS and JUN families. The observed correlations suggest that a lower expression of AP-1 complex components in cancer cell lines is indeed responsible for the lower expression of the consensus down-regulated genes. The RNA-seq data further confirmed that the genes coding 6 different AP-1 components are strongly down-regulated in cancer cell lines (Table S4), in some cases with expression levels one hundred times lower in cancer cell lines compared to mesenchymal stem cells. As an illustration of this phenomenon, the expression level of the FOS transcription factor (the main member of the FOS family) was plotted versus the expression level of the consensus down-regulated genes (Fig. 4E).

The role of AP-1 in tumorigenesis has been described to be ambivalent[29]. Some of the components of the AP-1 complex have been reported to be pro-oncogenic or anti-oncogenic depending on tumor type, stage and genetic background. However, the gene expression data that have been analyzed here show a very clear down-regulation of at least 6 AP-1 components in 44 cancer cell lines compared to mesenchymal stem cells. An enrichment

analysis using DAVID 6.7[25,26] revealed that 119 of the consensus down-regulated genes are membrane proteins and extracellular proteins, many of them being involved in cell attachment, such as fibronectin, thrombospondin, collagen, etc. (see Supplementary File SF3). It is known that cancer cells are less adhesive than normal human endothelial cells and fabricate less extracellular matrix, which favors their mobility and metastasis[30]. It is therefore possible that the down-regulation of AP-1 promotes cell migration and metastasis while at the same time could have anti-oncogenic effects in other stages of tumor development.

Transcriptional basis of cancer hallmark capabilities. In order to determine the relationship between the two large-scale transcriptional patterns (epithelial-mesenchymal transition and AP-1 down-regulation) that appear to differentiate cancer cell lines from healthy dividing cells and the hallmark capabilities of cancer[9], we performed enrichment analysis of KEGG[31,32] pathways using DAVID 6.7[25,26] (Supplementary file SF3) for the gene sets regulated by SP1, LEF1, and FOXO4 as well as for the consensus down-regulated genes and consensus up-regulated genes (found in both microarray and RNA-seq analysis). The mentioned analysis allowed us to identify the hallmark capabilities related to epithelial-mesenchymal transition and AP-1 down-regulation, respectively.

Hallmark capabilities enabled by epithelial-mesenchymal transition include *sustained proliferation*, with cell cycle components controlled by SP1, LEF1, and FOXO4 up-regulated in cancer cell lines. LEF1 also regulates the actin cytoskeleton, which is related to the formation of invasive protrusions involved in cell *invasion and metastasis*[30].

Hallmark capabilities enabled by putatively AP-1 and NFAT mediated down-regulation. Among the consensus down-regulated genes, KEGG pathway enrichment analysis revealed ECM-receptor interaction and focal adhesion, which are the features related to cell *invasion and metastasis*[30]. Loss of expression of cytokine-cytokine receptors is related to both *evading growth suppressors* and *resisting cell death*, as illustrated, for example, by the loss of the pro-apoptotic receptor Fas receptor, which triggers the extrinsic apoptotic program. In general, this down-regulation pattern results in the loss by cancer cells of their ability to integrate environmental signals of different types.

Hallmark capabilities enabled by alternative mechanisms. Fig. 2A–C shows that the up-regulation pattern associated to epithelial-mesenchymal transition is more pronounced in cancer cell lines than in mesenchymal stem cells. An enrichment analysis performed with DAVID 6.7 on the consensus up-regulated genes revealed the transcription factors E2F (p-value 1.4e-3) and NFY (p-value 1.4e-2). E2F is known to regulate the cell cycle, and the functional enrichment analysis of the consensus up-regulated genes revealed 10 components of the cell cycle to be up-regulated in cancer cell lines with respect to mesenchymal stem cells (Supplementary File SF3). Other enriched KEGG pathways among the consensus up-regulated genes were purine and pyrimidine metabolism, which are consistent with higher proliferation rates and an increased demand of biomass building blocks.

Alterations in metabolism as an emerging hallmark of cancer. The well-known review by Hannahan and Weinberg[9] indicates reprogramming energy metabolism as an emerging hallmark of cancer, which they describe as the shift to aerobic glycolysis or Warburg effect. Many cancer-specific metabolic features beyond the Warburg effect have been described in recent years[33]. Using a genome-scale metabolic model[34] and an algorithm based on flux balance analysis (supplementary material), a search for metabolic sub-networks associated with the identified transcriptional patterns was performed.

It was observed that LEF1 up-regulates 4 different histone lysine methylases: EHMT2 and EHMT1, which methylate lysine 9, as well as EZH2 and NSD2, which methylate lysine 27. Lysine 27 histone trimethylation has been reported to be responsible for gene silencing in cancer[35]. An enrichment test of genes repressed by this mechanism and the consensus down-regulated genes was performed, but no significant enrichment was detected (data now shown).

More importantly, cancer cell lines differ from healthy dividing cells in the higher expression of 5 enzymes involved in valine degradation (BCAT2, DBT, DLT, HADHA, and HIBADH), with 4 of them (BCAT2, DBT, DLT, and HADHA) being also involved in isoleucine degradation and 3 in leucine degradation (BCAT2, DBT and DLT) (Supplementary Fig. S2). This suggests that the degradation of the mentioned branched chain amino acids could play an important role in the energy supply of cancer cells. In order to quantify this role, we used the mentioned genome-scale metabolic model together with experimental metabolite uptake rates of the NCI-60 cell lines[36,37]. For each cell line, we computed a flux distribution satisfying the observed uptake and secretion rates and minimizing the sum of all the metabolic fluxes. From the obtained flux distribution, we estimated the total ATP production (which is equal to its consumption according to the pseudo-steady state assumption). The experimental lactic acid production rates and consumption rates of each of the mentioned branched chain amino acid were used to determine ATP produced by lactic fermentation of glucose and full degradation and oxidation of leucine, isoleucine, and valine. The fractions of each of the 4 ATP sources were plotted for each cell line (Fig. 5). It was found that between 12% and 55% of the total ATP is generated by the degradation of branched chain amino acids.

The 5 mentioned enzymes are not directly regulated by LEF1, FOXO4, or SP1 (according to GeneCodis); however, their expression pattern is identical to that of the genes associated with epithelial-mesenchymal transition (Supplementary Fig. S3), which suggests that the degradation of branched chain amino acids is triggered by the regulatory cascade associated with epithelial-mesenchymal transition.

Degradation of branched chain amino acids as a potential therapeutic window. The high fraction of ATP derived from the degradation of branched chain amino acids in cancer cell lines and its higher

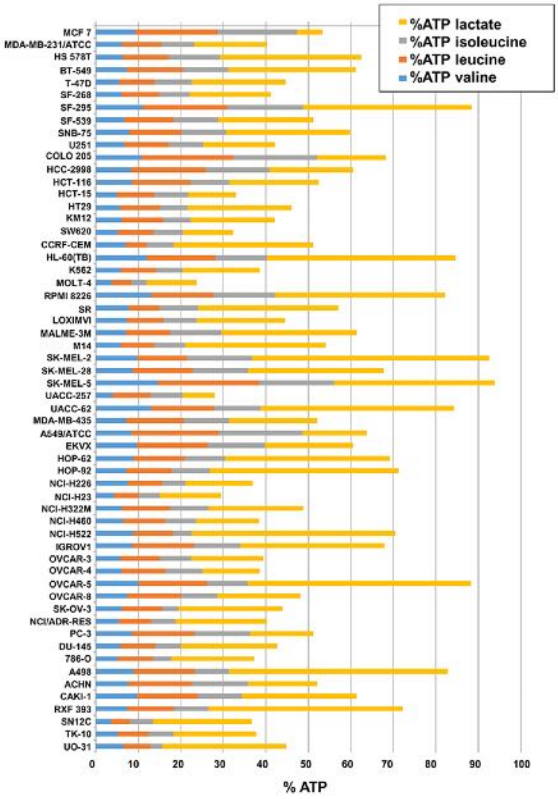

Figure 5. Estimated percentages of ATP obtained from lactic fermentation and valine, leucine, and isoleucine degradation for the NCI-60 cell lines.

activity compared to some healthy dividing cells suggests that suppressing the activity of enzymes in this pathway could be a valid therapeutic strategy (alone or in combination with other treatments). Here we focused on the BCAT2 enzyme that catalyzed the first step of the degradation of leucine, valine, and isoleucine (Supplementary Fig. S4). Firstly, we confirmed at the protein level the conclusion obtained from microarray analysis. We used the breast cancer cell line MCF-7 and primary cell culture prepared from breast tumor tissue (BCC) (see Materials and Methods). We introduced BCC in our experimental design in order to determine whether the conclusions obtained in widely used cancer cell lines can be extrapolated to cells from real tumors. As healthy dividing cells, we chose airway smooth muscle cell line (ASM) and breast epithelial cell line (MCF-10A). As shown in Fig. 6A,B, higher abundance of BCAT2 in cancer cells was observed as compared with healthy cells.

BCAT2 gene silencing experiments in cancer and normal cells were performed to assess the impact of branched chain amino acid degradation on cell proliferation. Reduced levels of the target protein after siRNA transfection were evaluated by Western blotting and immunocytochemical analysis (Fig. 6A,B; for full images of Western blots see Supplementary Fig. S6). BCAT2 siRNA decreased the number of MCF-7 and BCC cells by 16.6% ± 2.1% and 11.3% ± 1.5%, respectively (Fig. 6C). The number of ASM and MCF-10A remained unchanged (99% ± 0.8% and 106% ± 3.4%, respectively, compared to control).

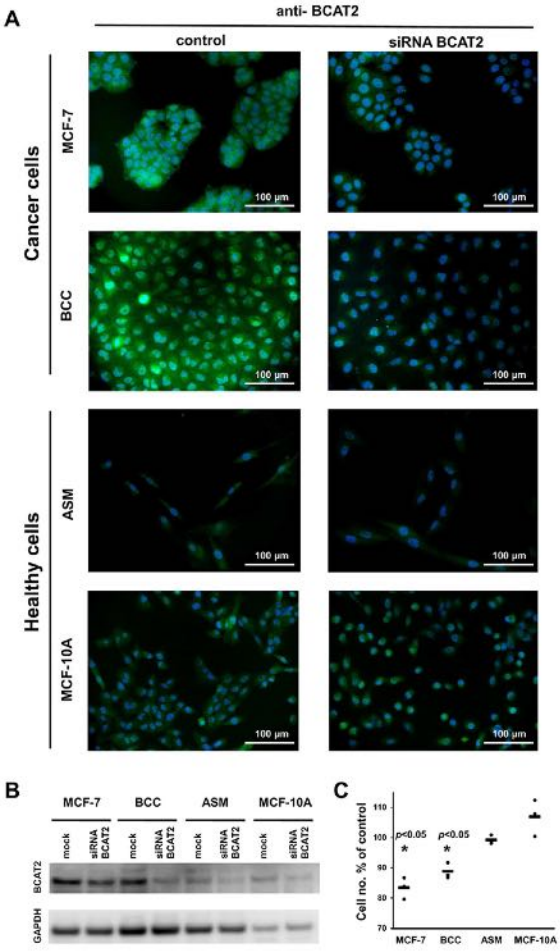

Figure 6. The effect of BCAT2 silencing on proliferation of breast cancer and normal cells. (**A**) Immunofluorescence of BCAT2 in cancer (MCF-7 and BCC) and normal (ASM and MCF-10A) cells in control and after BCAT2 siRNA transfection (green-secondary antibody to rabbit IgG-H&L conjugated with Alexa Fluor 488; blue-DAPI stained nucleus). (**B**) Representative Western blot showing BCAT2 expression levels after BCAT2 siRNA transfection compared to mock-treated controls. (**C**) Inhibition of cancer cell (MCF-7 and BCC) proliferation after BCAT2 silencing determined by flow cytometry assay. Data are expressed as a percentage of mock-treated controls (n = 3). All experiments were performed 24 h post-transfection.

There was no change in viability of all tested cancer and healthy BCAT2 siRNA-treated cells, as determined by Annexin V-PE/7-AAD staining (Supplementary Fig. S5). These results suggest that BCAT2 could be a suitable drug target with cytostatic effects on cancer cells.

Discussion

By analyzing 289 microarray samples and 50 RNA-seq libraries of cancer cell lines and healthy dividing cells, we have observed that cancer cell lines are generally characterized by two distinct regulatory events involving hundreds of genes.

The first identified event is associated with the phenomenon of epithelial-mesenchymal transition and appears to be more intense in cancer cell lines and healthy mesenchymal stem cells compared to epithelial stem cells. Based on gene enrichment analysis, the transcription factors SP1, LEF1, and FOXO4 have been identified as putative drivers of this large-scale transcriptional pattern. SP1 is already known to be involved in epithelial-mesenchymal transition, and our analysis revealed that among the genes up-regulated by SP1, there are 9 components of the Wnt signaling pathway, whose activation results in the phosphorylation of β-catenin, which binds the transcription factors coded by LEF1 and FOXO4, leading to the up-regulation of their target genes. The SP1 gene is itself among the FOXO4 targets and was found to be up-regulated in cancer cell lines. This suggests the existence of a positive activation feedback involving SP1, the canonical Wnt signaling pathway and FOXO4, resulting in a large-scale transcriptional change. It has been shown[38] that switches between two alternative cellular states (such as epithelial and mesenchymal) are typically regulated by sets of transcription factors forming feedback structures.

Interestingly, 5 enzymes involved in the degradation of branched chain amino acids (leucine, valine, and isoleucine) show a transcriptional pattern associated with epithelial-mesenchymal transition, even if they are not directly regulated by SP1, LEF1, and FOXO4. This general observation at the gene expression level was confirmed at the protein level for the enzyme BCAT2 in the cancer cell line MCF-7, the primary cell culture BCC isolated from tumor (which showed high BCAT2 levels), ASM and MCF-10A cells, in which it was lowly expressed. The silencing of the BCAT2 gene led to a significant decrease of cell proliferation for MCF-7 and BCC while had no effect on the proliferation of ASM cells, which proved the existence of a therapeutic window that could be exploited to develop cytostatic drugs targeting CICs preferentially while having lower effects on healthy dividing cells.

A second large-scale transcriptional pattern appeared to differentiate cancer cell lines from healthy mesenchymal stem cells. This pattern consists on the apparent failure of cancer cell lines to overexpress a large number of genes coding membrane proteins involved in phenomena such as ECM-receptor interaction, focal adhesion, cytokine-cytokine receptors, etc., as well as extracellular proteins that constitute the extracellular matrix. This down-regulation appears to confer the cells with the abilities of evading growth suppressors and cell death and diminishing cell adhesion, which leads to invasion and metastasis. In healthy cells, these genes appear to be up-regulated as a result of epithelial-mesenchymal transition; however, they seem to avoid overexpression in cancer cell lines. A gene enrichment analysis as well as a correlation analysis between the expression of the genes down-regulated in cancer cell lines and the expression of each transcription factor (using RNA-seq data) revealed a putative role of the AP-1 transcriptional complex on the observed regulatory pattern. Among the genes coding proteins that form the AP-1 complex, 6 of them also appeared to be down-regulated in cancer cell lines with respect to healthy mesenchymal stem cells. The role of AP-1 in cancer development is controversial and some of the components of the AP-1 complex have been reported to be pro-oncogenic or anti-oncogenic depending on tumor type, stage, and genetic background; however, our analysis revealed strong evidence of low AP-1 activity in cancer cell lines. Therefore, we believe that the AP-1 transcriptional complex deserves further attention for understanding the mechanisms leading to tumor formation and metastasis.

Our experiments on BCAT2 demonstrate how the described transcriptional hallmarks could potentially be exploited as therapeutic windows to target selectively cancer cells while keeping unaffected healthy dividing cells.

Materials and Methods

Microarrays. To extract the characteristic direction in gene expression that differentiates tumorigenic and healthy duplicating cells, we used the data in Table S1. The microarray set in Table S1 was normalized using the RMA method implemented in the *affy* R package.

Linear discrimination analysis and identification of differentially expressed genes was performed as described in the supplementary material (Statistical methods). The R code used in the analysis is reported in the supplementary material (R code to perform linear discrimination analysis).

As validation sets, we used the data summarized in Table S2. We used two validation datasets that included two different cancer cell lines originated in the same tissue (colon and breast, respectively) and compared them with stem cells from the same tissue.

Each validation set (colon and breast respectively) was normalized using the RMA method implemented in the *affy* R package.

RNA-seq analysis. Gene expression data for the 44 cancer cell lines (BioProject accession number PRJNA183192) included in the Human Proteome Atlas were downloaded from www.proteinatlas.com in the form of a comma-separated file that contains the expression of each gene in each cell line (given as RMPK). This file was parsed using a customized python script (available upon request). RNA-seq fastq files for 6 different mesenchymal stem cell lines (3 from placenta and 3 from bone-marrow) were downloaded from https://usegalaxy.org/u/cic19/h/mesenchymal-stem-cells-rnaseq. The reads were aligned on the complete list of human transcripts obtained from Ensembl BioMart using Bowtie2. The resulting alignment files were analyzed using a customized python script that is available upon request. Fold changes were calculated by dividing the average expression of each gene in cancer cells by the average expression in mesenchymal stem cells, p-values were calculated using the t-test, and correction for multiple testing was performed as described in the supplementary material.

Cell Lines and Culture Medium. BCC cells were prepared as described elsewhere (https://www.ncbi.nlm.nih.gov/pmc/articles/PMC4063716/) from part of the tumor tissue sample taken from a 41-year-old female patient suffering from invasive ductal carcinoma (T1 N0 M0 G2, ER(+), PR(+), HER2(3+)) during lumpectomy and sentinel lymph node biopsy surgery. The second part of the sample was used for histological and immunohistochemical

examination. Invasive ductal carcinoma staging (T (tumor), N (node), M (metastasis) and G (grade)) categories were assigned according to the Union for International Cancer Control (UICC) classification. Pathohistological diagnosis was proved at the Department of Pathology, Lithuanian University of Health Sciences. The patient provided written informed consent. This study was approved by the Kaunas Regional Biomedical Research Ethics Committee (license number BE-2–7), and all experiments were performed in accordance with the guidelines and regulations of the mentioned institution. BCC and MCF-7 (human breast adenocarcinoma cell line; CLS-Cell Lines Service, Eppelheim, Germany) were grown in Dulbecco's Modified Eagle Medium:Ham's F-12 (1:1; DMEM/F-12) (Life technologies, Carlsbad, CA, USA) medium with 10% fetal bovine serum (FBS) and antibiotics (penicillin 100 U/mL, streptomycin 100 µg/mL). Immortalized human airway smooth muscle (ASM) cells (kindly donated by Prof. R. Gosens, University of Groningen, Netherlands) were obtained as described elsewhere[35]. ASM cells were grown in DMEM medium containing 10% FBS and penicillin/streptomycin mix (100 U/mL penicillin and 100 µg/mL streptomycin). MCF-10A cells (ATCC, Wesel, Germany) were grown in DMEM/F-12 medium supplemented with 5% horse serum (GE Healthcare Life Sciences, Logan, USA), 20 ng/mL EGF (Life technologies, Carlsbad, CA, USA),10 µg/ml insulin (Life technologies, Carlsbad, CA, USA), 0.5 µg/mL hydrocortisone, and 100 ng/mL cholera toxin and penicillin/streptomycin mix. Cells were maintained in a humidified incubator at 37 °C/5% CO_2. All chemicals were purchased from Sigma Aldrich Corp. (Steinheim, Germany), unless indicated otherwise.

siRNA transfection. For BCAT2 gene silencing, jetPRIME transfection reagent (Polyplus-transfection® SA, France) and final concentration of 5 nM BCAT2 siRNA (sense 5′-CCAUGAACAUCUUUGUCUAtt-3′, antisense 5′-UAGACAAAGAUGUUCAUGGtt-3′, Invitrogen, USA) were used according to the manufacturer's instructions. All the following experiments were performed 24 h after siRNA transfection.

Immunocytochemistry. Cells grown in 24-well plates with glass coverslips on the bottom were fixed with 4% paraformaldehyde for 15 min and permeabilized with 0.2% Triton X-100 in PBS for 3 min. Samples then were incubated with primary antibody against BCAT2 (Abcam, Cambridge, UK) for 1 h at 37 °C, then rinsed with 1% BSA/PBS and incubated with secondary donkey anti-rabbit IgG H&L antibody conjugated with Alexa Fluor 488 (Life technologies, Carlsbad, CA, USA) for 30 min. Coverslips were attached with a Vectashield Mounting Medium with DAPI (Vector Laboratories, CA, USA). The analysis was performed with an inverted fluorescence microscope Olympus IX81 (Olympus Europa holding Gmbh, Hamburg, Germany) equipped with an Orca-R2 cooled digital camera (Hamamatsu Photonics K.K., Japan), the fluorescence excitation system MT10 (Olympus Life Science Europa Gmbh, Hamburg, Germany), and the fluorescence imaging system XCELLENCE (Olympus Soft Imaging Solutions Gmbh, München, Germany).

Western Blot analysis. For each cell type, 3×10^6 cells were lysed in ice-cold cell extraction buffer (Invitrogen, USA) containing 1 mM PMSF (Abcam, Cambridge, UK) and 20 µl/mL protease inhibitor cocktail (Sigma-Aldrich, Steinheim, Germany) for 30 min. The lysates were centrifuged at 13000 rpm for 10 min at 4 °C. The total protein concentration was determined by a Qubit® protein assay kit (Invitrogen, USA) using a Qubit 3.0 fluorometer (Invitrogen, USA). Cell lysates (30 µg) were separated by Bolt™ 4–12% Bis-Tris plus gels (Invitrogen, USA) and transferred to PVDF membranes (Millipore, USA). Proteins were detected using primary antibodies against BCAT2 (Abcam, Cambridge, UK) and GAPDH (Invitrogen, USA) and a WesternBreeze® chemiluminescent kit (Invitrogen, USA) according to the manufacturer's instructions. Bands were visualized using the G:Box Chemi Gel Documentation system (Syngene, USA).

Flow cytometry assay. Initially, 5×10^4 cells were seeded in a 6-well plate in 2 mL of full media. Mock-transfected and BCAT2 siRNA-transfected cells were washed twice with PBS, trypsinized, and collected by centrifugation. Afterwards, cells were incubated with Guava Nexin® Reagent (Millipore, USA) for 20 min at room temperature according to the manufacturer's instructions. Samples were quantified by a Guava PCA flow cytometer (Millipore, USA). The data were analyzed by guavaSoft 2.7 Nexin software.

Statistical analysis. Averaged experimental results are reported as means ± standard error of the mean. Statistical analysis was performed using two-tailed Student's t-test. Differences were considered statistically significant at $p < 0.05$. The calculations were performed using SigmaPlot.

References

1. Patrick, G. L. An introduction to Medicinal Chemistry. 489–553 (Oxford University Press, 2005)
2. Li, Y., Guo, Y. & Liu, Y. Cancer chemotherapy induces cardiotoxicity by targeting cardiac stem cells. *J. Cell. Mol. Med.* **14**, 2630–2632 (2010).
3. Stuelten, C. H. *et al.* Complex display of putative tumor stem cell markers in the NCI60 tumor cell line panel. *Stem Cells.* **28**, 649–660 (2010).
4. Reya, T., Morrison, S. J., Clarke, M. F. & Weissman, I. L. Stem cells, cancer, and cancer stem cells. *Nature* **414**, 105–111 (2001).
5. Parsons, D. W. *et al.* An integrated genomic analysis of human glioblastoma multiforme. *Science* **321**, 1807–1812 (2008).
6. Cancer Genome Atlas Research Network, Comprehensive genomic characterization defines human glioblastoma genes and core pathways. *Nature* **455**, 1061–1068 (2008)
7. Ding, L. *et al.* Somatic mutations affect key pathways in lung adenocarcinoma. *Nature* **455**, 1069–1075 (2008).
8. Negrini, S., Gorgoulis, V. G. & Halazonetis, T. D. Genomic instability – an evolving hallmark of cancer. *Nat. Rev. Mol. Cell. Biol.* **11**, 220–227 (2010).
9. Hannahan, D. & Weinberg, D. A. Hallmarks of Cancer: The Next Generation. *Cell* **144**, 646–674 (2011).
10. Clark, N. R. *et al.* The characteristic direction: a geometrical approach to identify differentially expressed genes. *BMC Bioinformatics* **15**, 79 (2014).
11. Carmona-Saez, P., Chagoyen, M., Tirado, F., Carazo, J. M. & Pascual-Montano, A. GENECODIS: A web-based tool for finding significant concurrent annotations in gene lists. *Genome Biol.* **8**, R3 (2007).
12. Nogales-Cardenas, R. *et al.* GeneCodis: interpreting gene lists through enrichment analysis and integration of diverse biological information. *Nucl. Acids Res.* **37**, W317–W322 (2009).

13. Tabas-Madrid, D., Nogales-Cadenas, R. & Pascual-Montano, A. GeneCodis3: a non-redundant and modular enrichment analysis tool for functional genomics. *Nucl. Acids Res.* **40**, W478–W483 (2012).
14. Zhang, K. *et al.* WNT/β-Catenin Directs Self-Renewal Symmetric Cell Division of hTERThigh Prostate Cancer Stem Cells. *Cancer Res.* **77**, 2534–2547 (2017).
15. Piccin, D. & Morshead, C. M. Wnt signaling regulates symmetry of division of neural stem cells in the adult brain and in response to injury. *Stem Cell* **29**, 528–538 (2011).
16. Gehrke, I., Gandhirajan, R. K. & Kreuzer, K. A. Targeting the WNT/β-catenin/TCF/LEF1 axis I solid and haematological cancers: Multiplicity of therapeutic options. *EJC* **45**, 2759–2767 (2009).
17. Aoki, M. *et al.* Nuclear endpoint of Wnt signaling: neoplastic transformation induced by transactivating lymphoid-enhancing factor 1. *Proc. Natl. Acad. Sci. USA* **96**, 139–44 (1999).
18. Hoogeboom, D. *et al.* Interaction of FOXO with beta-catenin inhibits beta-Catenin/T cell factor activity. *J. Biol. Chem.* **283**, 9224–9230 (2008).
19. Maiese, K., Chong, Z. Z., Shang, Y. C. & Hou, J. A. "FOXO" in Sight: Targeting Foxo Proteins from Conception to Cancer. *Med. Res. Rev.* **3**, 395–418 (2009).
20. Jungert, K. *et al.* Sp1 Is Required for Transforming Growth Factor-B–Induced Mesenchymal Transition and Migration in Pancreatic Cancer Cells. *Cancer Res.* **67**, 1563–1570 (2007).
21. Jia, Z. *et al.* Combined Treatment of Pancreatic Cancer with Mithramycin A and Tolfenamic Acid Promotes Sp1 Degradation and Synergistic Antitumor Activity. *Cancer Res.* **70**, 1111–1119 (2010).
22. Kwon, Y. *et al.* CYP1B1 Enhances Cell Proliferation and Metastasis through Induction of EMT and Activation of Wnt/β-Catenin Signaling via Sp1 Upregulation. *PLoS ONE* **11**, e0151598 (2016).
23. Moisan, A. *et al.* The WTX tumor suppressor regulates mesenchymal progenitor cell fate specification. *Dev. Cell* **20**, 583–596 (2011).
24. Roson-Burgo, B., Sanchez-Guijo, F., Del Cañizo, C. & De Las Rivas, J. Transcriptomic portrait of human Mesenchymal Stromal/Stem cells isolated from bone marrow and placenta. *BMC Genomics* **15**, 910 (2014).
25. Huang, T. *et al.* NFAT proteins repress canonical Wnt signaling via its interaction with Dvl and participate in regulating neural progenitor cell proliferation and differentiation. *J. Biol. Chem* **286**, 37399–37405 (2011).
26. Huang, D. W., Sherman, B. T. & Lempicki, R. A. Systematic and integrative analysis of large gene lists using DAVID Bioinformatics Resources. *Nature Protoc.* **4**, 44–57 (2009).
27. Huang, D. W., Sherman, B. T. & Lempicki, R. A. Bioinformatics enrichment tools: paths towards the comprehensive functional analysis of large gene lists. *Nucleic Acids Res.* **37**, 1–13 (2009).
28. Macián, F., López-Rodríguez, C. & Rao, A. Partners in transcription: NFAT and AP-1. *Oncogene* **20**, 2476–2489 (2001).
29. Wagner, E. F. & Eferl, R. AP-1: A double-edged sword in tumorigenesis. *Nat. Rev. Cancer* **3**, 859–868 (2003).
30. Ruoslahti, E. Fibronectin and its integrin receptors in cancer. *Adv. Cancer Res.* **76**, 1–20 (1999).
31. Kanehisa, M. & Goto, S. KEGG: Kyoto encyclopedia of genes and genomes. *Nucleic Acids Res.* **28**, 27–30 (2000).
32. Yamaguchi, H. & Condeelis, J. Regulation of the actin cytoskeleton in cancer cell migration and invasion. *Biochim. Biophys. Acta.* **1773**, 642–652 (2007).
33. Yizhak, K., Chaneton, B., Gottlieb, E. & Ruppin, E. Modeling cancer metabolism on a genome scale. *Mol. Syst. Biol.* **11**, 817 (2015).
34. Feizi, A. & Bordel, S. Metabolic and protein interaction sub-networks controlling the proliferation rate of cancer cells, and their impact on patient survival. *Sci. Rep.* **3**, 3041 (2013).
35. Kondo, Y. *et al.* Gene silencing in cancer by histone H3 lysine 27 trimethylation independent of promoter DNA methylation. *Nat. Genet.* **40**, 741–750 (2008).
36. Jain, M. *et al.* Metabolite profiling identifies a key role for glycine in rapid cancer cell proliferation. *Science* **336**, 1040–1044 (2012).
37. Dolfi, S. C. *et al.* The metabolic demands of cancer cells are coupled to their size and protein synthesis rates. *Cancer Metab.* **1**, 20 (2013).
38. Österlund, T., Bordel, S. & Nielsen, J. Controllability analysis of transcriptional regulatory networks reveals circular control patterns among transcription factors. *Integr. Biol.* **7**, 560–568 (2015).
39. Gosens, R. *et al.* Role of caveolin-1 in p42/p44 MAP kinase activation and proliferation of human airway smooth muscle. *Am J Physiol Lung Cell Mol Physiol.* **291**, L523–34 (2006).

Acknowledgements

This research was funded by a scholarship from the Swedish Institute (Visby program No. 11278/2013), a grant from the Olle Enkvist Foundation (No. 21210045) and a grant (No. SEN-04/2016) from the Research Council of Lithuania.

Author Contributions

Conceived the research and performed the computational analysis of microarrays and RNA-seq data: S.B. Designed the experiments: S.B., I.A., V.M., V.A.S. Performed experiments with the cells: I.A., V.M., I.C., G.M., V.A.S. Analyzed the results: S.B., I.A., V.M., V.A.S. Wrote the paper: S.B., I.A., V.A.S.

Additional Information

Supplementary information accompanies this paper at doi:10.1038/s41598-017-08329-8

Competing Interests: The authors declare that they have no competing interests.

Publisher's note: Springer Nature remains neutral with regard to jurisdictional claims in published maps and institutional affiliations.

PLOS ONE

RESEARCH ARTICLE

Genome scale metabolic models as tools for drug design and personalized medicine

Vytautas Raškevičius[1,2]*, Valeryia Mikalayeva[1], Ieva Antanavičiūtė[1], Ieva Ceslevičienė[1], Vytenis Arvydas Skeberdis[1], Visvaldas Kairys[2], Sergio Bordel[1,3]

1 Institute of Cardiology, Lithuanian University of Health Sciences, Kaunas, Lithuania, **2** Department of Bioinformatics, Institute of Biotechnology, Vilnius University, Vilnius, Lithuania, **3** Department Chemical Engineering and Environmental Technology, University of Valladolid, Valladolid, Spain

* vytautas.raskevicius@lsmuni.lt

OPEN ACCESS

Citation: Raškevičius V, Mikalayeva V, Antanavičiūtė I, Ceslevičienė I, Skeberdis VA, Kairys V, et al. (2018) Genome scale metabolic models as tools for drug design and personalized medicine. PLoS ONE 13(1): e0190636. https://doi.org/10.1371/journal.pone.0190636

Editor: Irina V Lebedeva, Columbia University, UNITED STATES

Received: June 1, 2017

Accepted: December 18, 2017

Published: January 5, 2018

Data Availability Statement: All data files and the HMR model are available from BioModels Database (https://www.ebi.ac.uk/compneur-srv/biomodels-main/MODEL1707250000) and GitHub (https://github.com/SergioBordel/pyTARG). All relevant data are within the paper and its Supporting Information files.

Funding: This research was funded by a scholarship from the Swedish Institute (Visby program no. 11278/2013), a grant from the Olle Engkvist Foundation (no. 21210045). The funders

Abstract

In this work we aim to show how Genome Scale Metabolic Models (GSMMs) can be used as tools for drug design. By comparing the chemical structures of human metabolites (obtained using their KEGG indexes) and the compounds contained in the DrugBank database, we have observed that compounds showing Tanimoto scores higher than 0.9 with a metabolite, are 29.5 times more likely to bind the enzymes metabolizing the considered metabolite, than ligands chosen randomly. By using RNA-seq data to constrain a human GSMM it is possible to obtain an estimation of its distribution of metabolic fluxes and to quantify the effects of restraining the rate of chosen metabolic reactions (for example using a drug that inhibits the enzymes catalyzing the mentioned reactions). This method allowed us to predict the differential effects of lipoamide analogs on the proliferation of MCF7 (a breast cancer cell line) and ASM (airway smooth muscle) cells respectively. These differential effects were confirmed experimentally, which provides a proof of concept of how human GSMMs could be used to find therapeutic windows against cancer. By using RNA-seq data of 34 different cancer cell lines and 26 healthy tissues, we assessed the putative anticancer effects of the compounds in DrugBank which are structurally similar to human metabolites. Among other results it was predicted that the mevalonate pathway might constitute a good therapeutic window against cancer proliferation, due to the fact that most cancer cell lines do not express the cholesterol transporter NPC1L1 and the lipoprotein lipase LPL, which makes them rely on the mevalonate pathway to obtain cholesterol.

Introduction

Predicting which ligands bind a particular protein and modify its activity is a fundamental step in drug-design, which is typically solved using molecular docking [1]. The structure of already known ligands can be used as a template to improve the prediction of drug-target interactions [2, 3]. Enzymes are important drug targets [4] for which some ligands are already known (their natural substrates), and are therefore particularly suitable for structure-based drug design. The assumption that molecules with similar structure to the natural substrate of an

had no role in study design, data collection and analysis, decision to publish, or preparation of the manuscript.

Competing interests: The authors have declared that no competing interests exist.

enzyme are likely to fit into the same binding site as the substrate, leading to competitive inhibition of the enzyme, can also be used to infer possible inhibitory effects of already existing drugs on enzymes different from their original targets, which would allow so called drug repositioning or repurposing [5]. This is particularly useful when it comes to the usage of approved drugs to treat new diseases, avoiding many of the clinical and preclinical trials necessary for a new compound. Here we show (as it was reasonable to expect) that drugs with a Tanimoto score higher than 0.9 with respect to a certain human metabolite are 29.5 times more likely to bind enzymes that have this metabolite as a substrate than a randomly chosen drug. Some drugs mimicking natural metabolites (known as antimetabolites) have been used for a long time as anticancer drugs (for example drugs mimicking the structure of folates interfere with DNA synthesis and impair cell growth). The analysis performed here revealed putative anticancer effects of compounds that are not currently being used as anticancer drugs.

The effects of a drug on a particular patient and disease, are not just reduced to its interaction with its targets, but have to be seen within the context of the whole cell. The effect of inhibiting the activity of a particular enzyme on a certain disease phenotype, depends on the activities of many other enzymes that form a complex network of metabolic reactions in which the products of a reaction are the substrates of others. Therefore, the response to a certain drug can be very different in different patients (or in different cell types), which leads to the emerging field of personalized medicine and personalized drug-choice [6]. Different effects of a drug on different cell types, depending on the activity of the whole metabolic network, are also related to the existence of so called therapeutic windows, that's the possibility of inflicting damage on a particular cell type (such as tumor cells) while minimizing the negative effects on healthy cells. The search for suitable therapeutic windows is a particularly important problem in cancer and the interest on metabolic enzymes as therapeutic windows is rapidly increasing [7]. Particularly suitable tools to deal with the mentioned problems (drug design, drug repurposing, personalized medicine and finding therapeutic windows) are Genome Scale Metabolic Models (GSMMs).

GSMMs [8, 9] are comprehensive compilations of all the metabolic reactions that take place in an organism. Each of the reactions is associated with one or more enzymes that are encoded by specific genes. Thus a direct gene-protein-reaction connection is established, which is an important feature of GSMMs. Given the stoichiometric coefficients of the different reactions in the network, it is possible to establish a stoichiometric matrix, which is a mathematical representation that provides quantitative information on how the different metabolites are linked to each reaction in the network. If the concentrations of all the internal metabolites are assumed to be in steady state, which is a reasonable assumption due to the fast turnover of intracellular metabolites, it is possible to constrain the fluxes to a space of feasible flux distributions and evaluate the metabolic capabilities of the cell (for example its capability to synthesize biomass building blocks). GSMMs have been applied to the study of cancer and other aspects of human metabolism following different approaches [10–12]. Many of those approaches consist in the generation of tissue specific models by integrating gene-expression, proteomics, metabolomics and other high throughput data [11, 13]. Tissue or cell specific models are usually presented as a sub-set of the total human metabolism, which is active in the tissue or cell of interest. Each human metabolic reaction is presented as present or absent, and no quantitative information on the reaction rates is embedded in the models. Other approach (the PRIME method) consists in setting maximal boundaries to a set of reaction rates, based on gene expression microarrays [14]. Here we use RNA-seq data to impose maximal rate boundaries on all the reactions in the model. Once the model is constrained according to the RNA-seq data from a particular cell type, we quantify the effects of decreasing the flux through the reactions targeted by a certain drug on an objective function, which in this case is the capability of

producing biomass building blocks for cell proliferation (uncontrolled cell proliferation is one of the main characteristics of cancer).

This approach has been used to identify drugs contained in the DrugBank database [15] that are putatively able to impair the growth of cancer cell lines while keeping their effects on healthy tissues as limited as possible. We have also shown experimentally that lipoamide analogs have a differential effect on the breast cancer cell line MCF7, compared to healthy ASM (airway smooth muscle) cells, which was predicted in-silico from RNA-seq profiles.

Results

Structure similarity as a guide to predict drug-enzyme binding

An updated human GSMM [16] was used to obtain a list of human metabolites with KEGG [17] identifiers. Based on their KEGG identifiers 1475 different chemical structures of human metabolites were obtained. Chemical structures were also obtained for every drug in DrugBank [15] and Tanimoto scores using FP4 fingerprints were calculated for each metabolite-drug pair using the software OpenBabel [18]. A set of 4231 drug-metabolite pairs with Tanimoto scores higher than 0.9 were extracted for further analysis (excluding the trivial cases in which the DrugBank compound and the metabolite were identical). EC numbers for the targets of each drug and for the enzymes associated to each metabolite were extracted from DrugBank and KEGG respectively. In 2817 cases both the drug and the metabolite had at least one target reported. For 644 pairs at least one of the targets was shared among the drug and the metabolite, which is 23% of the total pairs with Tanimoto scores over 0.9. As a control, we extracted 4000 random drug-metabolite pairs without any restriction on their Tanimoto scores and bootstrapped this procedure 1000 times (S1 Fig). On average, in 1% of the cases both the drug and the metabolite had reported shared target. An exact Fisher test resulted in a p-value of 2.2e-16 and an odds-ratio of 29.5.

For example, 7,8-dihydrobiopterin is described in DrugBank as an inhibitor of the enzyme dihydroneopterin aldolase, which catalyzes the conversion of its analog 7,8-dihydroneopterin to 6-hydroxymethyl-7,8-dihydropterin and glycolaldehyde (Fig 1).

Integration of RNA-seq data with GSMMs to predict phenotypes

GSMMs can be used to predict any phenotype that could be linked to the rate of production or consumption of one or several metabolites. In particular, cell growth can be described as the rate of assembly of biomass building blocks into macromolecules (amino acids into proteins for example). This is described in the models by a so called "biomass equation", which reflects the relative proportions in which different biomass building blocks are added to biomass. Predicting actual metabolic flux distributions would require knowing the kinetics of each metabolic reaction as well as other parameters outside metabolism, such as ribosome concentrations, protein synthesis rates, etc. The number of parameters to be adjusted from experimental data is too large for any realistic attempt to describe kinetically whole cell metabolic flux distributions, which makes necessary some rough assumptions. We assume that the maximal reaction rate of a metabolic reaction is proportional to the abundance of the enzyme catalyzing this reaction, which is itself proportional to the abundance of the transcript coding the enzyme. The proportionality constants might be very different for each reaction, however we will consider them to be equal. This assumption is far from reality but it is still able to capture the fact that increases in the expression of a gene are likely to result in a higher maximal flux through the reactions catalyzed by its gene products. The proportionality constant was set to be 0.027 mmol g-DW^{-1}h^{-1} for an expression level of 10 RPKM. This constant was chosen in order to fit the experimental growth rate of the cell line A549. Before setting each constraint,

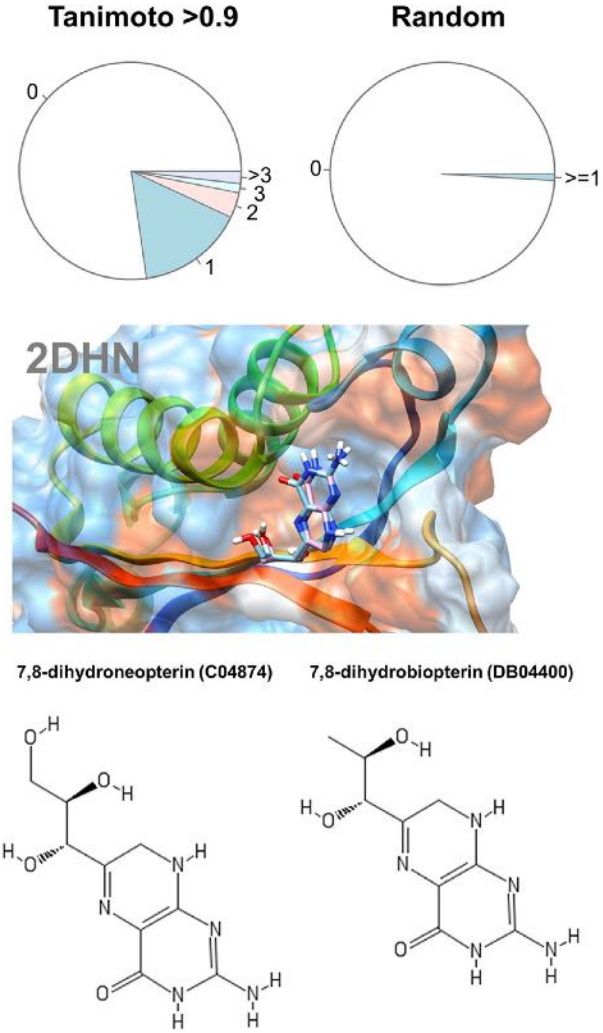

Fig 1. Analysis of drug-metabolite pairing. The upper panel shows the percentages of drug-metabolite pairs sharing 1, 2, 3 or more enzymes respectively for pairs with Tanimoto scores higher than 0.9 (left) and random pairs (right). The lower panel illustrates the docking of dihydroneopterin aldolase (2DHN) with its natural metabolite 7,8-dihydroneopterin (C04874, cyan sticks) and its structural analog 7,8-dihydrobiopterin (DB04400, pink sticks).

https://doi.org/10.1371/journal.pone.0190636.g001

the expression levels (in RPKM) were rounded up to the next multiple of 10. This proved to be an efficient way to avoid numerical problems while performing linear optimization. For reactions with several enzymes, the expression level was chosen to be the one of the most abundant enzyme. After constraining each reaction in the model based on the gene expression of its associated enzymes, the maximal value of the biomass production reaction (or any other reaction associated to a certain phenotype) can be computed by linear optimization (see Materials and methods). In order to perform the mentioned calculations, we have written a Python library (pyTARG), which is available at https://github.com/SergioBordel/pyTARG. We define as relative inhibition the fraction by which the original rates of the reactions affected by the drug are decreased (a relative inhibition of 0.9 means that the rate is 0.1 times its original value). Relative growth rate is the ratio of the maximal growth rate with inhibition to the maximal growth rate without inhibition. A value of 1 would mean that the cell is able to fully compensate the effects of the drug by using alternative metabolic pathways to produce all its biomass components. A relative growth equal to one minus the relative inhibition means that the cell cannot use any alternative pathway to compensate the effects of the drug. Values in between mean that there are alternative metabolic pathways that the cell can use, but they are not as efficient as the pathways targeted by the drug. The actual relative inhibition of a drug on a certain target would depend both on the concentration of the drug and its binding strength to the target. The problem of predicting this relative inhibition is out of the scope of this article. Here it is modeled only the impact that a certain relative inhibition would have on the global cell metabolism.

In order to check the ability of our Flux Balance Analysis approach to recapitulate (at least qualitatively), the actual uptake and secretion profiles of cell lines, we compared our predictions (see Materials and methods) with available experimental data [19] for the human lung adenocarcinoma epithelial cell line A549. The model showed to be able to reproduce (Fig 2) the largest uptake and secretion rates (glucose and glutamine uptake and lactic and citric acid secretion). Given the fact that the upper bounds imposed on the reaction rates are multiples of 0.027 mmol $g\text{-}DW^{-1}h^{-1}$, we cannot expect the model to predict fluxes below 0.027 mmol $g\text{-}DW^{-1}h^{-1}$ (as in the cases for isoleucine, leucine, valine and serine uptake rates). Remarkably, the model is able to reproduce the Warburg effect (aerobic production of lactic acid) as well as the secretion of substantial amounts of citric acid, which are common features of cancer cells.

In order to assess if our constraint-based modeling approach (pyTARG) can provide realistic estimations of metabolic fluxes we compare it with the existing method called PRIME [20]. PRIME works by constraining only the reactions associated to genes which expression levels are correlated to growth. The correlation coefficients between gene expression and growth rates were calculated using microarray data and growth rates from CellMiner (https://discover.nci.nih.gov/cellminer/) corresponding to the NCI-60 cell lines. A false discovery rate of 0.05 was used. The selected reactions are reported in the S2 Table together with correlation coefficients and p-values. Both PRIME and pyTARG work by maximizing the biomass production rate after imposing constraints on the model (see Methods). The flux distribution obtained after such maximization is just one among many possible flux distributions with the same optimal biomass production rate. In order to assess how accurately each of the methods reproduces experimental flux distributions, a set of alternative optimal results was computed for each cell line as described previously [21]. Using these sets we computed averages and standard deviations for the predictors of lactate production, glucose consumption and glutamate consumption obtained using pyTARG and PRIME, respectively. As it is shown in Fig 2 and Table 1, all the fluxes are predicted more accurately by pyTARG, with especially large differences for lactate production and glucose consumption.

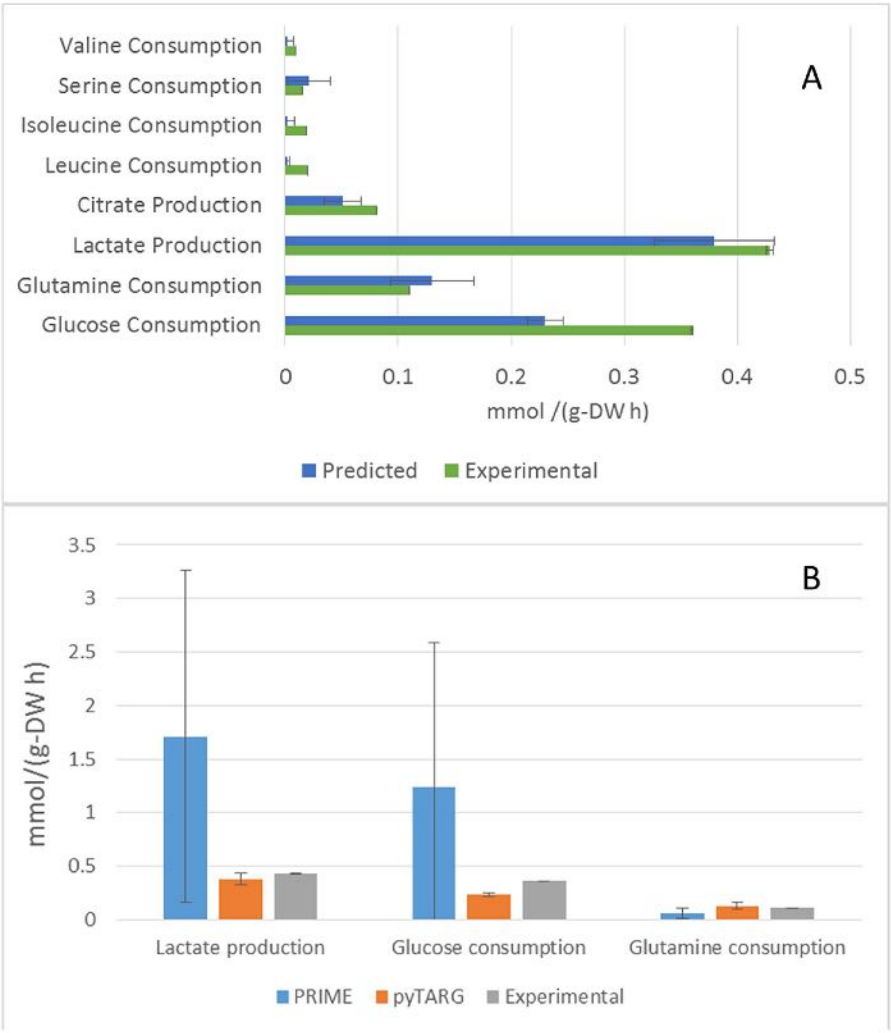

Fig 2. Consumption and production rates of metabolites. A. Uptake and secretion rates of the cell line A549, measured experimentally and predicted using Flux Balance Analysis. The error bars are standard deviations determined using a previously developed algorithm as it is mentioned in materials and methods. B. Average estimations of metabolic fluxes using pyTARG and PRIME and experimental metabolic fluxes, the error bars correspond to standard deviations.

https://doi.org/10.1371/journal.pone.0190636.g002

Table 1. Comparison of mean squared errors calculated by PRIME and pyTARG software for each metabolic flux in A549 cell line (mmol/g-DW h)^2.

A549	PRIME	pyTARG
Lactate production	4.04	0.0052
Glucose consumption	2.60	0.0171
Glutamine consumption	0.0055	0.0018

https://doi.org/10.1371/journal.pone.0190636.t001

Differential effects of a lipoamide analog on MCF7 and ASM cells (proof of concept of identification of therapeutic windows)

Structural similarity with natural metabolic intermediates is a well-known drug design principle, which is at the basis of the mechanism of anti-metabolites that interfere with DNA synthesis due to its structural similarity to pholates. Here we used the described modeling approach to assess the effects of lipoamide analogs on the growth capabilities of MCF7 and ASM cells. Fig 3 shows the relation between the relative inhibition of the enzymes that interact with

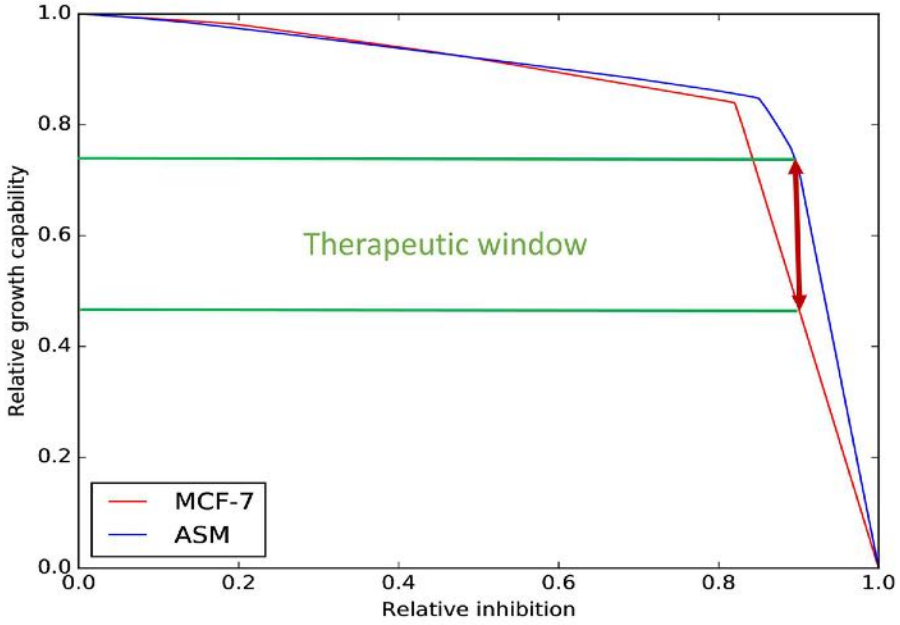

Fig 3. Identification of a therapeutic window. Relative growth rate depended on the relative inhibition of the reactions whose enzymes interact with lipoamide. The relative growth was computed for relative inhibitions from 0 to 1 in intervals of 0.001. No difference between the effects on MCF7 and ASM cells is observed at relative inhibitions lower than 0.8; however, at larger inhibitions a potential therapeutic window exists. This suggests that lipoamide analogs in the right dose, could lead to a substantial decrease of the proliferation rate of MCF7 cells while having milder effects on ASM cells.

https://doi.org/10.1371/journal.pone.0190636.g003

lipoamide (0.9 inhibition means that the reaction is constrained to 0.1 times its value estimated in absence of inhibition) and the relative growth capability, defined as the ratio between the estimated growth rate with and without inhibition.

We observe that at high relative inhibitions (around 0.9), the relative growth capability of ASM cells is 30% higher than the relative growth capability of MCF7 cells, which suggests the existence of a therapeutic window. We proceeded by looking for compounds with structural similarity to lipoamide. A compound with a pentagonal ring and an aliphatic chain that finishes with a polar group was tested (http://www.ambinter.com/reference/19149142) based on its similarity with lipoamide. The tested compound significantly decreased the growth of MCF7 cells while did not have statistically significant effects on ASM cells (Fig 4). The results suggest that Flux Balance analysis using GSMMs constrained according to RNA-seq data, could be used to predict therapeutic windows and help the development of new drugs.

Examples of drug repurposing

We have tested the relative effects of each of the compounds contained in DrugBank (see S1 Table, sheet Metabolite drug, for the structural analogies between DrugBank entries and metabolites in the HMR model) on each of the cell lines and healthy tissues for which there are RNA-seq data in the Human Protein Atlas (www.proteinatlas.com). The results for each

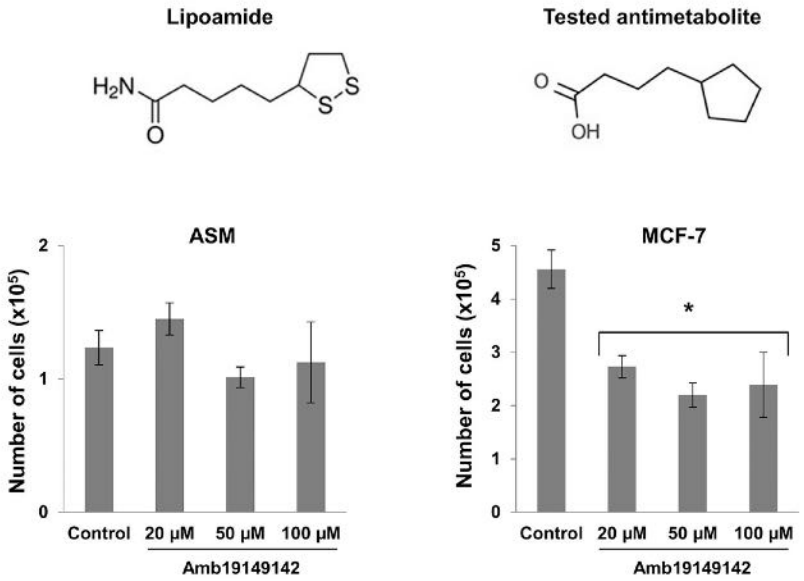

Fig 4. Effects of structural analog of lipoamide on MCF7 and ASM cell proliferation. The number of MCF7 cells was significantly lower after 120 h exposure to Amb19149142 (*, P<0.05) at all 3 tested concentrations, compared to control. No significant differences were observed in the case of ASM cells. Data are mean±SEM of three independent experiments.

https://doi.org/10.1371/journal.pone.0190636.g004

DrugBank entry and each tissue or cell type are reported in the S1 Table (sheet Drug effects). We aimed to identify drugs that tend to have larger effects on cancer cell lines compared to healthy tissues. This was done by performing a statistical t-test. The results are reported on the S1 Table (sheet Therapeutic windows).

First of all we noticed that many of the DrugBank entries correspond to actual human metabolites, which excludes their utilization as competitive inhibitors, however the obtained results still provide many valuable indications. The most significant putative therapeutic windows were associated to intermediates of the mevalonate pathway or ligands putatively binding enzymes in the mevalonate pathway. This pathway is responsible for the synthesis of cholesterol and its derivatives. This observation is particularly interesting because there are drugs in the market (such as statins or bisphosphonates) targeting this pathway. Looking closer on the reason why many of the tested (*in silico*) cancer cell lines are sensitive to a disruption of the mevalonate pathway, it was observed that these cells fail to express the cholesterol transporter NPC1L1 and the lipoprotein lipase LPL, involved in the assimilation of lipoproteins from the blood stream. This makes these cells unable to incorporate external cholesterol and dependent on the mevalonate pathway to synthesize it, while most of the healthy tissues are able to uptake external cholesterol. Inhibition of the mevalonate pathway has been already described as a way to target cancer stem cells [22]. Here we identify a possible mechanism of this effect.

We also remark the presence of xanthine among the candidates to affect selectively cancer cell lines. Xanthine is a natural human metabolite, which has a large structural similarity to caffeine, theobromine and theophylline. Caffeine has already been reported to inhibit the proliferation of glioma cells [23] and other cancer types [24]. Caffeine has a large range of mechanisms of action, among others inducing apoptosis [24]. Our results suggest that competitive inhibition of enzymes that have xanthine as a substrate could be one of the ways in which caffeine could inhibit proliferation of some cancer cell lines (besides other known mechanisms such as inhibition of phosphodiesterases).

Discussion

It has been shown that drug similarity to the natural substrates of metabolic enzymes (measured using Tanimoto scores) is a good predictor of the ability of a ligand to bind the chosen metabolic enzymes. One of the best known human biological network is metabolism, due to the fact that the accumulative knowledge of more than a century of biochemical research allows defining with precision the metabolic reactions catalyzed by each enzyme and these reactions have well known stoichiometry. All this stoichiometric information can be condensed in a GSMM which defines the metabolic capabilities of the cell. GSMMs can be used to predict the effects of constraining the rate of these metabolic reactions. Therefore, GSMMs can be also used to predict the putative effects of drugs targeting metabolic enzymes on the metabolic capabilities of the cell. This has an important practical application, which is finding therapeutic windows, that's drugs that affect the metabolic capabilities of a malignant cell type while having milder effects on healthy cell types. As a prove of concept it was shown experimentally that exposure to a lipoamide structural analog can reduce the proliferation rate of the cancer cell line MCF7 while having lower effects on healthy ASM cells. In order to further explore the potential of structural analogs to natural metabolites as selective anticancer agents, a statistical analysis was performed comparing the predicted effects of different metabolite-analogs on cancer cell lines and healthy mesenchymal stem cells. Mesenchymal stem cells were chosen because they share with metastatic cells the property of having undergone epithelial to mesenchymal transition. The compounds with the highest predicted selective effects included the analogs of intermediates of the mevalonate pathway as well as analogs to xanthine, such as

caffeine, theobromine and theophylline. These findings seem to agree with previous evidence from the literature.

Materials and methods

Analysis of drug-metabolite similarities

DrugBank and KEGG databases were parsed using the Perl library libwww-perl. OpenBabel [18] was used to obtain Tanimoto scores, further analysis was done using R. A script written in Perl was employed to loop over entire procedure using 1000 random drug-metabolite pairs (bootstrapping).

RNA-seq data

Gene expression data for the 34 cancer cell lines (BioProject accession number PRJNA183192) as well as healthy tissues included in the Human Proteome Atlas were downloaded from www.proteinatlas.com in the form of a comma separated file that contains the gene expression of each gene in each cell line (given as RMPK). This file was parsed using a customized python script (available upon request). The gene expression profile of ASM cells was obtained from the GEO database (accession number GSE52778) [25].

Integration of RNA-seq data and GSMMs

GSMMs are compilations of all the metabolic reactions that can be catalyzed in a particular organism. This information can be condensed in the so called stoichiometric matrix, which contains the stoichiometric coefficients of each metabolite in each reaction. If we consider the internal metabolites in steady state, the feasible metabolic flux distributions become constrained to the null space of the stoichiometric matrix S. The steady state condition for internal metabolites is expressed in Eq 1.

$$S\vec{v} = \vec{0} \tag{1}$$

Each reaction rate can be further constrained by imposing upper and lower boundaries. For irreversible reactions, the lower boundaries are set to zero. Upper boundaries and lower boundaries for reversible reactions are set as functions of the expression levels of their associated genes as described below.

$$b_j^{min} \leq v_j \leq b_j^{max} \tag{2}$$

The constraints represented by Eq 2 restrict the feasible metabolic flux distributions to a convex polytope in a multidimensional space (with as many dimensions as reactions in the metabolic network under consideration). In order to compute metabolic flux distributions among the many feasible solutions, a linear objective function (which often is chosen to be biomass production) is optimized using linear programming.

The prediction of metabolic flux distributions was done using the python library COBRApy (version 0.9.0 and solver glpk) [26] and the GSMM used was an updated version of the HMR human metabolic model [16]. A python library containing the necessary scripts (pyTARG) has been developed and is available at https://github.com/SergioBordel/pyTARG. The updated version of the HMR model is available in SBML format in the BioModels database (with the identifier MODEL1707250000) [27] and at https://github.com/SergioBordel/pyTARG (Human.xml). To model a particular cell line the upper bounds were constrained to be 0.0027 mmol g-DW^{-1}h^{-1} times the expression level of the most abundant enzyme associated to each reaction (measured in RPKM). The boundaries were set in a discrete way (by rounding up the

expression levels to their upper multiple of 10), this helped to avoid numerical problems while performing linear optimization. Numerical problems were observed trying to use a continuous spectrum of values for the reaction upper bounds. Other authors [28] have previously used a continuous spectrum of values but with GSMMs 10 times smaller than HMR. The model is allowed to uptake and secrete all the compounds present in HMR and whose uptake or secretion rates were measured experimentally in a previous study [19]. The bounds of these uptake and secretion rates are imposed by the expression levels of the corresponding transporters or the enzymes processing these metabolites.

The error bars in Fig 2 represent the standard deviation of the fluxes, calculated by maximizing the growth rate, constraining it to its optimal value and using a random sampling algorithm [21, 29]. The effect of adding a drug on the growth capabilities of a cell was simulated by first identifying all the metabolic genes that could be potentially targeted by the drug (based on its similarity to the natural substrates of the enzymes). The maximal rates of each reaction were set to be a certain fraction of their rates estimated in absence of the drug (0.1 in the default settings). The maximal growth rate is then computed again with the new constraints and its ratio to the maximal growth rate in absence of the drug is reported as an index of how much the cell is affected by the presence of the drug. An index of 1 would mean that the cell is not affected, and an index equal to the ratio by which the target reactions were decreased, would indicate the larger potential effect, meaning that there are not alternative pathways able to compensate for the drop of activity of the targeted reactions.

Cell culture

MCF-7 (human breast adenocarcinoma cell line; CLS-Cell Lines Service, Eppelheim, Germany) were cultivated in Dulbecco's Modified Eagle Medium: Ham's F-12 (1:1; DMEM/F-12) (Life technologies, Carlsbad, CA, USA) medium with 10% fetal bovine serum (FBS) and antibiotics (100 U/mL penicillin, 100 μg/mL streptomycin). Immortalized human airway smooth muscle cells (ASM) (kindly donated by Prof. R. Gosens; University of Groningen, Netherlands) were obtained as described elsewhere [30]. ASM cells were grown in DMEM medium supplemented with 10% FBS and mix of antibiotics (100 U/mL penicillin and 100 μg/mL streptomycin). Cells were maintained in 5% CO_2 humidified incubator at 37˚C. Unless indicated otherwise, all chemicals were purchased from Sigma Aldrich Corp. (Steinheim, Germany).

Cell proliferation assay

Cells were seeded in 6-well plates at a density 1.5×10^4 cells per well. Cell proliferation was observed 120 h after the treatment with Amb19149142 compound (20, 50, 100 μM) (Green-Pharma, France), as well as solvent control (0.1% ethanol). The total cell number was estimated using 0.4% Trypan Blue stain (Life technologies, Carlsbad, CA, USA) and Neubauer improved cell counting chamber (Sigma-Aldrich, Steinheim, Germany).

Statistical analysis

Averaged data are reported as means ± standard error of the mean. Statistical analysis was performed using two-tailed Student's t-test. Differences were considered statistically significant at $P < 0.05$. The error bars in Fig 2 correspond to standard deviations estimated using a previously developed algorithm [21, 29], which computes solutions corresponding to corners in the space of feasible flux distributions with optimal biomass production rates.

Supporting information

S1 Table. A file in Excel format with information about computationally investigated drugs containing 3 sheets:

Sheet Metabolite drug contains structural analogies between DrugBank entries and metabolites in the HMR model.

Sheet Drug effects contains predicted effect of drugs at 90% target inhibition.

Sheet Therapeutic windows contains drugs that tend to have larger effects on cancer cell lines compared to healthy tissues determined by a statistical t-test.
(XLSX)

S2 Table. A file in Excel format containing the selected reactions with their correlation coefficients and p-values.
(XLSX)

S1 Fig. Distribution of shared targets between random human metabolites and DrugBank compounds. The percentages were computed by extracting 4000 random metabolite-drug pairs. The process was repeated 1000 times.
(TIF)

Acknowledgments

This research was funded by a scholarship from the Swedish Institute (Visby program No. 11278/2013), a grant from the Olle Engkvist Foundation (No. 21210045).

Author Contributions

Conceptualization: Vytautas Raškevičius, Visvaldas Kairys, Sergio Bordel.

Data curation: Vytautas Raškevičius, Valeryia Mikalayeva, Sergio Bordel.

Formal analysis: Vytautas Raškevičius, Valeryia Mikalayeva, Ieva Antanavičiūtė, Vytenis Arvydas Skeberdis, Sergio Bordel.

Funding acquisition: Sergio Bordel.

Investigation: Vytautas Raškevičius, Valeryia Mikalayeva, Ieva Antanavičiūtė, Ieva Ceslevičienė, Vytenis Arvydas Skeberdis, Sergio Bordel.

Project administration: Vytenis Arvydas Skeberdis, Sergio Bordel.

Resources: Sergio Bordel.

Software: Sergio Bordel.

Supervision: Vytautas Raškevičius, Visvaldas Kairys, Sergio Bordel.

Visualization: Vytautas Raškevičius, Ieva Antanavičiūtė, Sergio Bordel.

Writing – original draft: Vytautas Raškevičius, Sergio Bordel.

Writing – review & editing: Vytautas Raškevičius, Valeryia Mikalayeva, Ieva Antanavičiūtė, Ieva Ceslevičienė, Vytenis Arvydas Skeberdis, Visvaldas Kairys, Sergio Bordel.

References

1. Yuriev E, Ramsland PA. Latest developments in molecular docking: 2010–2011 in review. J Mol Recognit. 2013; 26(5):215–39. https://doi.org/10.1002/jmr.2266 PMID: 23526775

2. Brylinski M, Skolnick J. FINDSITE LHM: a threading-based approach to ligand homology modeling. PLoS Comput Biol. 2009; 5(6):e1000405. https://doi.org/10.1371/journal.pcbi.1000405 PMID: 19503616
3. Lee HS, Im W. Identification of ligand templates using local structure alignment for structure-based drug design. J Chem Inf Model. 2012; 52(10):2784–95. https://doi.org/10.1021/ci300178e PMID: 22978550
4. Imming P, Sinning C, Meyer A. Drugs, their targets and the nature and number of drug targets. Nat Rev Drug Discov. 2006; 5(10):821–34. https://doi.org/10.1038/nrd2132 PMID: 17016423
5. Haupt VJ, Schroeder M. Old friends in new guise: repositioning of known drugs with structural bioinformatics. Brief Bioinform. 2011; 12(4):312–26. https://doi.org/10.1093/bib/bbr011 PMID: 21441562
6. Whirl-Carrillo M, McDonagh EM, Hebert JM, Gong L, Sangkuhl K, Thorn CF, et al. Pharmacogenomics knowledge for personalized medicine. Clin Pharmacol Ther. 2012; 92(4):414–7. https://doi.org/10.1038/clpt.2012.96 PMID: 22992668
7. Vander Heiden MG. Targeting cancer metabolism: a therapeutic window opens. Nat Rev Drug Discov. 2011; 10(9):671–84. https://doi.org/10.1038/nrd3504 PMID: 21878982
8. Duarte NC, Becker SA, Jamshidi N, Thiele I, Mo ML, Vo TD, et al. Global reconstruction of the human metabolic network based on genomic and bibliomic data. Proc Natl Acad Sci U S A. 2007; 104(6):1777–82. https://doi.org/10.1073/pnas.0610772104 PMID: 17267599
9. Thiele I, Swainston N, Fleming RM, Hoppe A, Sahoo S, Aurich MK, et al. A community-driven global reconstruction of human metabolism. Nat Biotechnol. 2013; 31(5):419–25. https://doi.org/10.1038/nbt.2488 PMID: 23455439
10. Folger O, Jerby L, Frezza C, Gottlieb E, Ruppin E, Shlomi T. Predicting selective drug targets in cancer through metabolic networks. Mol Syst Biol. 2011; 7(1):501.
11. Agren R, Bordel S, Mardinoglu A, Pornputtapong N, Nookaew I, Nielsen J. Reconstruction of genome-scale active metabolic networks for 69 human cell types and 16 cancer types using INIT. PLOS Comput Biol. 2012; 8(5):e1002518. https://doi.org/10.1371/journal.pcbi.1002518 PMID: 22615553
12. Feizi A, Bordel S. Metabolic and protein interaction sub-networks controlling the proliferation rate of cancer cells and their impact on patient survival. Sci Rep. 2013; 3:3041. https://doi.org/10.1038/srep03041 PMID: 24154670
13. Jerby L, Shlomi T, Ruppin E. Computational reconstruction of tissue-specific metabolic models: application to human liver metabolism. Mol Syst Biol. 2010; 6(1):401.
14. Yizhak K, Gaude E, Le Dévédec S, Waldman YY, Stein GY, van de Water B, et al. Phenotype-based cell-specific metabolic modeling reveals metabolic liabilities of cancer. eLife. 2014; 3:e03641.
15. Wishart DS, Knox C, Guo AC, Shrivastava S, Hassanali M, Stothard P, et al. DrugBank: a comprehensive resource for in silico drug discovery and exploration. Nucleic Acids Res. 2006; 34(suppl 1):D668–72.
16. Mardinoglu A, Agren R, Kampf C, Asplund A, Nookaew I, Jacobson P, et al. Integration of clinical data with a genome-scale metabolic model of the human adipocyte. Mol Syst Biol. 2013; 9(1):649.
17. Kanehisa M, Sato Y, Kawashima M, Furumichi M, Tanabe M. KEGG as a reference resource for gene and protein annotation. Nucleic Acids Res. 2016; 44(D1):D457–D462. https://doi.org/10.1093/nar/gkv1070 PMID: 26476454
18. O'Boyle NM, Banck M, James CA, Morley C, Vandermeersch T, Hutchison GR. Open Babel: An open chemical toolbox. J Cheminform. 2011; 3:33. https://doi.org/10.1186/1758-2946-3-33 PMID: 21982300
19. Jain M, Nilsson R, Sharma S, Madhusudhan N, Kitami T, Souza AL, et al. Metabolite profiling identifies a key role for glycine in rapid cancer cell proliferation. Science. 2012; 336(6084):1040–4. https://doi.org/10.1126/science.1218595 PMID: 22628656
20. Yizhak K, Gaude E, Le Dévédec S, Waldman YY, Stein GY, van de Vater B, et al. Phenotype-based cell-specific metabolic modeling reveals metabolic liabilities of cancer. eLife. 2014; 3: e03641.
21. Bordel S, Agren R, Nielsen J. Sampling the solution space in genome-scale metabolic networks reveals transcriptional regulation in key enzymes. PLOS Comput Biol. 2010; 6(7):e1000859. https://doi.org/10.1371/journal.pcbi.1000859 PMID: 20657658
22. Likus W, Siemianowicz K, Bieńk K, Pakuła M, Pathak H, Dutta C, et al. Could drugs inhibiting the mevalonate pathway also target cancer stem cells? Drug Resist Updat. 2016; 25:13–25. https://doi.org/10.1016/j.drup.2016.02.001 PMID: 27155373
23. Ku BM, Lee YK, Jeong JY, Ryu J, Choi J, Kim JS, et al. Caffeine inhibits cell proliferation and regulates PKA/GSK3β pathways in U87MG human glioma cells. Mol Cells. 2011; 31(3):275–9. https://doi.org/10.1007/s10059-011-0027-5 PMID: 21229324
24. Bode AM, Dong Z. The enigmatic effects of caffeine in cell cycle and cancer. Cancer Lett. 2007; 247(1):26–39. https://doi.org/10.1016/j.canlet.2006.03.032 PMID: 16709440

25. Himes BE, Jiang X, Wagner P, Hu R, Wang Q, Klanderman B, et al. RNA-Seq transcriptome profiling identifies CRISPLD2 as a glucocorticoid responsive gene that modulates cytokine function in airway smooth muscle cells. PloS One. 2014; 9(6):e99625. https://doi.org/10.1371/journal.pone.0099625 PMID: 24926665

26. Ebrahim A, Lerman JA, Palsson BO, Hyduke DR. COBRApy: COnstraints-Based Reconstruction and Analysis for Python. BMC Syst Biol. 2013; 7:74. https://doi.org/10.1186/1752-0509-7-74 PMID: 23927696

27. Chelliah V, Juty N, Ajmera I, Ali R, Dumousseau M, Glont M, et al. BioModels: ten-year anniversary. Nucleic Acids Res. 2015; 43: D542–D548. https://doi.org/10.1093/nar/gku1181 PMID: 25414348

28. Colijn C, Brandes A, Zucker J, Lun DS, Weiner B, Farhat MR, et al. Interpreting expression data with metabolic flux models: predicting Mycobacterium tuberculosis mycolic acid production. PLoS Comput Biol. 2009; 5(8):e1000489 https://doi.org/10.1371/journal.pcbi.1000489 PMID: 19714220

29. Bordel S. Experimental evidence suggests the existence of evolutionary conserved global operation principles governing microbial metabolism. Sci Rep. 2013; 3:3017. https://doi.org/10.1038/srep03017 PMID: 24145501

30. Gosens R, Stelmack GL, Dueck G, McNeill KD, Yamasaki A, Gerthoffer WT, et al. Role of caveolin-1 in p42/p44 MAP kinase activation and proliferation of human airway smooth muscle. Am J Physiol Lung Cell Mol Physiol. 2006; 291(3):L523–34. https://doi.org/10.1152/ajplung.00013.2006 PMID: 16617096

International Journal of
Molecular Sciences

MDPI

Article

Fatty Acid Synthesis and Degradation Interplay to Regulate the Oxidative Stress in Cancer Cells

Valeryia Mikalayeva [1], Ieva Ceslevičienė [1], Ieva Sarapinienė [1], Vaidotas Žvikas [2], Vytenis Arvydas Skeberdis [1], Valdas Jakštas [2] and Sergio Bordel [1,*]

1 Institute of Cardiology, Lithuanian University of Health Sciences, LT 44307 Kaunas, Lithuania; Valeryia.Mikalayeva@lsmuni.lt (V.M.); Ieva.Cesleviciene@lsmuni.lt (I.C.); Ieva.Sarapiniene@lsmuni.lt (I.S.); Arvydas.Skeberdis@lsmuni.lt (V.A.S.)

2 Institute of Pharmaceutical Technologies, Lithuanian University of Health Sciences, LT 44307 Kaunas, Lithuania; Vaidotas.Zvikas@lsmuni.lt (V.Ž.); Valdas.Jakstas@lsmuni.lt (V.J.)

* Correspondence: Sergio.Bordel@lsmuni.lt

Received: 30 January 2019; Accepted: 13 March 2019; Published: 18 March 2019

Abstract: Both cytosolic fatty acid synthesis (FAS) and mitochondrial fatty acid oxidation (FAO) have been shown to play a role in the survival and proliferation of cancer cells. This study aimed to confirm experimentally whether FAS and FAO coexist in breast cancer cells (BCC). By feeding cells with ^{13}C-labeled glutamine and measuring labeling patterns of TCA intermediates, it was possible to show that part of the cytosolic acetyl-CoA used in lipid synthesis is also fed back into the mitochondrion via fatty acid degradation. This results in the transfer of reductive potential from the cytosol (in the form of NADPH) to the mitochondrion (in the form of NADH and $FADH_2$). The hypothesized mechanism was further confirmed by blocking FAS and FAO with siRNAs. Exposure to staurosporine (which induces ROS production) resulted in the disruption of simultaneous FAS and FAO, which could be explained by NADPH depletion.

Keywords: cancer; metabolism; lipids; oxidative stress; metabolic flux analysis

1. Introduction

It has been known for more than 50 years that neoplastic tissues rely on de novo fatty acid synthesis (FAS) to proliferate [1]. The fatty acid synthase gene (*FASN*) was found to be a prognostic marker in breast [2] and prostate cancer [3]. ATP-citrate lyase, which is responsible for the synthesis of cytosolic acetyl-CoA in mammalian cells and fuels fatty acid synthesis, has also been shown to be necessary for cell transformation and tumor formation [4]. Acetyl-CoA carboxylase (ACC), which catalyzes the transformation of acetyl-CoA into malonyl-CoA and is necessary for fatty acid biosynthesis, was shown to induce growth arrest when inhibited chemically [5]. Overexpression of the oncogenic *Ras* has been associated with increased levels of long fatty acid chains [6] and non-small cell lung cancer tissues have also shown longer fatty acid chains [7], which suggests a higher activity of fatty acid elongases. A gene expression meta-analysis, in which genes were clustered forming metabolic sub-networks [8], revealed that the expression of metabolic sub-networks related to fatty acid synthesis and elongation, positively correlated with cell proliferation rates (using data from the NCI-60 collection) and negatively correlated with the survival prognosis of colon cancer patients. Interestingly, the same was observed for metabolic sub-networks related to fatty acid degradation and β-oxidation. These observations led to the hypothesis of both phenomena coexisting in the same cells.

The role of fatty acid oxidation (FAO) in the survival and proliferation of cancer cells is attracting growing attention [9,10]. FAO was found to inhibit apoptosis of leukemia cells [11]. *PPAR*-mediated fatty acid oxidation has been shown to protect cancer cells against apoptosis induced by loss of

attachment to the extracellular matrix [12]. Carnitine palmitoyltransferase 1C (*CPT1C*), an element of the carnitine shuttle involved in the transport of cytosolic fatty acids to the mitochondrion (where FAO takes place), has also been identified as an oncogene [13].

Given all the previously mentioned findings, Carracedo et al. [9] stated that "a big challenge is to unify the idea of FAO as an essential pathway in cancer cells with the fact that cancer cells also require active FAS in order to grow and divide." Simultaneous cytosolic FAS and mitochondrial β-oxidation has been considered impossible due to the inhibition of CPTI proteins by malonyl-CoA. CPTI proteins are responsible for the transfer of fatty acids from the cytosol to the mitochondrion via the so-called carnitine shuttle, while malonyl-CoA is an intermediate of FAS. However, malonyl-CoA can be produced by two enzymes, acetyl-CoA carboxylases 1 and 2 (ACC1 and ACC2), and genetic evidence suggests that while malonyl-CoA generated by ACC2 inhibits CPTI and therefore blocks fatty acid transport to the mitochondrion and its subsequent β-oxidation, malonyl-CoA generated by ACC1 does not exert suppressive effects on CPTI [14]. This is probably due to the direct channeling of malonyl-CoA from ACC1 to FASN, without being freely released in the cytosol.

Two main interpretations of the function of FAO in cancer cells are possible. First of all, it could be assumed that FAO plays a protective role only under conditions of metabolic stress such as loss of attachment to the extracellular matrix, during which glucose uptake and catabolism are suppressed [9]. Under such conditions, FAO would work as an alternative source of ATP [15] or NADPH [16], and FAS would have negative effects on cell survival as it would increase ATP and NADPH consumption [16]. Alternatively, FAO and FAS have been suggested to occur simultaneously and support each other [17]. This hypothesis is also supported by the fact that treatment of cells with orlistat (an inhibitor of lipid synthesis) resulted in decreased oxygen consumption rates [11], which was interpreted as the existence of simultaneous lipid synthesis and oxidation in the cells. Further evidence for a coexistence of FAS and FAO was provided by the fact that simultaneous targeting of FAS and FAO resulted in enhanced therapeutic effects in prostate cancer [18] and myeloma [19]. However, the available evidence is still indirect.

In this work we aimed to directly test the existence of simultaneous FAS and FAO by performing metabolic flux analysis using ^{13}C-labeled glutamine in combination with gene silencing using small interfering RNAs (siRNAs). Second, we examined the relevance of such a cycle for the resistance of breast cancer cells to oxidative stress.

2. Results

2.1. Assessment of Simultaneous FAS and FAO Using ^{13}C Labeling

Fatty acids are synthesized from cytosolic acetyl-CoA, which itself is partially derived from citric acid. Citric acid is originated in the tricarboxylic acid (TCA) cycle and transported to the cytosol, but can also be originated from glutamine via the reductive carboxylation of α-ketoglutarate [20]. FAO takes place in the mitochondrion (fatty acids are transported from the cytosol via the carnitine shuttle), resulting in mitochondrial acetyl-CoA, which feeds the TCA cycle. The simultaneous occurrence of both processes implies that part of the acetyl-CoA feeding the TCA cycle is derived from citrate. Supplying ^{13}C-labeled glutamine will result, via reductive carboxylation, in the production of citrate labeled in five carbons (M5 isotopomer) (Figure 1a), which itself will give rise to labeled cytosolic acetyl-CoA taking part in the synthesis of lipids. If these lipids are being simultaneously degraded, labeled acetyl-CoA will be entering the TCA cycle, resulting in the formation of fully labeled citric acid molecules (M6 isotopomer) (Figure 1a).

Alternatively, the presence of fully labeled citrate could be explained by the formation of labeled pyruvate obtained from malate via the malic enzyme (ME). Therefore, in order to assess if lipid metabolism is actually playing a role in the formation of fully labeled citrate, we combined labeling experiments with gene silencing using siRNAs. Previously described BCCs [21] were selected as a candidate for testing the existence of simultaneous FAS and FAO, as other two cell lines MCF7 and

BT-474 showed notably lower amount of fully labeled citrate. The percentage of M6 citrate in MCF7 and BT-474 was 1.15% and 0.5%, respectively (Figure 1b).

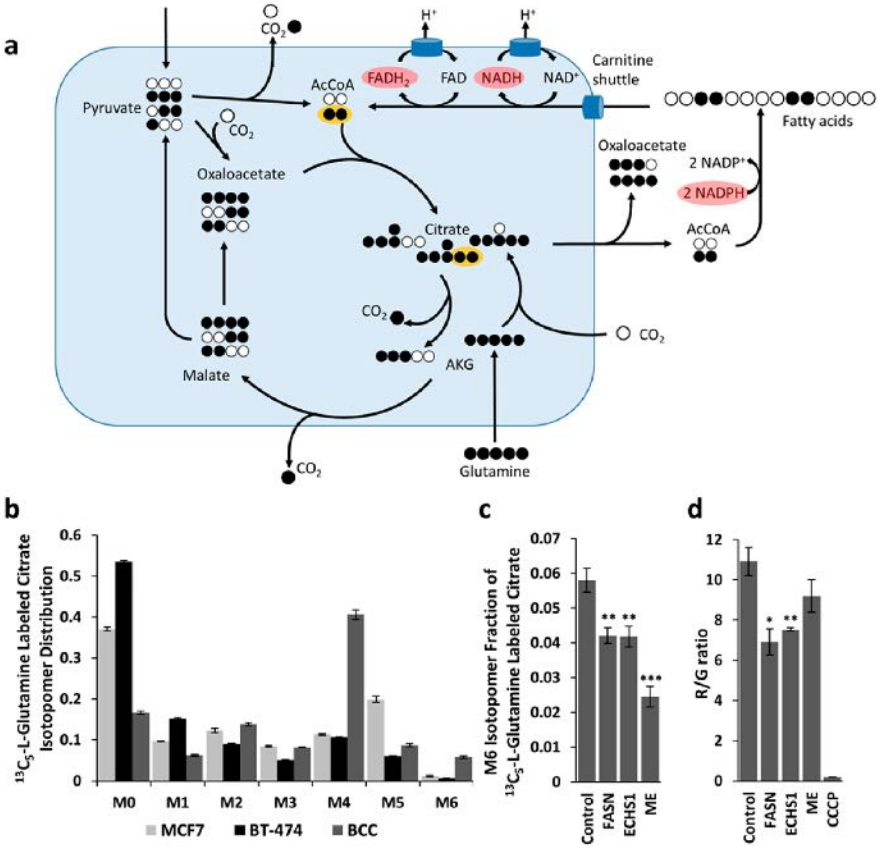

Figure 1. Experiments assessing the existence of simultaneous FAS and FAO. (**a**) Metabolic model with atomic transitions showing how degradation of fatty acids derived from glutamine or ME activity can result in the M6 citrate isotopomer, and scheme showing the shuttle of redox potential from cytosolic NADPH to the mitochondrion, formed by simultaneous FAS and FAO. Labeled carbon atoms entering the TCA cycle from FAO are indicated in yellow. (**b**) Percentages of fully labeled citrate in three different breast cancer cell lines which were fed with $^{13}C_5$-L-Glutamine. BCC showed 5 and 10 times more fully labeled citrate than MCF7 and BT-474 cell lines, respectively, which makes it more likely to have simultaneous FAS and FAO. Bar graphs represent mean ± SEM (n = 4). (**c**) Experimental changes in the fraction of M6 citrate resulting from the silencing of FASN, ECHS1, and ME, respectively. Bar graphs represent mean ± SEM (n = 4). (**d**) Effects of silencing FASN, ECHS1, and ME on the mitochondrial membrane potential. Bar graphs represent mean ± SEM of aggregate/monomer (R/G) ratios of JC-1 dye (n = 3). * $p < 0.05$, ** $p < 0.01$, *** $p < 0.001$.

BCC cells were alternatively transfected with siRNAs against the *FASN* and the *ECHS1* genes, which are involved in FAS and FAO, respectively, and compared to a mock transfection (see Methods). The cells were also transfected with siRNAs against the malic enzyme (*ME*1-3) genes, in order to assess the importance of the malic enzyme for the formation of fully labeled citric acid (western blot analysis is represented in Figure S1. The siRNAs against *FASN* and *ECHS1* resulted in a very similar

drop of the M6 fraction (Figure 1c), which was in both cases statistically significant (from 5.8 ± 0.3% to, respectively, 4.2 ± 0.2%.; n = 4; $p = 0.0054$ and 4.2 ± 0.3%; n = 4; $p = 0.0065$). This confirms that part of the fully labeled citrate appears to be generated via the hypothesized mechanism of simultaneous FAS and FAO. An even stronger drop (to 2.4 ± 0.3%; n = 4, $p = 0.0001$) was caused by siRNAs targeting ME (Figure 1c), which suggests that both mechanisms of formation of fully labeled citrate are active.

2.2. Assessment of Simultaneous FAS and FAO Using Measurements of Mitochondrial Membrane Potential

FAS occurs in the cytosol and requires the oxidation of two NADPH molecules per acetyl-CoA. On the other hand, mitochondrial FAO results in the generation of one NADH and one $FADH_2$ molecules per acetyl-CoA, both of which can be used to feed the respiratory chain (Figure 1a). This results in the transfer of redox potential from the cytosol to the mitochondrion, which can be used to maintain higher mitochondrial membrane potentials. ME catalyzes a reaction producing NADPH, which cannot be used in the respiratory chain. Therefore, if simultaneous FAS and FAO is taking place, it can be expected that silencing of FASN or ECHS1 will result in a drop of the mitochondrial membrane potential, while silencing of ME is not expected to have any significant impact upon it. Mitochondrial potential was estimated by flow cytometry using JC-1 dye (see Methods). Cells transfected with siRNAs targeting FASN and ECHS1 showed significant drops in mitochondrial membrane potential (from 10.9 ± 0.7 to, respectively, 6.9 ± 0.7; n =3; $p = 0.014$ and 7.5 ± 0.1; n = 3; $p = 0.009$; Figure 1d). Cells transfected with siRNAs targeting ME did not show a significant drop in membrane potential (9.2 ± 0.8; $p = 0.19$).

2.3. Metabolic Flux Analysis of BCC Cells

Experimental labeling patterns of citrate and malate were used to adjust the metabolic flux distributions in the central carbon metabolism. The flux distributions were calculated using a model that contained the TCA cycle, FAS, FAO, glutaminolysis, reductive carboxylation of α-ketoglutarate, malic enzyme, pyruvate carboxylase, and pyruvate dehydrogenase. The mitochondrial and cytosolic pools of citrate and α-ketoglutarate were treated as single pools, as if these compounds were freely transferred across the mitochondrial membrane. The cytosolic oxaloacetate produced by citrate lyase was assumed to be transferred back to the mitochondrion.

The EMU (elementary metabolic unit) framework [22] was used to model isotopic distributions. The fitting (based on minimizing relative errors between the experimental and predicted labeling patterns) was performed as described in Materials and Methods. The flux distributions are expressed relatively to the rate of pyruvate dehydrogenase.

Fitted metabolic flux distributions are represented in Figure 2a for the reference experiment and for the experiments with siRNAs (FASN, ECHS1, and ME). The data fitting revealed simultaneous FAS and FAO rates equal to 0.69 times the rate of pyruvate dehydrogenase and a flux of 0.48 in the ME reaction (for the control experiment). In the cells transfected with siRNAs against FASN or ECHS1, the solution minimizing the relative errors in isotopomer distributions (see Methods) corresponded to zero flux in the FAO reaction. Simultaneous transfection with siRNAs targeting three ME genes led to an estimated flux in the ME reaction of 0.03.

The experimental and fitted isotopomer distributions for malate and citrate in "control/reference" experimental conditions and after siRNA silencing are shown in Figure 2b–i, respectively. Reduced fractions of M6 citrate isotopomers indicate reduced FAS, FAO, or ME activity. The isotopomer distributions of malic acid are mainly determined by the rate of glutaminolysis and are not expected to be modified by changes in FAS, FAO, and ME activities.

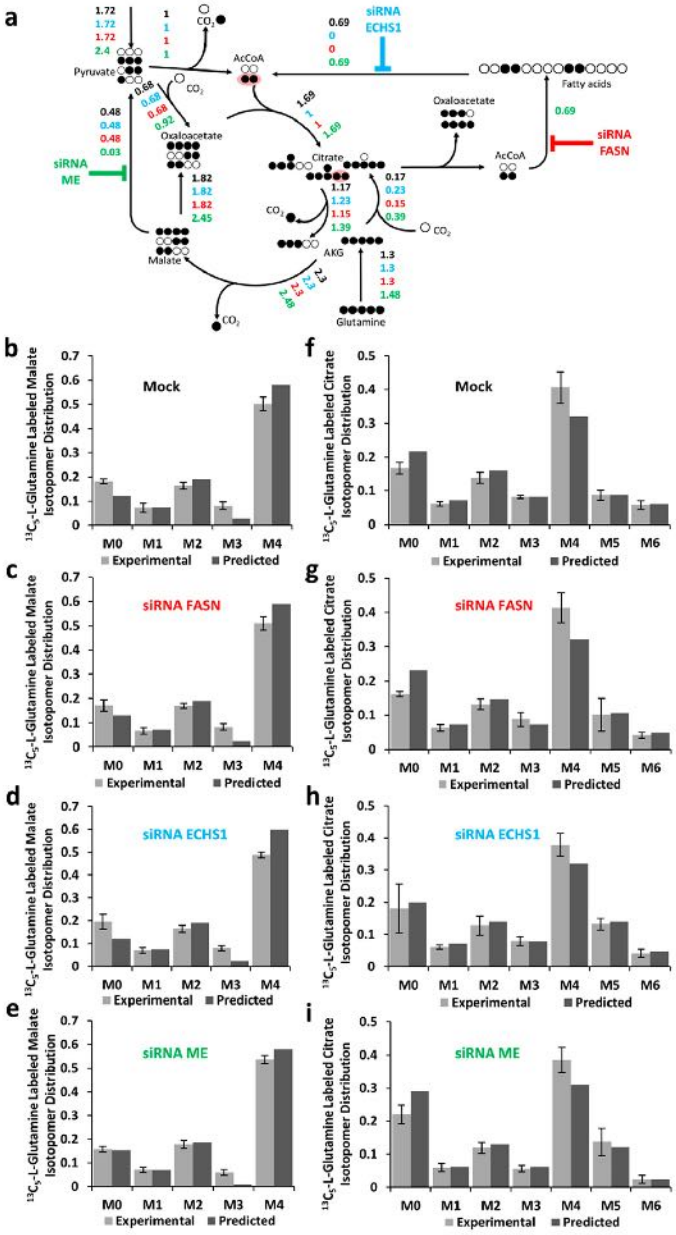

Figure 2. Estimated metabolic flux distributions and isotopomer distributions (simulated and experimental) of malate and citrate for BCC cells. (**a**) Metabolic model with atomic transitions and estimated flux distribution for the mock (black) and siRNAs against FASN (red), ECHS1 (cyan), and ME (green) transfected BCC cells. (**b**–**e**) Malate and (**f**–**i**) citrate isotopomer distribution in mock and siRNAs against FASN (red), ECHS1 (cyan), and ME (green) transfected BCC cells. The bar plots show the fractions of citrate and malate labeled in zero (M0) to six (M6) carbons. Error bars represent 95% confidence intervals (n = 4).

2.4. Effects of Oxidative Stress on Metabolic Fluxes

The overall effect of the described metabolic cycle formed by FAS and FAO is the shuttling of redox equivalents from the cytosol (in form of NADPH) to the mitochondrion (in form of NADH and $FADH_2$). Cytosolic NADPH has two main physiological roles: the biosynthesis of biomass components and the resistance to oxidative stress (the last one is coupled to glutathione reductase and glutathione peroxidase). Increased production of reactive oxygen species (ROS) is therefore expected to result in the depletion of cytosolic NADPH, and subsequently, to stop FAS and other processes that require NADPH. BCC cells treated with staurosporine, an alkaloid that induces high ROS levels [23], caused a strong drop of fully labeled citric acid (Figure 3), which is consistent with the expected arrest of FAS (a full arrest according to the metabolic flux analysis). This result suggests that BCC cells under normal conditions produce more cytosolic NADPH than what is necessary for their biosynthetic needs. In conditions of low oxidative stress, the excess redox potential is channeled into the mitochondrion, where it is ultimately used to produce ATP, while under conditions of high oxidative stress, the excess of NADPH can be directly used to eliminate cytosolic ROS.

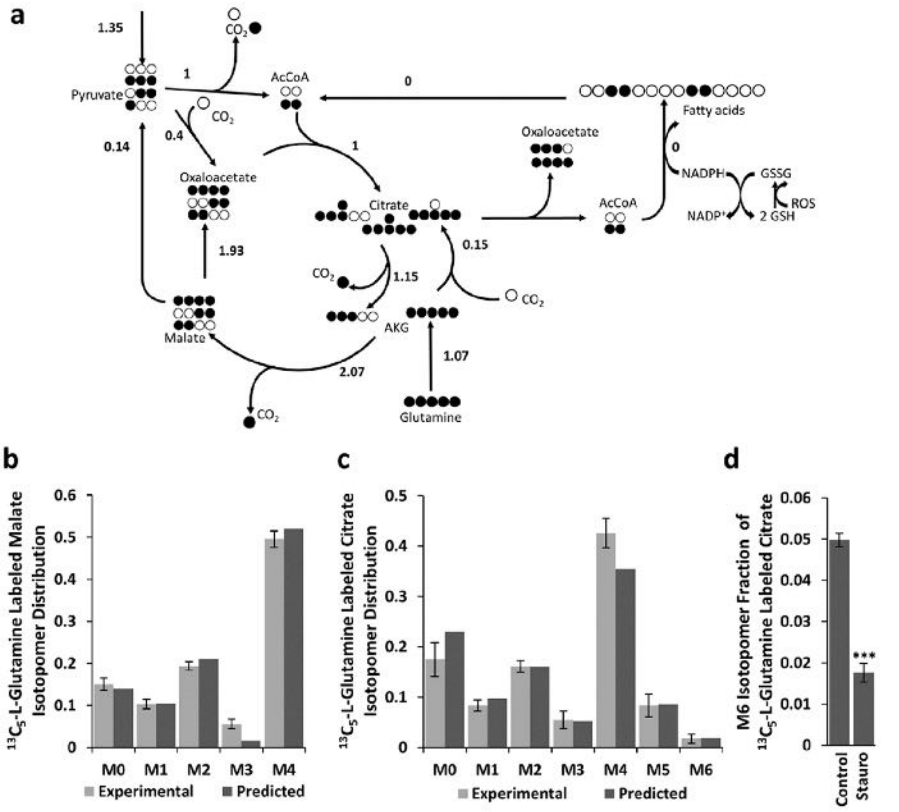

Figure 3. Estimated metabolic flux distributions and labeling patterns (simulated and experimentally observed) of malate and citrate for BCCs after treatment with staurosporine. (**a**) Estimated metabolic flux distributions for BCC cells treated with staurosporine. Simulated and observed labeling patterns of malate (**b**) and citrate (**c**) for BCCs treated with staurosporine. Error bars are 95% confidence intervals (n = 4). Drop of the fraction of M6 citrate caused by staurosporine (**d**). Bar graphs represent mean ± SEM (n = 4), *** $p < 0.001$.

2.5. Resistance of BCC and BT-474 Cells to Oxidative Stress

The previous results indicate that cells with simultaneous FAS and FAO have high cytosolic NADPH production rates, which confers to them the ability to counteract increases in oxidative stress. In contrast, we could expect cells not showing simultaneous FAS and FAO to have lower cytosolic NADPH production rates and also lower tolerance to increased oxidative stress. In order to test the mentioned hypothesis, we compared the effects of staurosporine on BCC and BT-474 cells. The choice of BT-474 cells for the comparison is due to the fact that they showed 10 times less M6 citrate than BCCs (Figure 1), which suggests that the loop formed by simultaneous FAS and FAO is not active in this cell line (Figure 4a). The ^{13}C-labeling data revealed a zero flux in FAO rate for BT-474 cells.

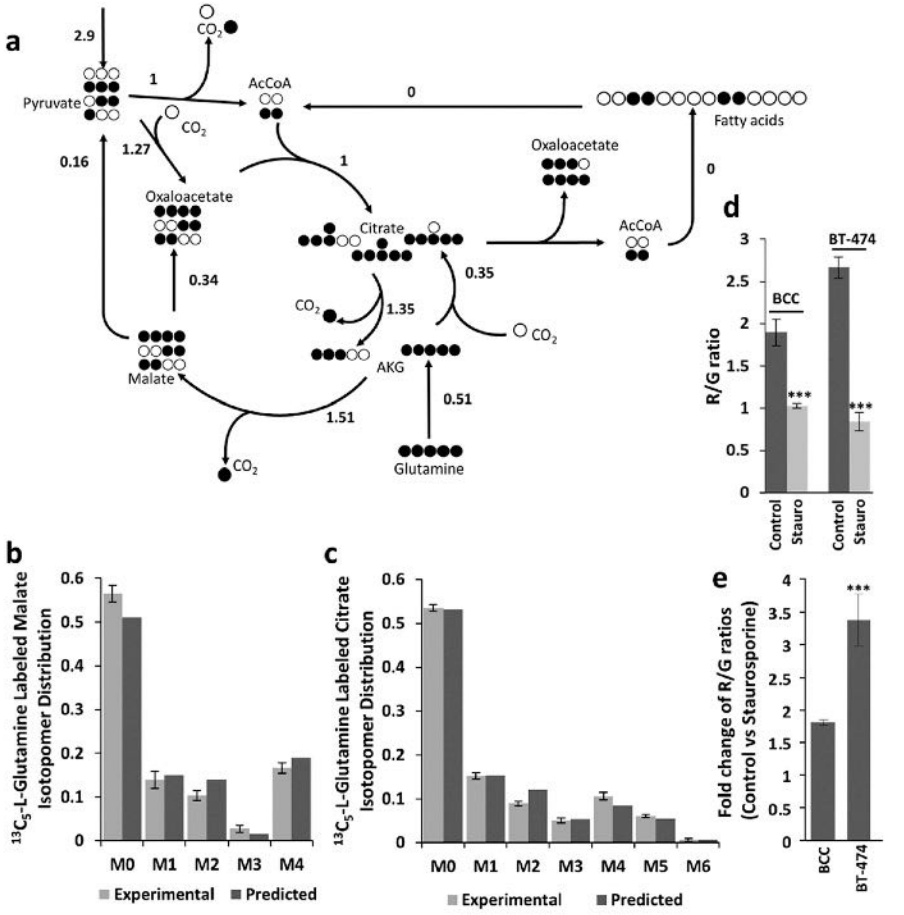

Figure 4. Estimated metabolic flux distributions and labeling patterns (simulated and experimental) of malate and citrate for BT-474 cells. (**a**) Estimated metabolic flux distributions for BT-474 cells. Simulated and observed labeling patterns of malate (**b**) and citrate (**c**). Error bars represent 95% confidence intervals (n = 4). (**d**) Staurosporine-induced mitochondrial depolarization in BT-474 and BCC cells. (**e**) Fold change of R/G ratios in BCC and BT-474 cells after staurosporine treatment. Bar graphs represent mean ± SEM (n = 4), *** $p < 0.001$.

Staurosporine treatment induced stronger mitochondrial depolarization in BT-474 cells compared to BCC, which was determined by the decrease of R/G ratio 3.4 ± 0.4 and 1.8 ± 0.05-fold ($p < 0.001$), respectively (Figure 4d,e). These results are consistent with our hypothesis of BCC cells being more resistant to oxidative stress.

3. Discussion

FAO has been recently shown to play a key role on the survival of cancer cells. On the other hand, FAS is also necessary for cancer cell growth and proliferation. There are two possible solutions in this apparently contradictory situation. It is possible that FAO helps cell survival in situations of metabolic stress when other sources of energy and redox cofactors are not available; on the other hand, even if FAS and FAO have traditionally been considered incompatible due to the inhibitory effects of malonyl-CoA on the carnitine shuttle (responsible for the transport of fatty acids into the mitochondrion), growing evidence is supporting the hypothesis of both phenomena coexisting and feeding each other in some cancer cells. In this work, we demonstrate that this is the case in BCC cells. The coexistence of FAS and FAO is the best explanation for the impact that siRNAs targeting the FASN and ECHS1 genes had on the amount of fully labelled citrate (when ^{13}C-labelled glutamine is supplied to the cells) and the mitochondrial membrane potential. Blocking of FAS resulted in a very similar drop of fully labeled citrate and mitochondrial potential than blocking FAO. This is also consistent with previous observations [11] in which blocking lipid synthesis resulted in lower oxygen consumption.

A possible physiological role of this simultaneous occurrence of FAS and FAO is the shuttling of reductive potential contained in cytosolic NADPH to the mitochondrion. This would allow the cells to recycle the excess NADPH produced in the cytosol and channel its reductive potential into the respiratory chain. If cells are challenged by sudden increases of oxidative stress, this excess production of cytosolic NADPH could be immediately diverted to eliminate ROS, stopping lipid synthesis. This phenomenon indeed appears to take place in BCCs treated with staurosporine, in which a strong drop in the fraction of fully labelled citrate was observed compared to the untreated cells.

Metabolic cycles involving the oxidation of overproduced NADPH have previously been observed in microorganisms [24], where this apparent waste of energy could be compensated for by an increased robustness against sudden increases of oxidative stress. The case presented here suggests that human cells could also use analogous mechanisms.

Cells not showing this cooperative operation of FAS and FAO such as BT-474 are therefore likely to have lower production rates of cytosolic NADPH and to be more sensitive to sudden ROS increases. This could be one of the reasons for the stronger effects of exposure to staurosporine observed in BT-474 compared to BCC.

The presented findings contribute to the understanding of the interplay between FAS, FAO, and NADPH metabolism in cancer cells and confirm FAO as a suitable anticancer metabolic target for some cancer types.

4. Methods

4.1. Cell Lines and Culture Medium

BT-474 (human breast ductal carcinoma cell line; ATCC HTB-20, Manassas, VA, USA), MCF7 (human breast adenocarcinoma cell line; CLS-Cell Lines Service, Eppelheim, Germany), and BCC cells [21] were grown in Dulbecco's Modified Eagle Medium:Ham's F-12 (1:1; DMEM/F-12) (Life technologies, Carlsbad, CA, USA) medium, supplemented with 10% fetal bovine serum (FBS), 100 U/mL penicillin and 100 µg/mL streptomycin. Cells were maintained at 37 °C in a humidified incubator with 5% CO_2. For treatment with staurosporine (Calbiochem, Darmstadt, Germany), cells were incubated for 4 h with 0.25 µM of latter compound.

4.2. siRNA Transfection

We used a jetPRIME transfection reagent (Polyplus-transfection® SA, France) and siRNAs for gene silencing according to the manufacturer's instructions. Final concentrations of 10 nM ECHS1 siRNA (ATGATGTGTGATATCATCTAT; Qiagen, Germantown, MD, USA) or FASN siRNA (CAGGCTTCAGCTCAACGGGAA; Qiagen) were used. Cells were simultaneously transfected with three different siRNAs against the different malic enzyme (ME1, ME2, and ME3) genes: 4nM ME1 (UGCCAUGACUCAGCGUUCtt; Ambion, Waltham, MA, USA), 4 nM ME2 (GGGUGUCUAUGGAAUGGGAtt; Ambion), 4 nM ME3 (GCCUUUACCCUUGAAGAAAtt; Ambion). All following procedures were performed 24 h after siRNA transfection. Mock transfection was used as control.

4.3. ^{13}C Labeling

Cells were incubated in DMEM without glucose, L-Glutamine and piruvate (Sigma, Schnelldorf, Germany), supplemented with 10% FBS and antibiotics. L-Glutamine-$^{13}C_5$ (Aldrich, Hamburg, Germany) was added to the final concentration of 4 mM. Cells were incubated for 24 h. Metabolite extraction was performed as described earlier [25].

4.4. UPLC-ESI-MS Conditions

Separation of organic acids in samples was carried out with an Acquity H-Class UPLC system (Waters, Milford, MA, USA) equipped with a YMC-Triart C18 (100 × 2.0 mm, 1.9 µm) column (YMC, Kyoto, Japan). Triple quadrupole tandem mass spectrometer Xevo TQD (Waters, Milford, MA, USA) with an electrospray ionization (ESI) source was used to obtain mass spectroscopy (MS) data. The column temperature was maintained at 40 °C. Gradient elution was performed with a mobile phase consisting of 0.1% formic acid water solution (solvent A) and acetonitrile (solvent B) with the flow rate set to 0.4 mL/min. The initial conditions were set to 95% of solvent A. Linear gradient profile was applied with following proportions of solvent A: 0 to 0.2 min was set to 95%, 0.2 to 1.5 min–10%, 1.5 min to 1.8 min was maintained at 90%, and 1.8 to 2 min set back to initial conditions. Total time of analysis with equilibration was 3 min. Negative electrospray ionization was applied for analysis with the following settings: capillary voltage was set to negative 2 kV, source temperature applied at 150 °C, desolvation temperature of supplied nitrogen gas was set to 400 °C, desolvation gas flow -700 L/h, cone gas flow -20 L/h. Cone voltage was set to 25 V. MS data was collected in full scan mode in the 50 *m/z* to 250 *m/z* range. MS spectra and chromatograms of citrate isotopomers are presented in the Figure S2.

4.5. Fitting of Metabolic Flux Distributions

Mass distributions were calculated using a Python function (available in the Supplementary Material). This function uses a simplified model of central carbon metabolism containing the reactions depicted in Figure 1. The function is an implementation of the EMU framework [22]. The model contained seven independent reaction rates. One of them (pyruvate dehydrogenase—PDH) was set to 1 and all the other fluxes were given relative to the flux in PDH. The remaining independent reactions were the FAO rate, the malic enzyme, the formation of α-ketoglutarate derived from glutaminolysis, the carboxylation of α-ketoglutarate, pyruvate carboxylase, and the import of pyruvate into the mitochondrion.

The objective function to be minimized was the squared sum of relative errors in the labeling patterns of malate and citrate:

$$F = \sum_{i=1}^{4} \left(\frac{M_i^{mal} - \left(M_i^{mal}\right)_{exp}}{\left(M_i^{mal}\right)_{exp}} \right)^2 + \sum_{i=1}^{6} \left(\frac{M_i^{cit} - \left(M_i^{cit}\right)_{exp}}{\left(M_i^{cit}\right)_{exp}} \right)^2 \quad (1)$$

The contribution of M_0 was not included due to being redundant (the sum of all the mass fractions has to be equal to 1). Previous to the fitting, an identification analysis was performed by numerically calculating the Jacobian matrix of the system and performing its singular value decomposition. The value of the lowest singular value of the Jacobian matrix measures how far the columns of this matrix are from being linearly dependent. A lowest singular value equal to zero would mean that there are many different flux distributions leading to the same labeling patterns and the system is therefore not identifiable. In order to assess the contribution of each flux to the identifiability of the system, new Jacobian matrices were calculated by subtracting the column corresponding to the tested flux and performing singular value decomposition on the new matrix (see Supplementary Methods). The higher that the new lowest singular value was, the more difficult to identify was the subtracted flux. The results of this analysis are presented in the Figures S3 and S4. FAO (the flux most interesting in this work) was the most difficult flux to identify. In order to circumvent this problem, we performed a global optimization for the experiments corresponding to the mock transfection and the silencing of *FASN* and *ECHS1*. This approach is based on the assumption that all the independent fluxes, except FAO are unaffected by the siRNAs. The carboxylation rate of α-ketoglutarate was also allowed to change between conditions, as this flux has been reported to be very sensitive to small perturbations in the concentrations of α-ketoglutarate and citric acid [20].

The fitting of the fluxes corresponding to ME silencing, was performed by fixing the rate of FAO to the value estimated in the previous fitting and allowing all the other fluxes to change. Fitting of flux distributions after treatment with staurosporine and of BT-474 cells were performed allowing all the independent reactions to change.

For each fitting, the values of all the fluxes were sequentially incremented or diminished by 0.001 (without allowing them to take negative values) and if this increment resulted on a reduction of the objective function, the new values were kept and the process reiterated. Different initial sets of flux distributions were used and the fitting leading to the lowest relative error was kept.

4.6. Western Blot Analysis

BCC cells (3×10^6) were lysed in ice-cold cell extraction buffer (Invitrogen, Carlsbad, CA, USA) supplemented with 20 µL/mL protease inhibitor cocktail (Sigma-Aldrich, Germany) and 1 mM PMSF (Abcam, Cambridge, U.K.) for 30 min. The lysates were centrifuged at 13,000 rpm for 10 min at 4 °C. Qubit®protein assay kit (Invitrogen) was used to determine total protein concentration by Qubit 3.0 fluorometer (Invitrogen). Cell lysates (30 µg) were separated by Bolt™ 4–12% Bis-Tris plus gels (Invitrogen) in MES SDS running buffer and transferred to 0.45 µm PVDF membranes (GE Healthcare, U.K.). Proteins were detected using primary antibodies against ECHS1 (ab174312) and FASN (ab99359) (Abcam), PPAR-δ (PA1-823A), ME1 (MA5-23524), ME2 (PA5-38007), ME3 (PA5-36494), and GAPDH (AM4300) (Thermo Fisher Scientific, USA), and a WesternBreeze®chemiluminescent kit (Invitrogen) according to the manufacturer's instructions. Bands were visualized by G:Box Chemi Gel Documentation system (Syngene, Frederick, MD, USA).

4.7. Flow Cytometry Assay

Initially, 5×10^4 cells were seeded in a 35 mm dishes in 2 mL of full media. Mock-transfected and siRNA-transfected cells were incubated with media containing 1 mg/L JC-1 dye (Biotium, Fremont, CA USA) for 20 min at room temperature. Afterwards, cells were washed with PBS, trypsinized, and collected using centrifugation. Then cells were resuspended in PBS with 5 mg/L 7-AAD dye (Millipore, Burlington, MA, USA) and incubated for 10 min. For positive control 10 µM carbonyl cyanide m-chlorophenylhydrazone (CCCP) was used. Samples were quantified using a Guava PCA flow cytometer (Millipore). The data were analyzed by guavaSoft 2.7 InCyte software. Mitochondrial membrane potential was represented as the JC-1 aggregates (red fluorescence) to monomers (green fluorescence) ratio (R/G).

4.8. Statistical Analysis

Error bars correspond to standard errors (number of samples specified in the figure legends) when two experiments were compared to each other. When predicted isotopomer distributions were compared to calculated ones, error bars of the experimental values correspond to 95% confidence intervals. Comparisons between two values were performed using the Student *t*-test. Statistical analysis was performed using Excel and the library scipy.stats.

Supplementary Materials: Supplementary materials can be found at http://www.mdpi.com/1422-0067/20/6/1348/s1.

Author Contributions: Conceived the research and performed the metabolic flux analysis: S.B. Designed the experiments: S.B., V.M., I.S., V.A.S. Performed experiments with the cells: V.M., I.C., I.S., V.A.S. Performed MS analysis: V.Ž., V.J. Analyzed the results: S.B., V.M., I.S., V.A.S. All authors reviewed the manuscript.

Funding: This research was funded by a grant (No. SEN-04/2016) from the Research Council of Lithuania.

Conflicts of Interest: The authors declare no financial and non-financial competing interests.

References

1. Medes, G.; Thomas, A.; Weinhouse, S. Metabolism of neoplastic tissue. IV. A study of lipid synthesis in neo-plastic tissue slices in vitro. *Cancer Res.* **1953**, *13*, 27–29. [PubMed]
2. Kuhajda, F.P.; Jenner, K.; Wood, F.D.; Hennigar, R.A.; Jacobs, L.B.; Dick, J.D.; Pasternack, G.R. Fatty acid synthesis: A potential selective target for antineoplastic therapy. *Proc. Natl. Acad. Sci. USA* **1994**, *91*, 6379–6383. [CrossRef] [PubMed]
3. Swinnen, J.V.; Vanderhoydonc, F.; Elgamal, A.A.; Eelen, M.; Vercaeren, I.; Joniau, S.; Heyns, W.; Verhoeven, G. Selective activation of the fatty acid synthesis pathway in human prostate cancer. *Int. J. Cancer* **2000**, *88*, 176–179. [CrossRef]
4. Bauer, D.E.; Hatzivasssiliou, G.; Zhao, F.; Andreadis, C.; Thompson, C.B. ATP citrate lyase is an important component of cell growth and transformation. *Oncogene* **2005**, *24*, 6314–6322. [CrossRef] [PubMed]
5. Beckers, A.; Organe, S.; Timmermans, L.; Scheys, K.; Peeters, A.; Brusselmans, K.; Verhoeven, G.; Swinnen, J.V. Chemical inhibition of acetyl-CoA carboxylase induces growth arrest and cytotoxicity selectively in cancer cells. *Cancer Res.* **2007**, *67*, 8180–8187. [CrossRef] [PubMed]
6. Quijano, C.; Cao, L.; Fergusson, M.M.; Romero, H.; Liu, J.; Gutkind, S.; Rovira, I.I.; Mohney, R.P.; Karoly, E.D.; Finkel, T. Oncogene-induced senescence results in marked metabolic and bioenergetics alterations. *Cell Cycle* **2012**, *11*, 1383–1392. [CrossRef] [PubMed]
7. Marien, E.; Meister, M.; Muley, T.; Fieuws, S.; Bordel, S.; Derua, R.; Spraggins, J.; Van de Plas, R.; Dehairs, J.; Wouters, J.; et al. Non-small cell lung cancer (NSCLC) is characterized by dramatic changes in phospholipid profiles. *Int. J. Cancer* **2015**, *137*, 1539–1548. [CrossRef]
8. Feizi, A.; Bordel, S. Metabolic and protein interaction sub-networks controlling the proliferation rate of cancer cells and their impact on patient survival. *Sci. Rep.* **2013**, *3*, 3041. [CrossRef]
9. Carracedo, A.; Cantley, L.C.; Pandolfi, P.P. Cancer metabolism: Fatty acid oxidation in the limelight. *Nat. Rev. Cancer* **2013**, *13*, 227–232. [CrossRef]
10. Qu, Q.; Zeng, F.; Liu, X.; Wang, Q.J.; Deng, F. Fatty acid oxidation and carnitine palmitoyltransferase I: Emerging therapeutic targets in cancer. *Cell Death Dis.* **2016**, *4*, e532. [CrossRef]
11. Samudio, I.; Harmancey, R.; Fiegl, M.; Kantarijan, H.; Konopleva, M.; Korchin, B.; Kaluarachchi, K.; Bornmann, W.; Duvvuri, S.; Taegtmeyer, H.; et al. Pharmacologic inhibition of fatty acid oxidation sensitizes human leukemia cells to apoptosis induction. *J. Clin. Invest.* **2010**, *120*, 142–156. [CrossRef]
12. Carracedo, A.; Weiss, D.; Leliaert, A.K.; Bhasin, M.; de Boer, V.C.; Laurent, G.; Adams, A.C.; Sundvall, M.; Song, S.J.; Ito, K.; et al. A metabolic prosurvival role for PML in breast cancer. *J. Clin. Invest.* **2012**, *122*, 3088–3100. [CrossRef]
13. Zaugg, K.; Yao, Y.; Reilly, P.T.; Kannan, K.; Kiarash, R.; Mason, J.; Huang, P.; Sawyer, S.K.; Fuerth, B.; Faubert, B.; et al. Carnitine palmitoyltransferase 1C promotes cell survival and tumor growth under conditions of metabolic stress. *Genes Dev.* **2011**, *25*, 1041–1051. [CrossRef]

14. Abu-Elheiga, L.; Matzuk, M.M.; Abo-Hashema, K.A.; Wakil, S.J. Continuous fatty acid oxidation and reduced fat storage in mice lacking acetyl-CoA carboxylase 2. *Science* **2001**, *291*, 2613–2616. [CrossRef]
15. Schafer, Z.T.; Grassian, A.R.; Song, L.; Jiang, Z.; Gerhart-Hines, Z.; Irie, H.Y.; Gao, S.; Puigserver, P.; Brugge, J.S. Antioxidant and oncogene rescue of metabolic defects caused by loss of matrix attachment. *Nature* **2009**, *461*, 109–113. [CrossRef]
16. Jeon, S.M.; Chandel, N.S.; Hay, N. AMPK regulates NADPH homeostasis to promote tumor cell survival during energy stress. *Nature* **2012**, *485*, 661–665. [CrossRef]
17. Caro, P.; Kishan, A.U.; Norberg, E.; Stanley, I.A.; Chapuy, B.; Ficarro, S.B.; Polak, K.; Tondera, D.; Gounarides, J.; Yin, H.; et al. Metabolic signatures uncover distinct targets in molecular subsets of diffuse large B cell lymphoma. *Cancer Cell* **2012**, *22*, 547–560. [CrossRef]
18. Schlaepfer, I.R.; Rider, L.; Rodrigues, L.U.; Gijón, M.A.; Pac, C.T.; Romero, L.; Cimic, A.; Sirintrapun, S.J.; Glodé, L.M.; Eckel, R.H.; et al. Lipid catabolism via CPT1 as a therapeutic target for prostate cáncer. *Mol. Cancer Ther.* **2014**, *13*, 2361–2371. [CrossRef]
19. Tirado-Velez, J.M.; Joumady, I.; Saez-Benito, A.; Cozar-Castellano, I.; Perdomo, G. Inhibition of fatty acid metabolism reduces human mieloma cells proliferation. *PLoS ONE* **2012**, *7*, e46484. [CrossRef]
20. Fendt, S.M.; Bell, E.L.; Keibler, M.A.; Olenchock, B.A.; Mayers, J.R.; Wasylenko, T.M.; Vokes, N.I.; Guarente, L.; Vander Heiden, M.G.; Stephanopoulos, G. Reductive glutamine metabolism is a function of α-ketoglutarate to citrate ratio in cells. *Nat. Commun.* **2013**, *4*, 2236. [CrossRef]
21. Antanavičiutė, I.; Mikalayeva, V.; Ceslevičienė, I.; Milašiūtė, G.; Skeberdis, V.A.; Bordel, S. Transcriptional hallmarks of cancer cell lines reveal and emerging role of branched chain amino acid catabolism. *Sci. Rep.* **2017**, *7*, 7820. [CrossRef]
22. Antoniewicz, M.R.; Kelleher, J.K.; Stephanopoulos, G. Elementary metabolite units (EMU): A novel framework for modeling isotopic distributions. *Metab. Eng.* **2007**, *9*, 68–86. [CrossRef]
23. Kruman, I.; Guo, Q.; Mattson, M.P. Calcium and reactive oxygen species mediate staurosporine-induced mitochondrial disfunction and apoptosis in PC12 cells. *J. Neurosci. Res.* **1998**, *51*, 293–308. [CrossRef]
24. Borgos, S.E.F.; Bordel, S.; Sletta, H.; Ertesvag, H.; Jakobsen, O.; Bruheim, P.; Ellingsen, T.E.; Nielsen, J.; Valla, S. Mapping global effects of the anti-sigma factor MucA in Pseudomonas fluorescensSBW25 through genome-scale metabolic modeling. *BMC Syst. Biol.* **2013**, *7*, 19. [CrossRef]
25. Sellick, C.A.; Hansen, R.; Stephens, G.M.; Goodacre, R.; Dickson, A.J. Metabolite extraction from suspension-cultured mammalian cells for global metabolite profiling. *Nat. Protoc.* **2011**, *6*, 1241–1249. [CrossRef]

PRIEDAI

KAUNO REGIONINIS BIOMEDICININIŲ TYRIMŲ ETIKOS KOMITETAS

Lietuvos sveikatos mokslų universitetas, A. Mickevičiaus g. 9, LT 44307 Kaunas, tel. (+370) 37 32 68 89;el.paštas: kaunorbtek@lsmuni.lt

LEIDIMAS ATLIKTI BIOMEDICININĮ TYRIMĄ

2017-01-12 Nr. BE-2-6

Biomedicininio tyrimo pavadinimas:	**"Fliuksominių metodų kūrimas ir taikymas naviko ląstelių metabolizmui tirti**
Protokolo Nr.:	**2**
Data:	**2016-06-01**
Versija:	**3**
Asmens informavimo forma	**2016-12-28, versija 2**
Pagrindinis tyrėjas:	**Habil. Dr. Vytenis Arvydas Skeberdis**
Biomedicininio tyrimo vieta: Įstaigos pavadinimas: Adresas:	**LSMUL VšĮ Kauno klinikos,** **Chirurgijos klinika, Krūtinės chirurgijos skyrius** Eivenių g. 2A, LT-50009, Kaunas **Lietuvos sveikatos mokslų universitetas** A. Mickevičiaus g. 9, LT-44307, Kaunas **LSMU Kardiologijos institutas,** **Ląstelių kultūrų laboratorija** Sukilėlių per. 17, LT-50009, Kaunas **LSMU Kardiologijos institutas,** **Vaistinių medžiagų ikiklinikinių tyrimų laboratorija** Eivenių g. 4, LT-50103, Kaunas

Išvada:

Kauno regioninio biomedicininių tyrimų etikos komiteto posėdžio, įvykusio **2016 m. liepos mėn. 8 d.** (protokolo Nr. BE-10-10) sprendimu pritarta biomedicininio tyrimo vykdymui.

Mokslinio eksperimento vykdytojai įsipareigoja: (1) nedelsiant informuoti Kauno Regioninį biomedicininių Tyrimų Etikos komitetą apie visus nenumatytus atvejus, susijusius su studijos vykdymu, (2) iki sausio 15 dienos – pateikti metinį studijos vykdymo apibendrinimą bei, (3) per mėnesį po studijos užbaigimo, pateikti galutinį pranešimą apie eksperimentą.

Kauno regioninio biomedicininių tyrimų etikos komiteto nariai			
Nr.	Vardas, Pavardė	Veiklos sritis	Dalyvavo posėdyje
1.	Prof. Romaldas Mačiulaitis	Klinikinė farmakologija	taip
2.	Prof. Edgaras Stankevičius	Fiziologija, farmakologija	taip
3.	Doc. Eimantas Peičius	Filosofija	ne
4.	Dr. Ramunė Kasperavičienė	Kalbotyra	taip
5.	Med. dr. Jonas Andriuškevičius	Chirurgija	taip
6.	Agnė Krušinskaitė	Teisė	taip
7.	Prof. Skaidrius Miliauskas	Pulmonologija, vidaus ligos	ne
8.	Med. dr. Rokas Bagdonas	Chirurgija	ne
9.	Eglė Vaižgelienė	Visuomenės sveikata	ne

Kauno regioninis biomedicininių tyrimų etikos komitetas dirba vadovaudamasis etikos principais nustatytais biomedicininių tyrimų Etikos įstatyme, Helsinkio deklaracijoje, vaistų tyrimėjimo Geros klinikinės praktikos taisyklėmis.

Kauno RBTEK pirmininkas Prof. Edgaras Stankevičius

LIETUVOS SVEIKATOS MOKSLŲ UNIVERSITETAS * KAUNO REGIONINIS BIOMEDICININIŲ TYRIMŲ ETIKOS KOMITETAS

CURRICULUM VITAE

Name, Surname:	Ieva Ceslevičienė
Address:	Departament of Surgery, Hospital of Lithuanian University of Health Sciences Kauno klinikos, Eivenių 2, LT-50161 Kaunas, Lithuania
E-mail:	ieva.cesleviciene@lsmuni.lt

Education:

2007 06 28	Master's Degree in Medicine and Doctor's Qualification, Kaunas University of Medicine, Kaunas, Lithuania
2008 06 26	Professional qualification of medical doctor, Kaunas University of Medicine, Kaunas, Lithuania
2014 06 26	Professional Qualification of General Surgeon, Lithuanian University of Health Sciences, Kaunas, Lithuania
2017 09 07	Breast Cancer Surgeon Professional Training Course, Lithuanian University of Health Sciences, Kaunas, Lithuania
2008–2011	Doctor assistant, Jonava Hospital, Jonava, Lithuania
2008–2010	Doctor assistant, Hospital of Lithuanian University of Health Sciences Kauno klinikos, Pediatric surgery clinic, Kaunas, Lithuania

Work experience:

2008–2011	Junior resident doctor, Hospital of Lithuanian University of Health Sciences Kauno klinikos, Surgical clinic, Kaunas, Lithuania
2011–2014	Senior resident doctor, Hospital of Lithuanian University of Health Sciences Kauno klinikos, Surgical clinics, Kaunas, Lithuania
2014–Present	Assistant Lithuanian University of Health Sciences, Kaunas, Lithuania
2014–Present	General Surgeon, Hospital of Lithuanian University of Health Sciences Kauno klinikos, Surgical clinics, Kaunas, Lithuania

PADĖKA

Dėkoju mokslinam vadovui dr. Sergio Bordel Velasco už idėjas, pamokymus ir patarimus.

Dėkoju prof. habil. dr. Vyteniui Arvydui Skeberdžiui už pagalbą ir patarimus vykdant doktorantūros metu numatytus darbus, bei pagalbą rengiant disertaciją.

Dėkoju prof. habil. dr. Algirdui Boguševičiui už rekomendacijas, padrąsinimą bei supratimą.

Dėkoju Ląstelių kultūrų laboratorijos kolegoms: dr. Ievai Sarapinienei, dr. Valerijai Mikalayevai, Gintarei Milašiūtei už pagalbą atliekant eksperimentus ir jų analizę, patarimus ir nuoširdų bendravimą.

Dėkoju LSMU mokslo fondui už suteiktą finansinę paramą.

Dėkoju Lietuvos fiziologų draugijai už suteiktą finansinę paramą dalyvaujant tarptautinėje konferencijoje.

Esu dėkinga savo šeimai už įvairiapusį palaikymą.